EVALUATION OF ELECTRIC POWERED WHEELCHAIRS AND EXPOSURE TO WHOLE-BODY VIBRATION

by

Erik Jason Wolf

BS, Bioengineering, University of Pittsburgh, 2000

MS, Bioengineering, University of Pittsburgh, 2003

Submitted to the Graduate Faculty of

School of Engineering in partial fulfillment

of the requirements for the degree of

Doctor of Philosophy in Bioengineering

University of Pittsburgh

2006

UNIVERSITY OF PITTSBURGH

SCHOOL OF ENGINEERING

This dissertation was presented

by

Erik J. Wolf

It was defended on

November 21, 2006

and approved by

Michael, L. Boninger, MD

Shirley G. Fitzgerald, PhD

Carmen P. DiGiovine, PhD

Dissertation Director: Rory A. Cooper, PhD

EVALUATION OF ELECTRIC POWERED WHEELCHAIRS AND EXPOSURE TO WHOLE-BODY VIBRATION

Erik J. Wolf, PhD

University of Pittsburgh, 2006

The detrimental results of whole-body vibration (WBV) and their effect on humans in the seated position have been documented. Although wheelchair users are subjected to WBV little research has been conducted to assess, or attempt to reduce them. Whole-body vibrations were measured in power and manual wheelchairs driving over a standard poured sidewalk surfaces and eight interlocking paver surfaces to determine if vibration transmitted to users differed between surfaces. A sensor for detecting ground forces and moments on power wheelchairs while driving was developed. Twenty-two individuals, twenty without a physical disability and two with a physical disability drove two power wheelchairs over an activities of daily living (ADL) course to evaluate effectiveness of suspension in power wheelchairs at attenuating vibration. The suspension elements of the two power wheelchairs were characterized and a spring-mass model was developed to determine the transfer function between the force input and the vibration measured at the seat. The results showed that there were differences in surfaces with some of the interlocking paver surfaces transmitting lower amounts of vibration to users. Ground reaction force and moment sensors ($SMART^{HUB}$ and $SMART^{CASTER}$) were successfully developed, calibrated, and tested while driving over the ADL course. There were differences in the amount of vibration experienced by users for different suspension settings. The suspension model developed to predict the vibrations at the seat based on the input force, underestimated the

accelerations at the seat. Alternative suspension models that would further reduce vibrations transmitted to users were also examined. Results showed that an additional suspension element below the seat could further reduce vibrations. Although suspension in power wheelchairs reduced the amount of whole-body vibration transmitted to users, they do not attenuate them enough to adequately reduce the possibility of secondary injuries, such as disc degeneration and low-back pain. Future research should focus on analysis of whole-body vibration experienced by power wheelchair users over longer periods of time and should be collected during everyday use. Additionally, alternative suspension designs that could reduce the amount of whole-body vibrations transmitted to users and maintain or increase power wheelchair performance should be developed and tested.

TABLE OF CONTENTS

LIST OF TABLES

LIST OF FIGURES

ACKNOWLEDGEMENTS

First, I would like to thank my dissertation committee: Dr. Michael Boninger, Dr. Shirley Fitzgerald, and Dr. Carmen DiGiovine. The support and guidance that each of you has given me over the years is immeasurable and I will be forever grateful. Special thanks are reserved for my dissertation advisor Dr. Rory Cooper. I cannot begin to thank you enough for not only my past eight years at HERL, but also for giving me the tools to succeed in the future. You have contributed to all that I have learned about conducting research, being a mentor and advisor, and have fueled my passion of the rehabilitation engineering discipline.

I would like to thank all of the students whom I have met during my time at the HERL, who have provided me with not only their knowledge and wisdom, but with their friendship. Additionally, I would like to thank all of the staff at HERL, especially Paula Stankovic who has always offered me reassurance and advice in important decisions. They offered assistance whenever it was requested even if it was at the most inconvenient times.

Last but not least I must thank my family. Through all of the good times and the bad my Mother and Father have been unwavering in their support and have given me strength when I had none left. They have sacrificed more than their fair share for me and I love them very much. To Megan. Our friendship became much more, even though it took me too long to finally see it. Your love and support has shown me what is truly important.

1.0 INTRODUCTION

The detrimental results of whole-body vibrations, and their effect on humans in the seated position have been documented [1-12]. In 1957, Dieckmann [1] performed a study on the effects of vibration on humans in the standing and seated positions. He concluded that adding dampeners to the seat would reduce vibrations that may be uncomfortable or even dangerous. Seidel and Heide [2] reviewed the literature on the long term effects of whole-body vibration and concluded that occupational groups (including but not limited to; Drivers of buses, trucks and tractors, operators of vibrating equipment such as crane operators, and helicopter pilots) exposed to whole-body vibrations near or exceeding the International Standards Organization (ISO) 2631-1 (1997) exposure limit were at an increased risk for musculoskeletal ailments as well as injuries to the peripheral nervous system. The ISO 2631-1 Standard was developed to define the risks associated with exposure to whole-body vibrations and also the methods involved in measuring WBVs.

Some of the disorders that have been acknowledged as a result of whole-body vibration are muscle aches, spinal deformities, motion sickness, and most prevalent low-back pain. Kumar et al [3], reported on the difference in self-reported symptoms of backaches in tractor driving farmers versus non-tractor driving farmers. The prevalence of low back symptoms was significantly higher in farmers who operated a tractor than in those who did not, presumably from exposures to whole-body vibrations.

Although wheelchair users are regularly subjected to whole-body vibrations little research has been conducted to assess these vibrations or attempt to reduce them [13-16]. Additionally, wheelchair users are predominantly in a seated position and are exposed to whole-body vibrations over long periods of time and are therefore at risk for secondary injuries (i.e. injuries other than those requiring them to use a wheelchair) such as low-back pain and spinal disc deformities [10]. Wheelchairs that can reduce the amount of vibrations transmitted to the user present a useful solution to harmful whole-body shocks and vibrations. Whole-body vibrations must be minimized to reduce an individual's vulnerability to secondary injuries.

The purpose of section one was to examine different sidewalk surfaces, including a poured concrete sidewalk surface, which represented the standard, and eight interlocking concrete and brick paving surfaces, to determine the amounts of whole-body vibration transmitted to users while driving manual and power wheelchairs over the surfaces.

The purpose of section two was the development, calibration, and testing of ground reaction force and moment drive wheel and caster sensors ($SMART^{HUB}$ and $SMART^{CASTER}$) for use on power wheelchairs. The collection of this data is important to evaluate the forces and moments that power wheelchairs undergo during driving, in order to develop more durable and cost-effective power wheelchair frames, and more effective suspension systems that prevent the transmission of whole-body vibration to power wheelchair users. The methodology and results included are from the second attempt to design these devices. In the initial development and testing, some problems occurred and the results were not acceptable. The first problem was with the bonding of the strain gages. The gages were not coated with polymer and eventually lost their bond with the core sensor. This problem was remedied in the second attempt by applying a polymer coating to the gages after they were bonded to the core sensor, wired, and checked for

reliability. The second problem was with the calibration testing. The testing was incomplete because only static loads were applied and also unreliable because of the previous problem with the strain gages. This problem was addressed by employing a dynamic and more thorough calibration of each wheel.

The purpose of section three was to evaluate differences in suspension in two electric power wheelchairs during driving over an activities of daily living course. This study also examined if suspension systems in power wheelchairs were proficient at reducing the amounts of whole-body vibration transmitted to power wheelchair users, and if the levels of whole-body vibration that users are exposed to while driving over obstacles that are commonly encountered, are at potentially harmful levels according to the ISO 2631-1 Standard.

The purposes of section four were to characterize the spring-damper elements used in the two suspension power wheelchairs, to examine a spring mass model of two suspension power wheelchairs and determine the effectiveness at predicting whole-body vibration experienced at the wheelchair seat based on the input ground reaction force in the vertical direction, and to examine a theoretical suspension power wheelchair spring mass model with an added suspension seat to determine if vibrations can be further attenuated through the use of additional or modified suspension.

2.0 LONGITUDINAL ASSESSMENT OF VIBRATIONS DURING MANUAL AND ELECTRIC POWERED WHEELCHAIR DRIVING OVER SELECTED SIDEWALK SURFACES

2.1 INTRODUCTION

Wheelchair users, both manual and powered, use their wheelchairs for mobility for extended periods of time each day [17]. This extensive use, combined with the bumps, uneven driving surfaces, and other obstacles, can expose wheelchair users to harmful whole-body vibrations (WBVs) which can lead to secondary injuries such as low-back and neck pain, muscle ache and fatigue, and other harmful effects [10]. Few studies have reported the levels of vibration that are experienced by manual wheelchair users, and even fewer have reported on powered wheelchairs or their users. This study will examine different sidewalk surfaces and the resulting whole-body vibrations that are transmitted during manual and power wheelchair driving. Differences in vibration exposure over years will also be examined.

A review of the literature revealed that little research has been conducted on exposure to whole-body vibration over various surfaces during wheeled mobility, including bicycle riding, in-line skating, baby stroller use, and scooters. Thompson et al [18] looked at vibration during in-line skating; however it was only over a standard paved road and did not examine any other surfaces. A study done in Italy by Frendo et al [19] examined vibration during motorscooter driving over different street surfaces including heavy paved brick, light paved brick, and cobblestone. Results revealed differences between the surfaces, with the light paved brick resulting in the lowest transmitted vibration and the cobblestone surface producing the highest.

Multiple studies have shown the negative effects associated with the exposure to whole-body vibrations on humans in the seated positions [20-22]. Occupations where WBVs are a concern include heavy machinery operation, bus and truck driving, and helicopter piloting. These industries, as well as the automotive industry, have taken measures to reduce the amounts of WBVs transmitted to their users while operating these vehicles [23-25].

This problem has been recognized by the wheelchair community and efforts have been made to quantify the amounts of vibrations transmitted to wheelchair users during propulsion. VanSickle et al [13] showed that manual wheelchair users traveling over a simulated road course experience levels of vibrations that exceed the "fatigue-decreased performance boundary" and that may cause fatigue and injury. Wolf et al [26] evaluated vibration exposure to wheelchair users while traveling over sidewalk surfaces. They showed differences between interlocking concrete pavement (ICPI) surfaces and a standard poured concrete surface. In some cases, the ICPI surfaces caused lower WBV than the standard poured concrete surface. Maeda et al [27] issued questionnaires to 33 wheelchair users and tested 10 wheelchair users on a vibration platform. Results from the questionnaire revealed that wheelchair users did feel WBV at the neck, back, and buttocks during propulsion, and that users sensed differences while traveling over different surfaces and obstacles.

Wheelchair companies have attempted to address this problem by adding suspension to manual and powered wheelchairs, however studies have demonstrated that these additions do not necessarily reduce the amounts of oscillatory and shock WBVs. Additionally, in the case of manual wheelchairs, titanium rigid framed wheelchairs without suspension performed better than some wheelchairs with suspension [28-30].

The ISO 2631-1 – Evaluation of Human Exposure to Whole-Body Vibration Standard was established to define the methods of collection, the effects, and the health concerns associated with WBV [31]. The standard defines a health guidance caution zone (Figure 1) which characterizes the amount of WBV that is considered unsafe. When evaluating exposure of WBVs over long periods of time, lower cumulative levels of WBV are considered harmful (less than 1 m/s^2 of weighted Root Mean Squared (RMS) acceleration at eight hours of exposure). Some of the harmful effects of WBVs may be negated by an eight hour rest period (for example a good nights sleep); however through days, months and years the cumulative exposure to WBVs can result in secondary injuries.

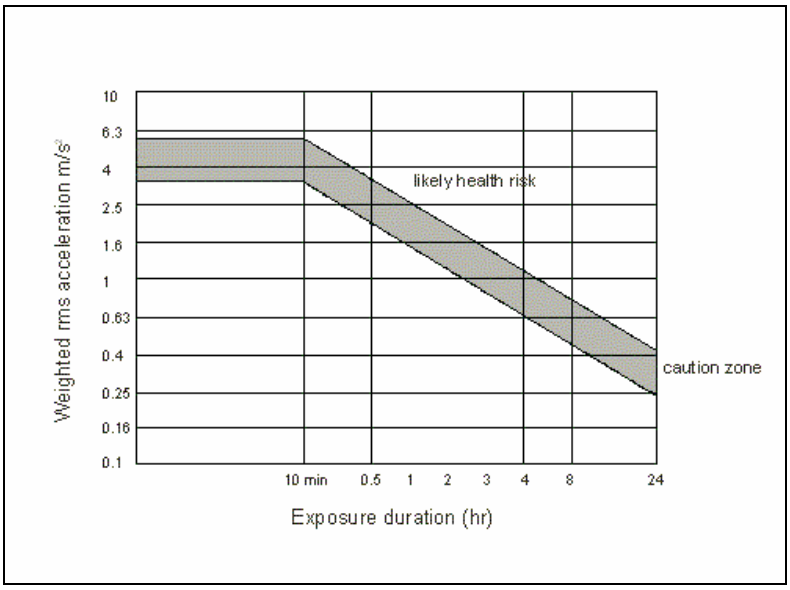

Figure 1 - Limit boundaries of vibration exposure as defined by the ISO-2631 Standard

The goal of this research was to evaluate the whole-body vibrations experienced while driving a manual and electric powered wheelchair over selected sidewalk surfaces, and differences in exposure over years. We hypothesized that different surfaces would induce significantly different whole body vibrations, suggesting that some are less likely to cause secondary injuries to wheelchair users. Furthermore, we hypothesized that over time, due to weather-related wear, the surfaces would become smoother and thus induce significantly lower vibrations.

2.2 METHODS

Six different sidewalk surfaces were tested in three consecutive years (May 2002, July 2003, and June 2004). All of the sidewalk surfaces were approximately 1.2 meters wide and 7.6 meters long. Surface 1 was a poured concrete sidewalk with a brush finish which acted as the control surface. Surfaces 2, 3, and 4 were made from interlocking concrete pavement installed to industry specifications [32], and were installed with a 90-degree herringbone pattern. The interlocking concrete blocks used to construct Surface 2 had no bevel, blocks used for Surface 3 had 2 mm beveled edges, and blocks for Surface 4 had 8 mm beveled edges. Sidewalk surfaces 5 and 6 were constructed of fired clay bricks, and were constructed using a 45-degree herringbone pattern. Blocks used for Surface 5 had 4 mm beveled edges and blocks used for Surface 6 had no bevel. In year three, three additional concrete surfaces were added. Surfaces 7 and 8 both had a 6mm bevel and were installed using a 90 degree and 45 degree herringbone pattern respectively. Surface 9 had a 4 mm bevel and was installed using a 90 degree

herringbone pattern. The specifications of the surfaces can be seen in Table 1. An Interlocking Concrete Pavement Institute (ICPI) certified contractor installed all of the sidewalks.

Table 1 - Specifications of Surfaces Tested

				Dimension (mm)			
#	Name	**Edge Detail**	**Composition**	**A**	**B**	**C**	**Pattern Installed**
1	Pour concrete (Control)	Not applicable	Concrete	N/A	N/A	N/A	smooth
2	Holland Paver	Square - no chamfer	Concrete	198	98	60	90^o
3	Holland Paver	2 mm chamfer	Concrete	198	98	80	90^o
4	Holland Paver	8 mm chamfer	Concrete	198	98	60	90^o
5	Whitacre-Greer	4 mm chamfer	Brick	204	102	57	45^o
6	Pathway Paver	Square - no chamfer	Brick	204	102	57	45^o
7	Holland Paver	6 mm chamfer	Concrete	198	98	60	90^o
8	Holland Paver	6 mm chamfer	Concrete	198	98	60	45^o
9	Holland Paver	4 mm chamfer	Concrete	198	98	60	90^o

Ten able-bodied subjects were recruited in each of the three testing years. Efforts were made to recruit either the same subject each year or subjects with matching weights and heights in order to make sure variability in subject population was accounted for. Subject demographics, averages and standard deviations of heights and weights, can be seen in Table 2. A repeated measures ANOVA showed that there were no significant differences between subjects heights (p=0.7548) and weights (p=0.3962) over years.

Table 2 - Subject Descriptive Statistics (Mean values are in bold)

	Height (cm)	Weight (kg)
Year 1	**170.43**	**71.18**
	11.32	18.98
Year 2	**170.94**	**71.95**
	11.55	19.43
Year 3	**170.94**	**72.95**
	10.78	20.58

This study was approved by the Veterans Affairs Pittsburgh Healthcare Systems Institutional Review Board. Study requirements stated that subjects be between the ages of 18-65, free of any shoulder pain that would prevent them from propelling, no history of cardiopulmonary disease, and free of a physical disability. After giving their written informed consent, subjects were asked to propel a manual wheelchair (at 1 m/s) (Figure 2) and drive an electric powered wheelchair (at 1 m/s and 2 m/s) over six sidewalk surfaces a total of three times each.

Figure 2 - Setup of the Quickie GP manual wheelchair

The manual wheelchair (Quickie GP, Sunrise Medical Ltd.) was a rigid frame design with 127 mm (5”) diameter polyurethane tires, and standard 610 mm (24”) diameter rear wheels. The seat width was 406 mm, the seat depth was 458 mm, and the backrest height was 410 mm. The rear axles were placed 45 mm in front of the backrest tubes. The SMART^{Wheels} were used as the rear wheels during this study [33]. They were used in the first year of testing to evaluate that there were no differences in work during propulsion over all of the surfaces [26], and therefore used each of the following years for congruency. SMART^{Wheels} use solid foam inserts. The approximate mass of the manual wheelchair was 15.5 kg with the SMART^{Wheels} attached.

The electric powered wheelchair (Quickie P200, Sunrise Medical Ltd.) had a rigid frame with 203 mm (8”) front casters, and 254 mm diameter rear wheels (Figure 3).

Figure 3 - Setup of the Quickie P200 electric powered wheelchair

The seat width was 406 mm, the seat depth was 415 mm, and the backrest height was 435 mm. A standard position-sensing joystick was mounted to the right side armrest, and the manufacturer default controller settings were used. All tires were properly inflated to the rated air pressure (248.2 kPa for the caster, and 344.7 kPa for the rear wheels). The approximate mass of the electric powered wheelchair with batteries was 89 kg. The frame of the electric powered wheelchair was made from aircraft quality aluminum. All subjects sat on a 50 mm thick linear polyurethane foam cushion during all testing. Both wheelchairs were not used in between years of testing to ensure minimal deterioration (specifically to the tires, and frames) or other changes over time.

A tri-axial accelerometer was used to collect vibrations in three orthogonal axes at the seat and the footrest. Acceleration data were collected at 200 Hz. The ISO Standards describe the minimum collection rate for accelerations as 160 Hz. The seat accelerometer was attached to a 40.64 cm x 40.64 cm x .64 cm aluminum plate. The footrest accelerometer was attached to a 7.62 cm x 15.24 cm x .95 cm aluminum plate which in turn was attached to the wheelchair footplates. Based upon the ISO 2631-1 Standard [31], the whole-body vibrations defined along the z-axis (vertical, along the spine of a seated subject and along the legs transmitted through the footrest) were analyzed using the Root Mean Square method (Equation 1). The choice to only measure the z-axis acceleration direction was based on the ISO 2631-1 standard which states that the results of the measurements should be made on the direction which presents the highest vibrations. Once acceleration data were collected at the seat and the footrest for each trial, frequency weightings, as described by the ISO 2631-1 standard were applied. The frequency weighted accelerations in the vertical direction are given as a_{wz} and the time of the trial is T. The result is the root mean squared acceleration in the vertical direction (RMS_z).

$$RMS_z = \left[\frac{1}{T} \int_0^T a_{wz}^2(t)dt \right]^{\frac{1}{2}} \quad [1]$$

The acceleration data were calibrated and converted for analyses in custom software written using Matlab (The Mathworks Inc., Natick, MA).

Statistical analyses were done using SAS (SAS Institute, Inc., Cary, NC). Data were analyzed using a mixed model to evaluate the differences in RMS vertical vibrations at the seat and the footrests between surfaces and between years. Analyses between years only included surfaces 1 through 6 because surfaces 7, 8 and, 9 were only tested in the third year. Post-hoc analysis was completed using a Tukey pairwise comparison.

2.3 RESULTS

Data were analyzed for normality. Outliers were identified using the Chi-Squared test for Normality and removed (one subject performed a wheelie during a manual wheelchair trial) and data were found to be normally distributed.

Table 3 - Average Seat RMS (m/s^2). Surfaces significantly lower (p=0.05) than surface 1 are denoted by *. Surfaces significantly higher (p=0.05) than surface 1 are denoted by #.

	Manual Wheelchair	Power Wheelchair (1 m/s)	Power Wheelchair (2 m/s)
Surface 1	0.47±.07	0.37±.09	1.17±.21
Surface 2	0.32±.06 *	0.28±.06 *	0.60±.12 *
Surface 3	0.39±.07 *	0.33±.08	0.67±.12 *
Surface 4	0.76±.16 #	0.85±.19 #	0.89±.14 *
Surface 5	0.46±.09	0.33±.10	0.75±.15 *
Surface 6	0.47±.08	0.37±.09	0.90±.14 *
Surface 7	0.59±.09 #	0.59±.08 #	0.76±.10 *
Surface 8	0.78±.09 #	0.38±.05	0.89±.15 *
Surface 9	0.48±.06	0.40±.05	0.66±.08 *

Table 4 - Average Footrest RMS (m/s^2). Surfaces significantly lower (p=0.05) than surface 1 are denoted by *. Surfaces significantly higher (p=0.05) than surface 1 are denoted by #.

	Manual Wheelchair	Power Wheelchair (1 m/s)	Power Wheelchair (2 m/s)
Surface 1	1.36±.22	0.53±.10	1.26±.31
Surface 2	0.81±.18 *	0.32±.08 *	0.67±.21 *
Surface 3	1.09±.23 *	0.38±.09 *	0.79±.19 *
Surface 4	2.30±.44 #	0.66±.16 #	1.21±.28
Surface 5	1.34±.32	0.43±.09	0.84±.21 *
Surface 6	1.41±.25	0.47±.09	0.94±.23 *
Surface 7	1.79±.29 #	0.43±.08	0.78±.70 *
Surface 8	2.19±.32 #	0.46±.13	0.86±.26 *
Surface 9	1.35±.18	0.32±.06 *	0.67±.16 *

Table 5 - Average Seat RMS (m/s^2) vibrations over three years. Years not significantly different are denoted by *.

Seat			
	Manual Wheelchair	Power Wheelchair (1 m/s)	Power Wheelchair (2 m/s)
Year 1	0.439 ± 0.171	0.399 ± 0.190	0.784 ± 0.214
Year 2	0.494 ± 0.154 *	0.450 ± 0.228	0.825 ± 0.229
Year 3	0.501 ± 0.178 *	0.420 ± 0.196	0.885 ± 0.224

Table 6 - Average Footrest RMS (m/s^2) vibrations over three years. Years not significantly different are denoted by *.

Footrest	Manual Wheelchair	Power Wheelchair (1 m/s)	Power Wheelchair (2 m/s)
Year 1	1.272 ± 0.526	0.477 ± 0.173 *	0.942 ± 0.316
Year 2	1.390 ± 0.504	0.448 ± 0.137	0.902 ± 0.286
Year 3	1.492 ± 0.571	0.467 ± 0.142 *	1.020 ± 0.326

2.3.1 Manual Wheelchair

2.3.1.1 Surfaces

Results of collected vibrations, shown in Tables 3 and 4, at the seat and the footrest for the manual wheelchair revealed that there were significant differences between the surfaces ($p<.0001$). Post-hoc analysis revealed that the standard poured concrete surface was significantly higher than surfaces 2 and 3, significantly lower than 4, 7, and 8, and not significantly different from surfaces 5 and 6.

2.3.1.2 Years

For RMS vibrations at the seat and the footrest, shown in tables 5 and 6, there were significant differences between the three years ($p < 0.0001$). Post-hoc analysis revealed that for RMS vibrations at the seat, year 1 was significantly lower than years 2 and 3. Year 2 was not significantly different ($p = 0.3257$) than year 3. For RMS vibrations at the footrest all three years were significantly different ($p < 0.0001$).

2.3.2 Powered Wheelchair

2.3.2.1 Surfaces

At 1 m/s, for vibrations at the seat and the footrest, shown in Tables 3 and 4, significant differences were found between surfaces ($p<.0001$). Post-hoc analysis of the 1 m/s speed revealed that at the seat surface 2 was significantly lower than surface 1. Surfaces 3, 5, 6, 8, and 9 were not significantly different than the standard poured concrete surface. Surface 4 and surface 7 were significantly higher than surface 1. At the footrest, surfaces 2, 3, and, 9 were significantly lower than surface 1, surfaces 5, 6, 7, and, 8 were not significantly different, and surface 4 was significantly higher.

At 2 m/s, for vibrations at the seat and the footrest, shown in Tables 3 and 4, significant differences were found between surfaces ($p<.0001$). Post-hoc analysis of the 2 m/s speed revealed that at the seat, all surfaces were significantly lower than the standard poured concrete surface. At the footrest, all surfaces were significantly lower than the standard poured concrete surface except Surface 4, which was not significantly different.

2.3.2.2 Years

For RMS vibrations at the seat and the footrest, shown in tables 5 and 6, there were significant differences in years at 1 m/s ($p=0.0008$ and $p=0.0005$) and at 2 m/s ($p<0.0001$ and $p<.0001$). Post-hoc analysis revealed that year 1 was not significantly different from year 3 ($p=0.1756$) at the footrest at 1 m/s.

2.4 DISCUSSION

Based on its nature, a wheelchair represents a system where its user will be subjected to whole-body vibrations in a seated position for long durations. Because the ISO 2631-1 standard requires an eight hour rest period to negate the damaging effects of any transmitted vibration [31], and because powered wheelchair users typically rely on their wheelchair for all of their mobility, they characterize a population that is potentially at high risk of secondary injuries due to WBVs.

The results of this study showed that surfaces other than poured concrete should be considered for pedestrian access routes. Interlocking concrete and brick surfaces that have small bevels may decrease the amount of whole-body vibrations that are transmitted to wheelchair users during propulsion, especially at higher speeds. Whole-body vibration transmission is related to the speed users are traveling while driving over surfaces. Based on the results it appears that the breaks in the poured concrete sidewalk result in higher transmitted WBV than interlocking pavers while traveling at higher speeds.

The results showing differences in the surfaces were expected based on previous studies [26] as well as the physical properties of the surfaces. Surface 4 has the largest bevel (8 mm) and would expectantly cause the most vibration. Surface 2 has the smallest bevel (0 mm) and resulted in the lowest RMS vibration.

2.4.1 Manual Wheelchair

Results for the manual wheelchair showed that surfaces 2 and 3 produce significantly lower RMS vibrations than the poured concrete surface. These surfaces present a good alternative to the standard poured concrete because they transmit lower amounts of whole-body vibration to

wheelchair users. This result contradicts the statement from the Rights-of-Way Advisory Board that claim that surfaces comprised of individual units are undesirable due to the vibrations they cause. Results showed that there were differences in RMS vibration over surfaces between years for the manual wheelchair at both the seat and the footrest with RMS vibrations trending to increase over time.

2.4.2 Power Wheelchair

Results for the power wheelchair also showed promising results for the use of alternative surfaces to reduce the amount of whole-body vibrations transmitted to wheelchair users. At 1 m/s surface 2 was significantly lower at the seat than the standard poured concrete surface and surfaces 2, 3, and 9 were significantly lower at the footrest. At 2 m/s all surfaces were significantly lower than the standard concrete surface at the seat and only surface 4 was not significantly different at the footrest while all other surfaces were significantly lower. The results from the data collected at 2 m/s most likely are caused by the breaks in the poured concrete surface. The higher speed of the wheelchair causes larger transmission of shocks from the breaks in the sidewalk. Results also showed that there were significant differences in years at the seat and the footrest for both speeds of the power wheelchair. There appeared to be no trend for increase or decrease of RMS vibrations over years. The results from the change in the surfaces over years suggests that data has not been collected for a long enough period of time to show either an increase or decrease in vibration. Data should continue to be collected to more appropriately analyze the trend of change over time.

We hypothesized that due to weather conditions and use, one might expect that the wear on the bevels would reduce the amounts of vibrations experienced by the wheelchair. The results

however show an increase in RMS vibration at the seat and the footrest for the manual wheelchair and the power wheelchair at 2 m/s. There are multiple reasons that this result may have occurred. The nine tested surfaces are isolated and do not see normal wear due to travel and use, which would result in similar results over multiple years. Heaving and settling of the interlocking concrete and brick pavers may occur over time and would cause sharper transitions resulting in higher RMS vibrations. Finally, there may be no significant difference over time if results are followed for longer periods.

Limitations of this study include no use of a standard non-vibration surface such as smooth tile to compare surfaces to a baseline control. However the standard poured concrete was used as the control surface because it is the most common outdoor pedestrian surface. There was no additional pedestrian wear on any of the surfaces. In a real world situation there would be wear on surfaces from normal use. However keeping the surfaces in a controlled environment allows the comparison to be more accurate since the wear on all surfaces is equal. Only one manual and power wheelchair was used for this study. It is understood that certain wheelchairs are capable of reducing the amounts of whole-body vibration transmitted to wheelchair users, however since differences in surfaces are being examined, rigid frame manual and power wheelchairs were selected for this study.

The uses of able-bodied subjects as well as using different subject over the years are further limitations to this study. Although there are differences in the sitting biomechanics of wheelchair users and able-bodied subjects, this subject population was used for ease of recruitment over multiple years and because the metric of interest was the differences between a standard poured concrete surface and interlocking concrete or brick surfaces. Additionally by

matching the height and weight of the replacement subjects we hoped to control for a main factor in whole-body vibration measurements.

These results do demonstrate that some interlocking pavement surfaces should be considered for wheelchair access routes and may reduce the amount of WBVs that are transmitted to wheelchair users, specifically the surfaces with the smallest bevels. The results clearly show that many of the ICPI surfaces are just as good if not better than the standard poured concrete surface at reducing the amounts of WBV transmitted to wheelchair users. It would be useful to use Interlocking paver surfaces to reduce the amount of whole-body vibrations transmitted to wheelchair users.

3.0 DEVELOPMENT OF A SMART^{HUB} AND SMART^{CASTER} FOR AN ELECTRIC POWERED WHEELCHAIR

3.1 INTRODUCTION

With the exponential progression of wheelchair technology in the past quarter century, including the development of new assistive devices, and the advancements of devices already in production, along with the requisite for evidence based practices, the demand for research on wheelchairs and other assistive devices has never been more necessary. Advanced and accurate research calls for existing instrumentation such as kinematics motion capture, electromyography, metabolic data, as well as uniquely designed instrumentation, including measurement of wheelchair propulsion kinetics, ground reaction forces and moments, and wheelchair speed and acceleration.

The purpose of this study was to create ground reaction force sensors for use on an electric powered wheelchair (SMART^{HUB} and SMART^{CASTER}), to calibrate the sensors, and to measure ground reaction forces on two suspension power wheelchairs while traveling over an activities of daily living course. The SMART^{HUB} and SMART^{CASTER} are sensors that measure reaction forces at the drive axle and at the caster of a powered wheelchair during driving. The SMART^{HUB} and SMART^{CASTER} were developed at the Human Engineering Research Laboratories. The SMART^{HUB} measures forces and moments in six directions at the drive wheel

of a powered wheelchair. The SMART^{CASTER} measures forces in three directions and the moment in one direction (because of the bearing at the hub and the bearing at the caster spindle).

Instrumentation has been developed to examine variables associated with wheelchair use that existing devices cannot measure. Multiple avenues have been explored to examine the same problems. The evaluation of propulsion kinetics has been studied through different instruments. Van der Woude et al [34] used a force transducer located at the wheel center and attached to the pushrim to evaluate torques during wheelchair propulsion. The SMART^{wheel} is a device which uses strain gauges, which are mounted to three beams attached to the pushrim [33]. The SMART^{wheel} is capable of measuring forces and moments in three directions during wheelchair propulsion. Richter et al [35] used a wheel instrumented with a six degree of freedom load cell placed at the center of the wheel and attached to the pushrim.

VanSickle et al [36] designed a SMART^{HUB} and SMART^{CASTER} for use with a manual wheelchair. The development of these devices was guided by the need for data that would accurately reflect the forces and moments experienced by the wheelchair frame during propulsion. Dynamic forces and moments collected during wheelchair propulsion through the use of these unique devices could be used with Computer Aided Design and Finite Element Analysis to design lighter, more durable wheelchairs. Previous studies have examined stresses experienced by manual wheelchair frames by affixing strain gauges directly to the frame [37]. However these results are not generalizable between different types of wheelchairs. A system that could measure the input forces and moments through the wheels is preferred because comparisons can be made between many different wheelchairs. Another use of these devices is determining the amount of whole-body vibration transferred through the wheelchair frame or in some cases suspension elements to wheelchair users. Wolf et al [38] measured the absorbed

power transferred to wheelchair users during propulsion over an activities of daily living course. Through the use of the SMART^{HUB}, the absorbed power, a measure of harmful energy transferred to the wheelchair user through exposure to external forces, could be evaluated.

With the incredible advancements in power wheelchair technology over the past decade users are able to go further distances, for longer periods of time, and over coarser terrain. Increased use and harsher treatment of power wheelchairs causes increased loads experienced by the frame and in turn by the user. The power wheelchair SMART^{HUB} and SMART^{CASTER} can be used to evaluate the forces and moments experienced during driving, and to model the suspension elements in powered wheelchairs.

3.2 METHODS

The developments of the power wheelchair SMART^{HUB} and power wheelchair SMART^{CASTER} were based on current technology in use at the Human Engineering Research Laboratories. Before machining, Computer Aided Designs (CADs) were created using FeatureCAM (Delcam USA, Salt Lake City, UT) to ensure accurate viability, design and construction. Additional FeatureCAM drawings can be seen in Appendix A.

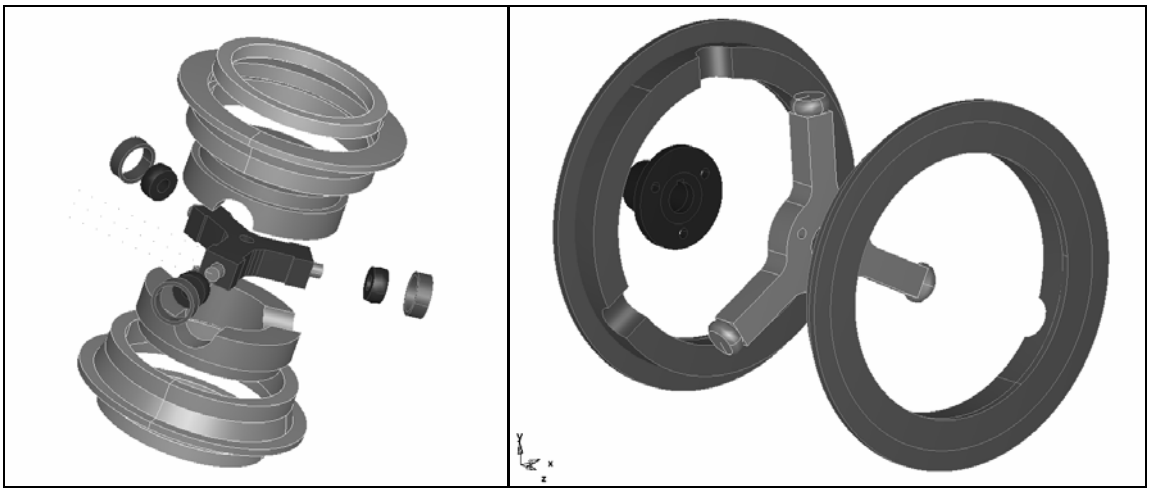

Figure 4 - FeatureCAM drawings of the SMART^{CASTER} and SMART^{HUB}

The SMART^{HUB} and SMART^{CASTER} work by attaching strain sensors to a three beam core which is attached to the power wheelchair. When the three beam core is placed under load, there is strain that is experienced by each of the three beams, which is measured by the strain sensors mounted to each beam. The signal from those sensors can then be amplified and outputted to a data collection device. Calibration coefficients can then be calculated to describe the relationship between external loads applied to the SMART^{HUB} or SMART^{CASTER} and the voltages measured by the strain sensors. Requirements for the development of these devices are that they are able to attach to a large variety of power wheelchairs and that they are capable of measuring forces equal to 2000 N per wheel, moments of 500 N-m per wheel, and linearity of greater than 90%. These values were selected based on the average weight of a power wheelchair and user and the system being exposed to 4g shock vibrations.

The core sensor of the SMART^{HUB} and SMART^{CASTER} is constructed of titanium (Grade 5 – 6AL-4V), and has three beams mounted with 350 Ohm general purpose, stress analysis strain gages (Micro Measurements, EA-06-125PC-350).

Figure 5 - Strain gage mounted on one of the three titanium beams

The mechanical properties of titanium allow for maximum strength while at the same time allowing maximum beam flexibility. Three beams were chosen as the minimal amount, to still allow for force and moment measurement in three directions. The outer hub of the device is constructed of aircraft aluminum (6061T6), for its strength and light weight. The dimensions of the core sensors were dependant on three factors: the minimum size to allow for the strain gauges, the size of the solid insert drive wheel and caster, and the strength and flexibility of the titanium.

Machining of the core sensors of the SMART^{HUB} and SMART^{CASTER} was completed using a Wire EDM machine, a CNC Mill, and a CNC Lathe. The use of these machines allows for extreme precision in the manufacturing process.

The ends of each beam in the core sensors are rounded and polished to slide within a carbide bushing at the interface with the outer hub. This ensures a very low friction environment to

reduce error and hysteresis. The SMART^{HUB} is designed to use a 14-inch solid foam insert tire and to connect to an electric power wheelchair via an axle attachment. This design allows for use on many electric powered wheelchairs, because a specific axle attachment can simply be created. The SMART^{CASTER} is constructed using an 8-inch solid foam insert tire and a standard caster fork. This allows for attachment to any power wheelchair using an 8-inch caster.

Each beam is instrumented with four strain gages, two on each opposing side. The four gages are wired into a Wheatstone bridge [39], which is modified to contain a potentiometer in one of the bridges (Figure 6). The potentiometers are used to equalize the output voltages from each of the channels to the data logger.

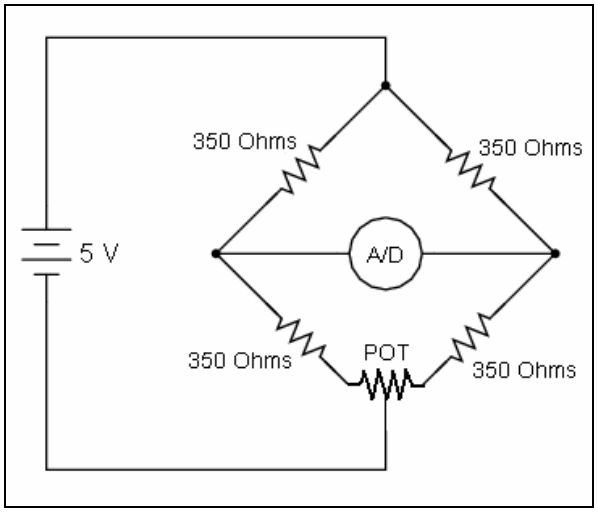

Figure 6 - Wheatstone bridge formed by four 350 Ohm strain gages

The Tattletale 8v2 data logger is used to collect the strain gage data from the SMART^{HUB} and SMART^{CASTER}. This data logger was selected because it has 1 MB of memory, and is capable of a maximum of 16 MHz processing speed. This data logger provided all of the required data and collection rate specifications as well as 8 A/D input channels. An amplifier

board was designed to preprocess the strain gage data running to the data logger. A diagram of the amplifier board can be seen in Appendix B. The board amplifies each of the six strain gage channels, and increases the resolution of the signals being collected.

The Tattletale 8v2 data logger software is based in the C programming language. A provided sample data logger program was used as a starting point to create the program for the SMART^{HUB} and SMART^{CASTER}. The software collects seven channels of data from each of the four instrumented wheels: the six strain gauge channel and a channel of encoder data to determine the orientation of the beams in the SMART^{HUB} during driving.

A tri-axial accelerometer (Crossbow, LP Series) was used to determine the level of vibrations that the wheelchair user is experiencing during the testing. These accelerometers have been used for testing in the past and have shown good reliability and high resolution [13-16, 26, 28-30]. From these collected variables we will be able to determine the functionality of the suspension elements and their abilities to absorb the vibrations from wheelchair driving.

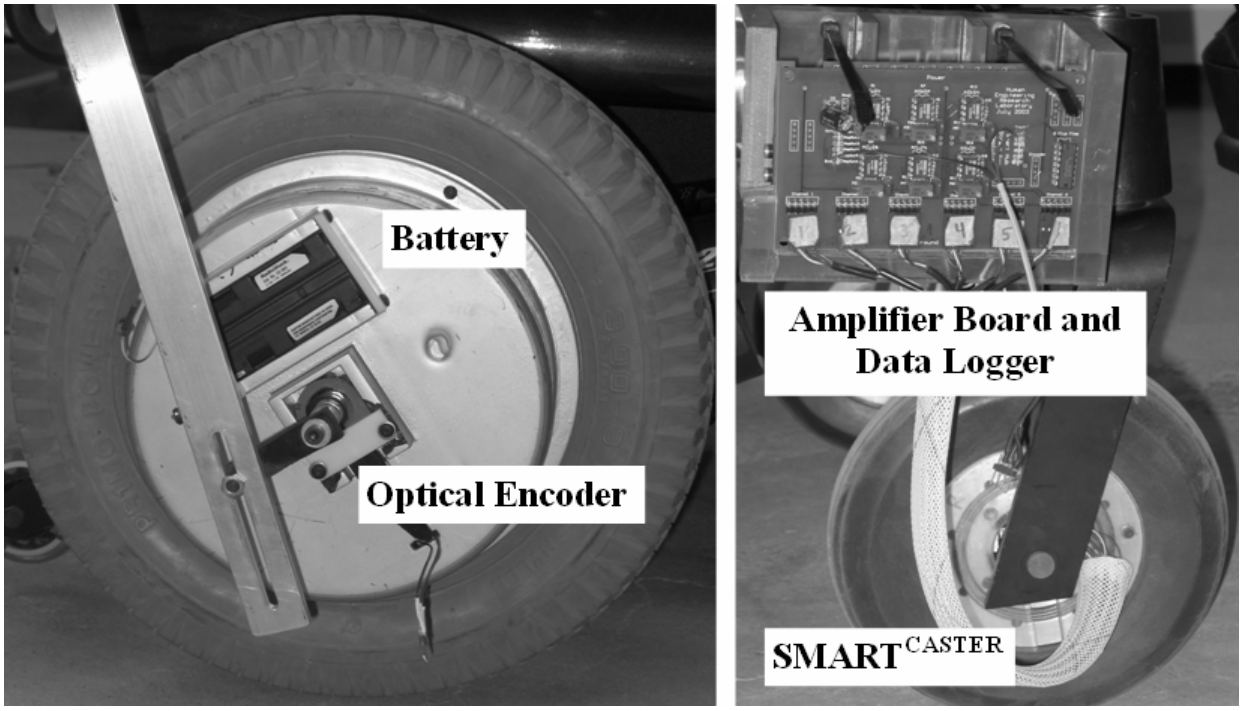

Figure 7 - Completed SMART^{HUB} and SMART^{CASTER}

3.2.1 Calibration

Calibration of the SMART^{HUBS} and SMART^{CASTERS} was completed by applying known dynamic loads from a MTS Material Testing System. Forces of varying frequency and magnitude were applied to the SMART^{HUBS} and SMART^{CASTERS}. Force data and resultant voltage data from the SMART^{HUBS} and SMART^{CASTERS} were collected during all tests. A linear regression was then completed to compute the regression coefficients (K and C), which can be seen in Figure 8.

$$\begin{bmatrix} F_{Lateral} \\ F_{Fore-Aft} \\ F_{Vertical} \\ M_{Lateral} \\ M_{Fore-Aft} \\ M_{Vertical} \end{bmatrix} = \begin{bmatrix} K_L & 0 & K_L & 0 & K_L & 0 \\ 0 & K_F \cdot \sin(\theta) & 0 & K_F \cdot \sin(\theta + \frac{2\pi}{3}) & 0 & K_F \cdot \sin(\theta + \frac{4\pi}{3}) \\ 0 & K_V \cdot \cos(\theta) & 0 & K_V \cdot \cos(\theta + \frac{2\pi}{3}) & 0 & K_V \cdot \cos(\theta + \frac{4\pi}{3}) \\ 0 & C_L \cdot L & 0 & C_L \cdot L & 0 & C_L \cdot L \\ C_F \cdot L & 0 & C_F \cdot L & 0 & C_F \cdot L & 0 \\ C_V \cdot L & 0 & C_V \cdot L & 0 & C_V \cdot L & 0 \end{bmatrix} * \begin{bmatrix} V_1 \\ V_2 \\ V_3 \\ V_4 \\ V_5 \\ V_6 \end{bmatrix}$$

Figure 8 - Relationship between the voltages and the forces and moments

Directions of testing included; Vertical direction, Fore-aft direction, and Moment about the Fore-aft direction for the SMART^{CASTERS}. Because of the design of the SMART^{CASTERS} there is no force in the lateral direction because the core sensor is pinched by a caster axle. There is no moment about the vertical direction because of the swivel from the attachment to the wheelchair, and there is no moment about the lateral direction because of ball bearings that allow the caster to spin. For the SH the directions of testing included the radial direction (which includes the vertical and fore-aft directions), the lateral direction, the moment about the lateral direction (or the torque of the drive wheels), and the moment about the radial direction.

Both SMART^{HUBS} and SMART^{CASTERS} were tested to determine the sensor noise. Data were collected from each sensor with no force application, and the resultant outputs were tested for normality.

Once calibration was completed, the SMART^{HUB} and SMART^{CASTER} were used to collect force data from two suspension power wheelchairs, the Invacare 3G Torque SP and the Quickie S-626, while driving over an activities of daily living course. Six suspension settings were tested. The Invacare 3G Torque SP was tested with its suspension setting and a solid aluminum insert to represent a rigid frame power wheelchair. The Quickie S-626 was tested with its adjustable suspension set in a least stiff, mid stiff, and most stiff setting and with a solid

aluminum insert to represent a rigid frame power wheelchair. The course was comprised of six obstacles that power wheelchairs commonly encounter; deck surface, door threshold, 50 mm curb descent, dimple strip, smooth surface, and carpet. Eight able-bodied subjects completed the testing. All subjects completed an inclusion/exclusion criteria questionnaire after signing the informed consent document but prior to participating in the study. Forces in the vertical direction were compared for all subjects, per obstacle and a mixed model ANOVA (p<0.05) was completed to evaluate if differences existed between suspension settings.

3.3 RESULTS

3.3.1 SMART^{CASTERS} – Left Caster Calibration

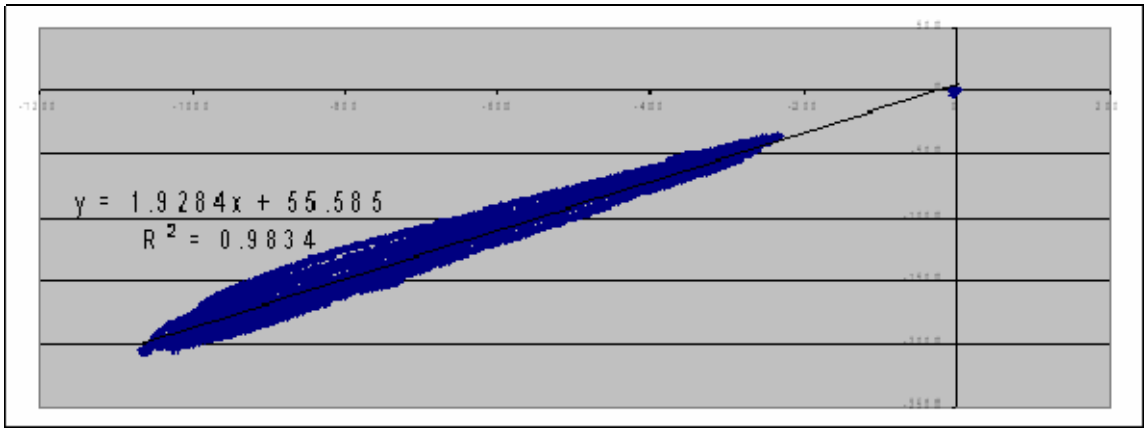

Figure 9 - Left Caster Vertical Direction (Newtons)

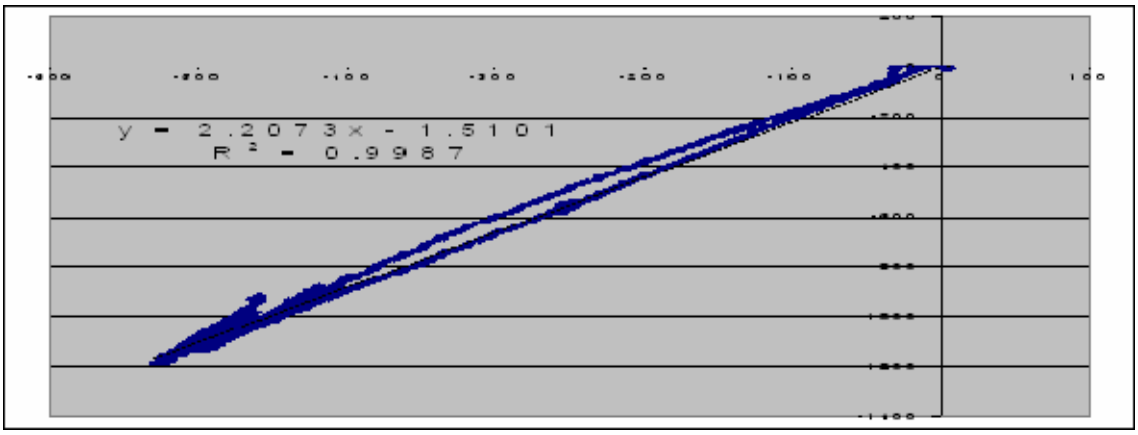

Figure 10 - Left Caster Fore-Aft Direction (Newtons)

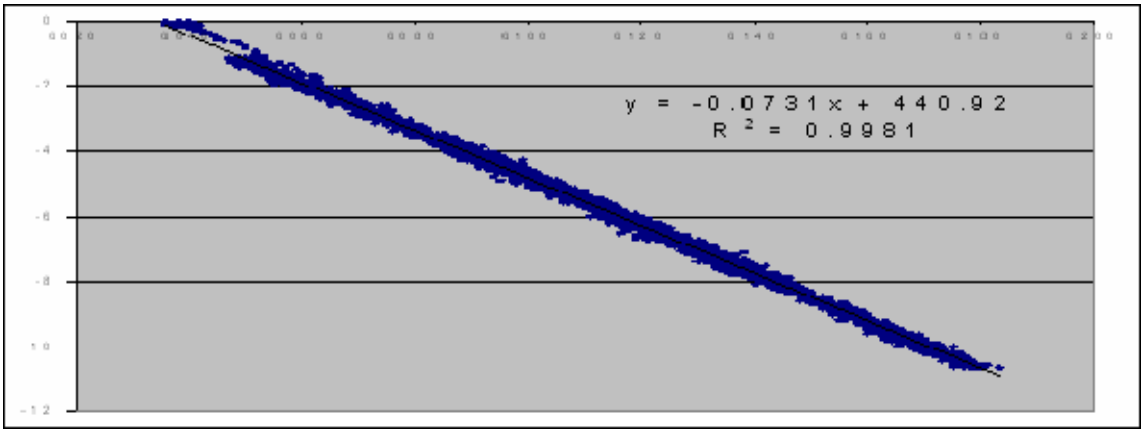

Figure 11 - Left Caster Moment about Vertical Axis (Newton-meters)

3.3.2 SMART^{CASTERS} – Right Caster Calibration

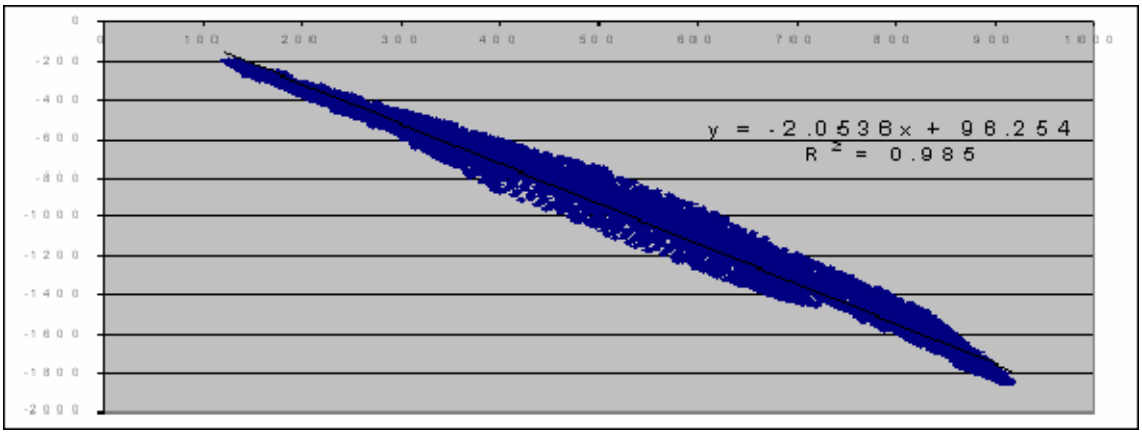

Figure 12 - Right Caster Vertical Direction (Newtons)

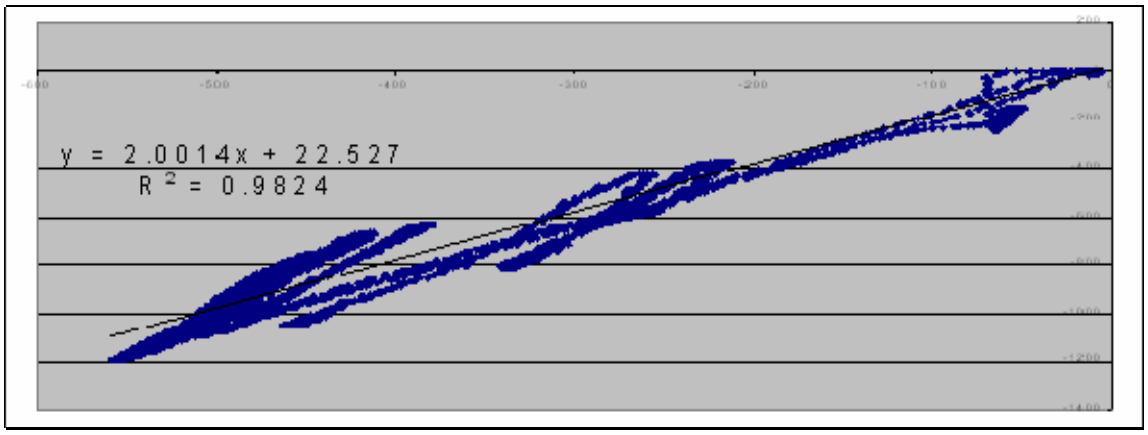

Figure 13 - Right Caster Fore-Aft Direction (Newtons)

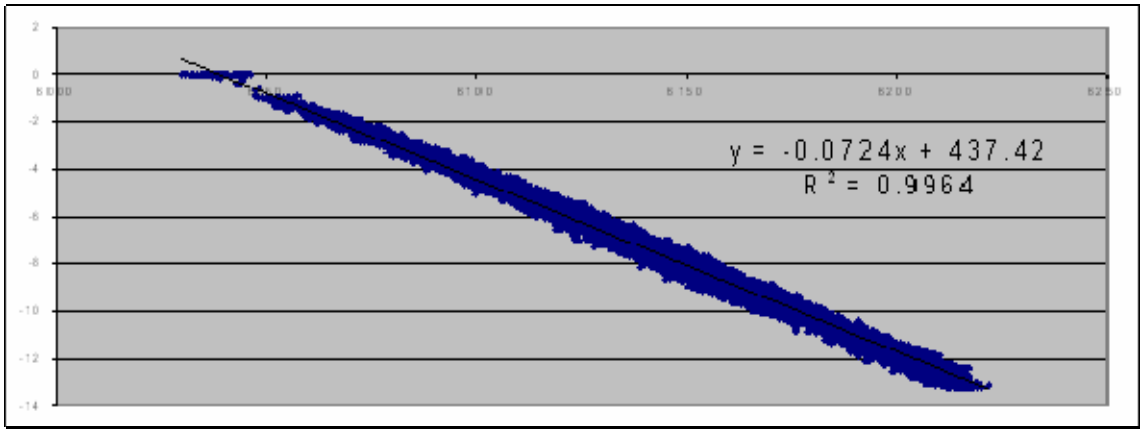

Figure 14 - Right Caster Moment about Vertical Axis (Newton-meters)

3.3.3 SMART^{HUBS} – Left Hub Calibration

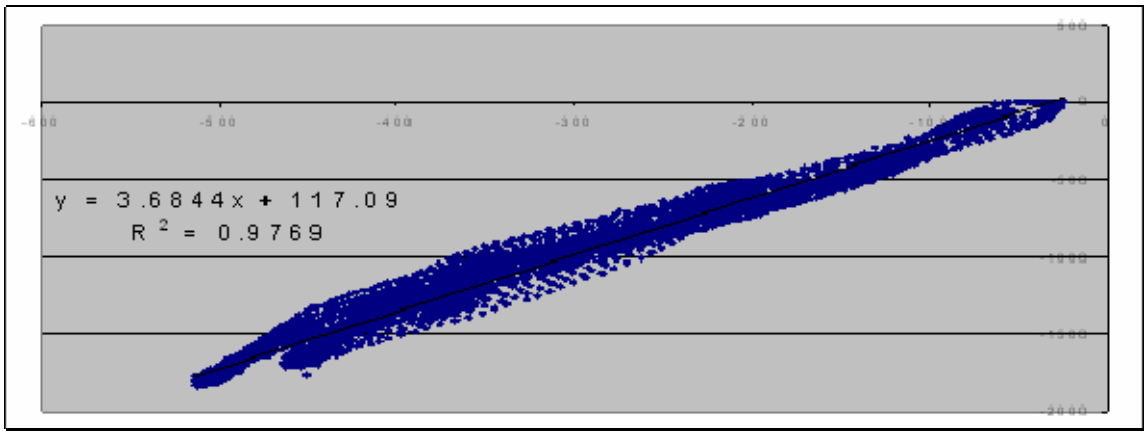

Figure 15 - Left Hub Radial Direction (Newtons)

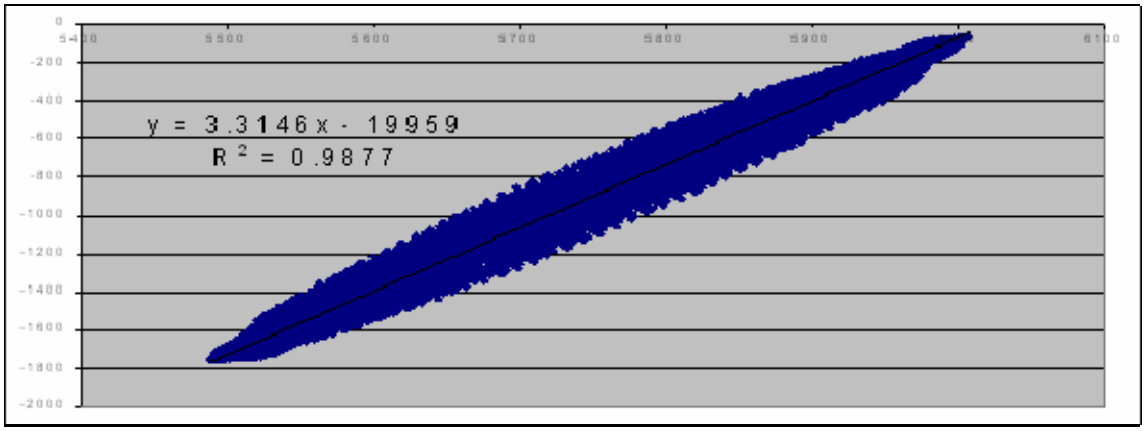

Figure 16 - Left Hub Lateral Direction (Newtons)

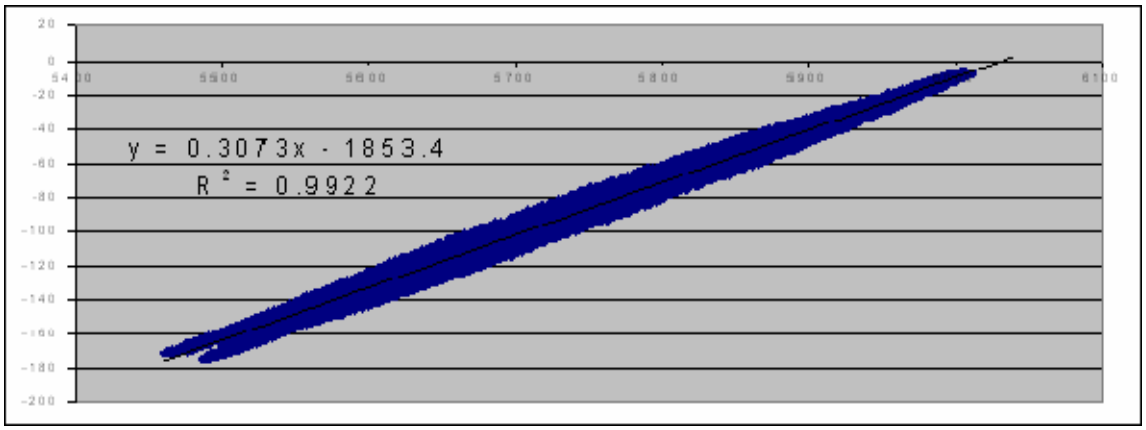

Figure 17 - Left Hub Moment about Radial Direction (N-m)

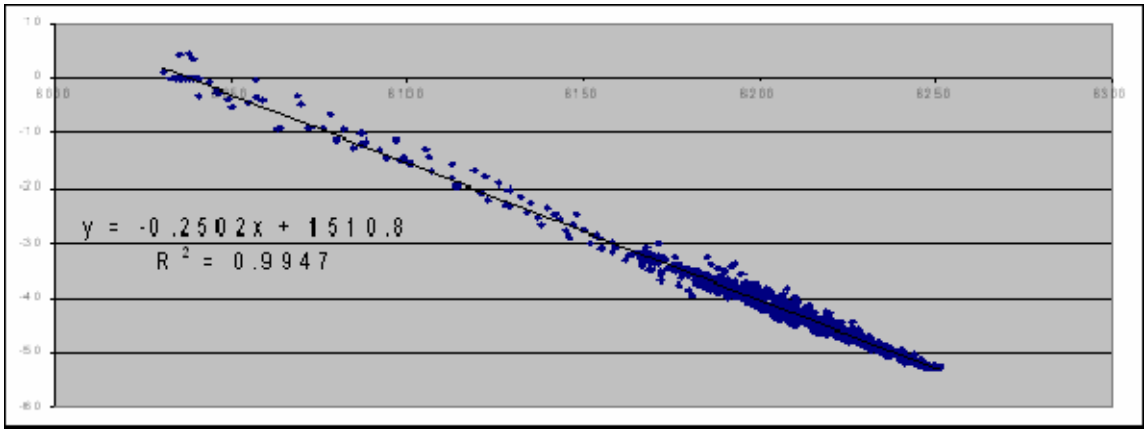

Figure 18 - Left Hub Moment about Lateral Direction (N-m)

3.3.4 SMART^{HUBS} – Right Hub Calibration

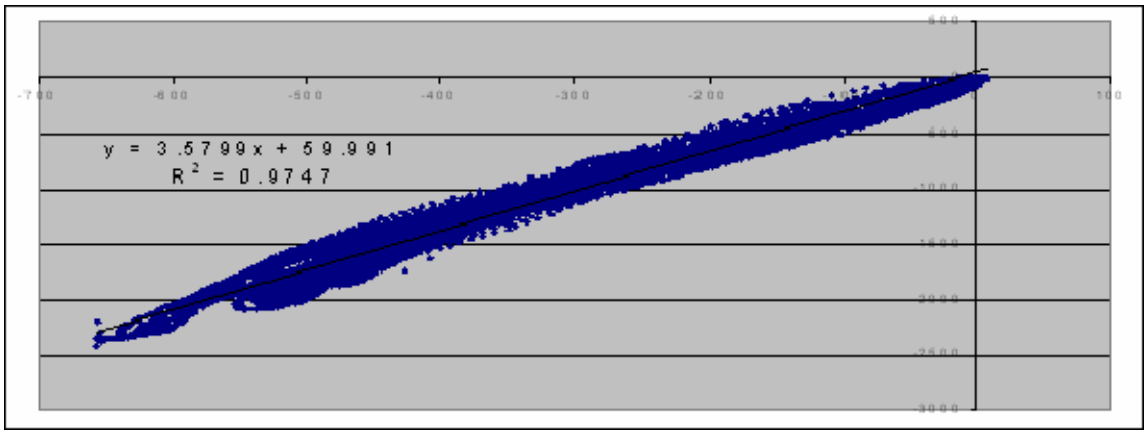

Figure 19 - Right Hub Radial Direction (Newtons)

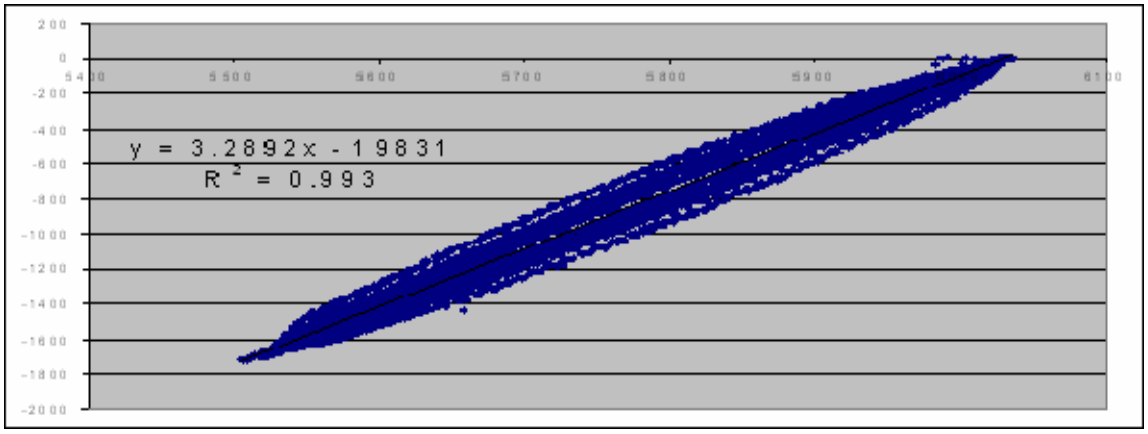

Figure 20 - Right Hub Lateral Direction (Newtons)

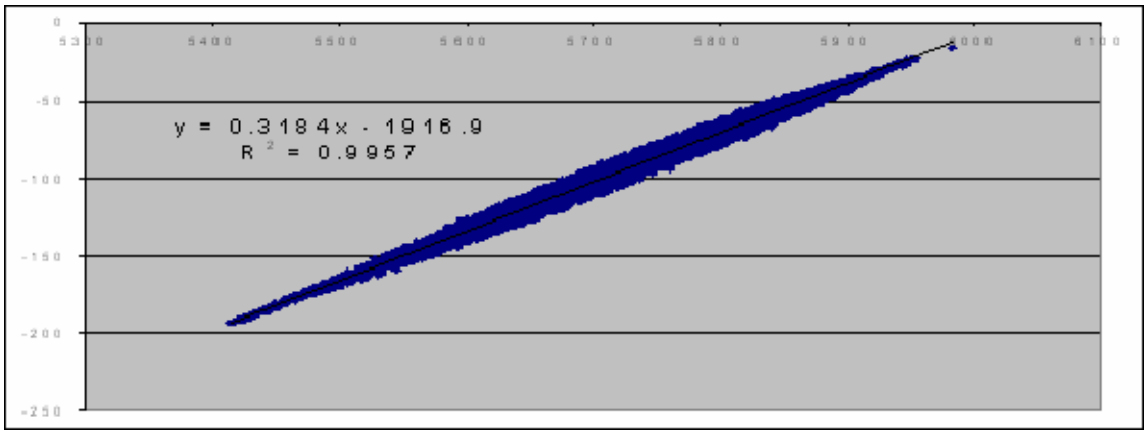

Figure 21 - Right Hub Moment about Radial Direction (N-m)

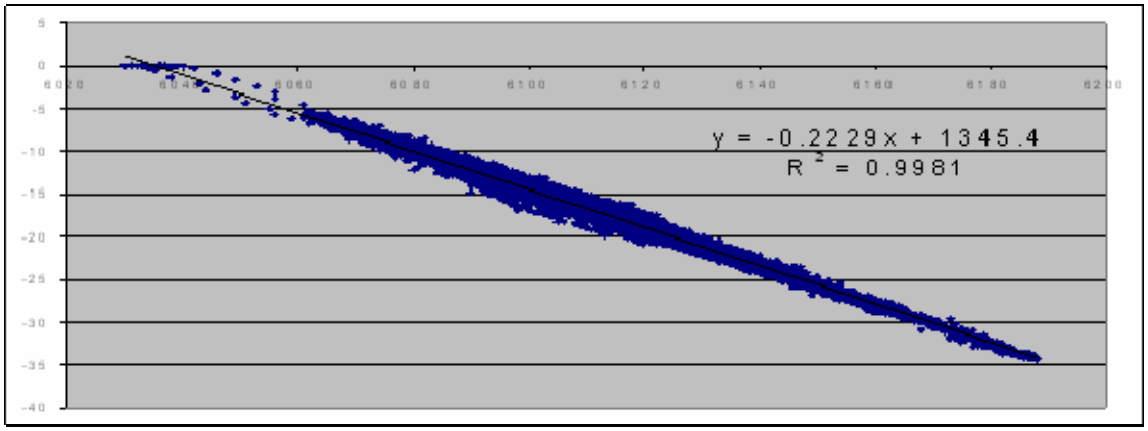

Figure 22 - Right Hub Moment about Lateral Direction (N-m)

Table 7 shows the calibration coefficients, A/D units per Newton (AU/N), calculated from the linear regression and the corresponding R^2 values. These resultant calibration constants can be used to convert the raw voltage data collected from the SMART^{HUBS} and SMART^{CASTERS} during power wheelchair driving.

Table 7 - Calibration coefficients for both SMART^{HUBS} and SMART^{CASTERS}

Left Caster

Fore-Aft Force		Vertical Force		Fore-Aft Moment	
AU/N	R^2	AU/N	R^2	AU/N	R^2
2.2073	0.9987	1.9284	0.9834	-0.0731	0.9981

Right Caster

Fore-Aft Force		Vertical Force		Fore-Aft Moment	
AU/N	R^2	AU/N	R^2	AU/N	R^2
2.0014	0.9824	-2.0536	0.985	-0.0724	0.9964

Left Hub

Radial Force		Lateral Force	
AU/N	R^2	AU/N	R^2
3.6844	0.9769	3.3146	0.9877
Radial Moment		Lateral Moment	
AU/N	R^2	AU/N	R^2
-0.3073	0.9922	-0.2502	0.9947

Right Hub

Radial Force		Lateral Force	
AU/N	R^2	AU/N	R^2
3.5799	0.9747	3.2892	0.993
Radial Moment		Lateral Moment	
AU/N	R^2	AU/N	R^2
0.3184	0.9957	-0.2229	0.9981

The cross axis sensitivities during each test were also calculated to ensure that no cross talk existed in opposing directions (i.e. that there is no force in the lateral direction during vertical testing).

3.3.5 SMART^{CASTERS} – Left Caster Cross Axis Sensitivity

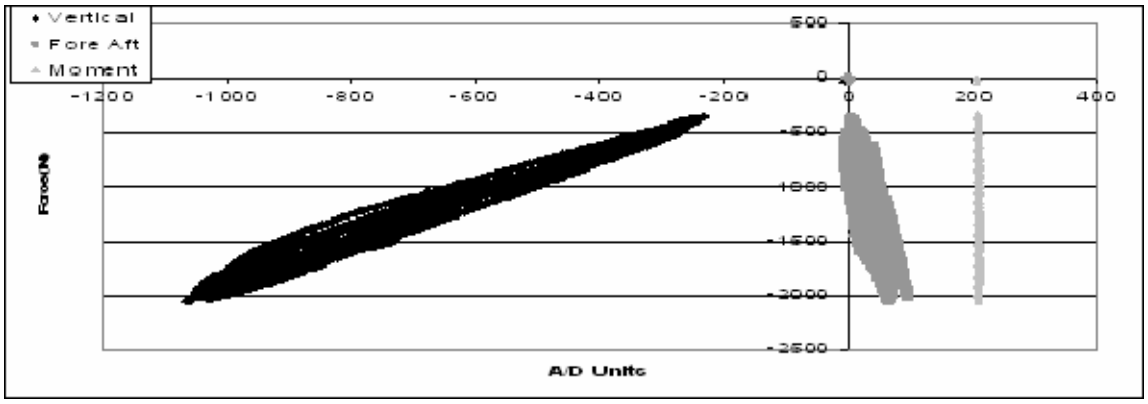

Figure 23 - Cross Axis Sensitivity During Vertical Testing

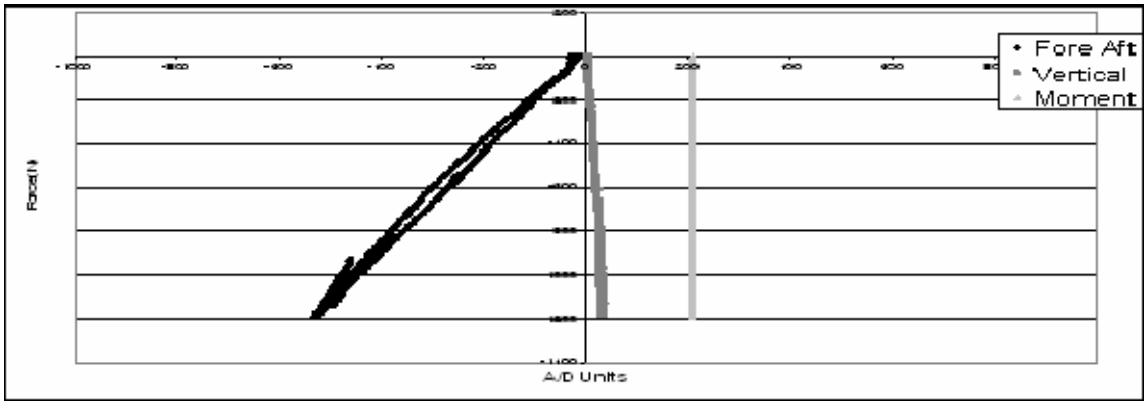

Figure 24 - Cross Axis Sensitivity During Fore Aft Testing

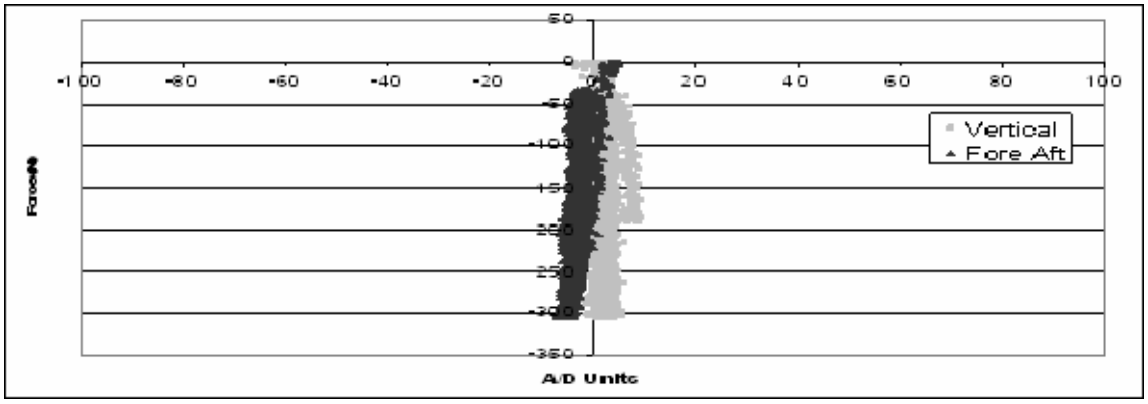

Figure 25 - Cross Axis Sensitivity During Moment Testing

3.3.6 SMART^{CASTERS} – Right Caster Cross Axis Sensitivity

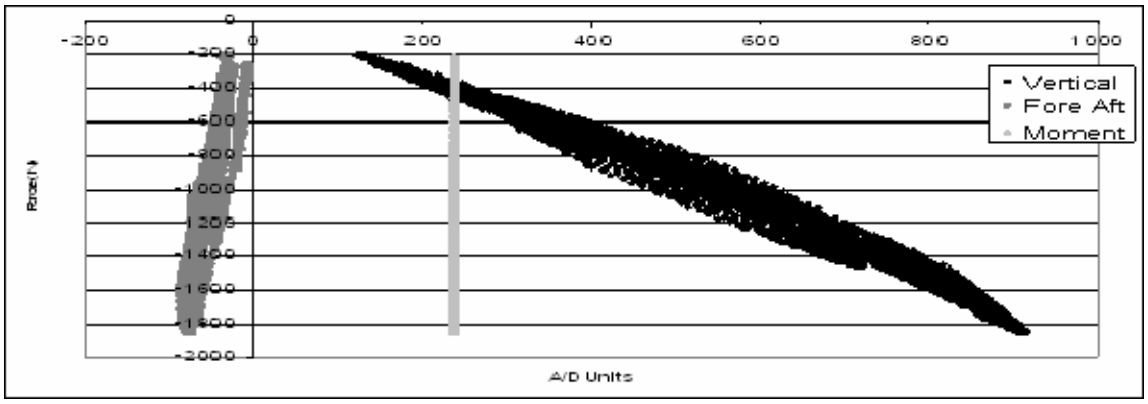

Figure 26 - Cross Axis Sensitivity During Vertical Testing

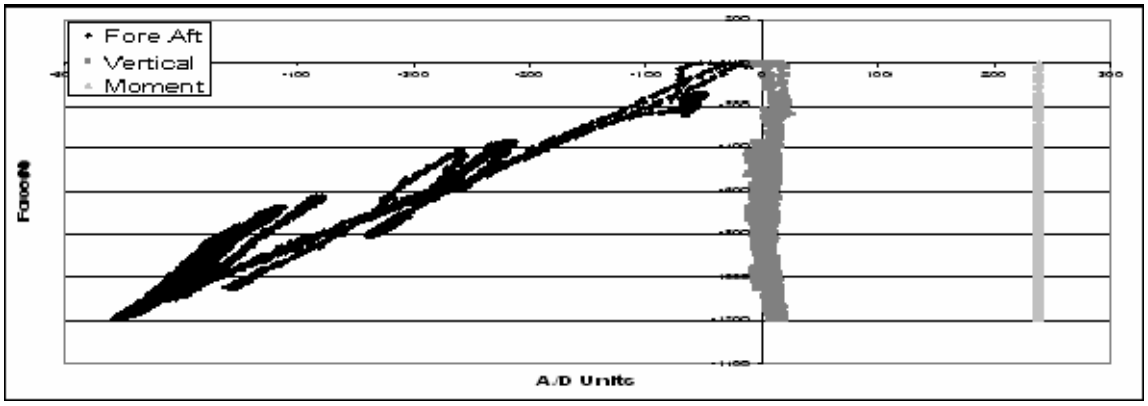

Figure 27 - Cross Axis Sensitivity During Fore Aft Testing

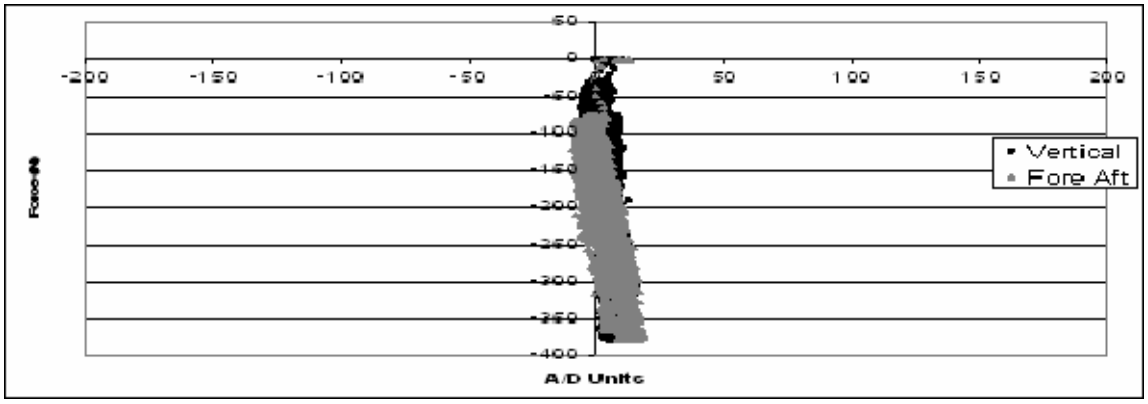

Figure 28 - Cross Axis Sensitivity During Moment Testing

3.3.7 SMART^{HUBS} – Left Hub Cross Axis Sensitivity

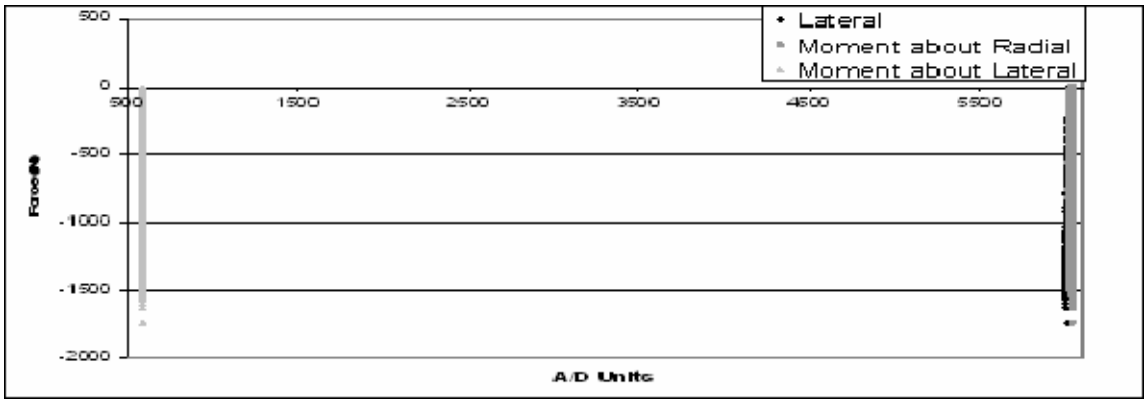

Figure 29 - Cross Axis Sensitivity During Radial Testing

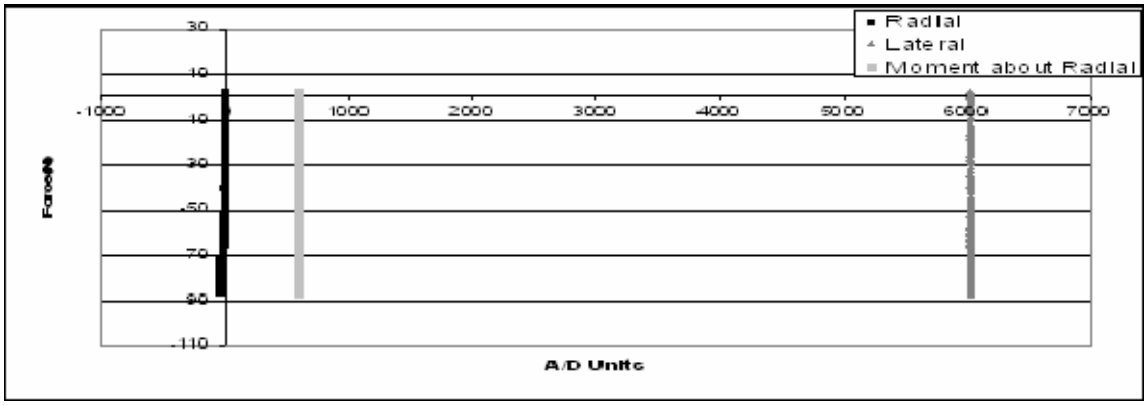

Figure 30 - Cross Axis Sensitivity During Moment about Lateral Testing

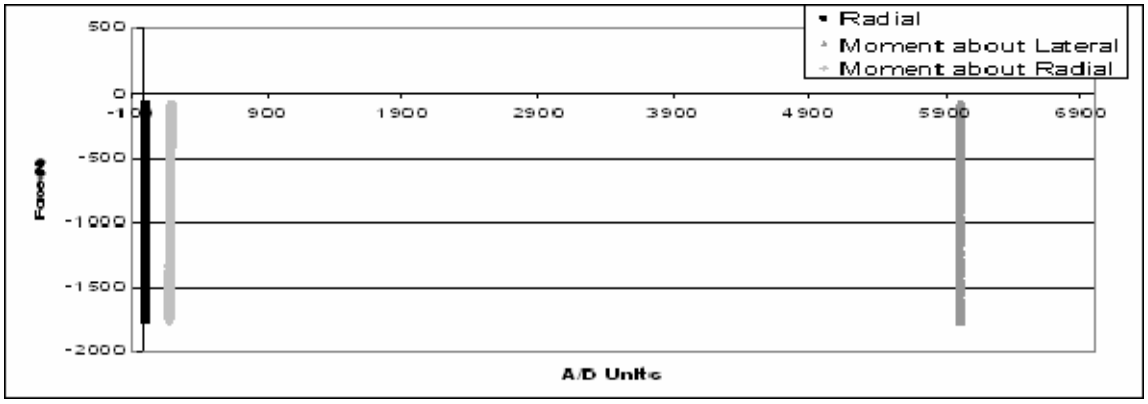

Figure 31 - Cross Axis Sensitivity During Lateral Testing

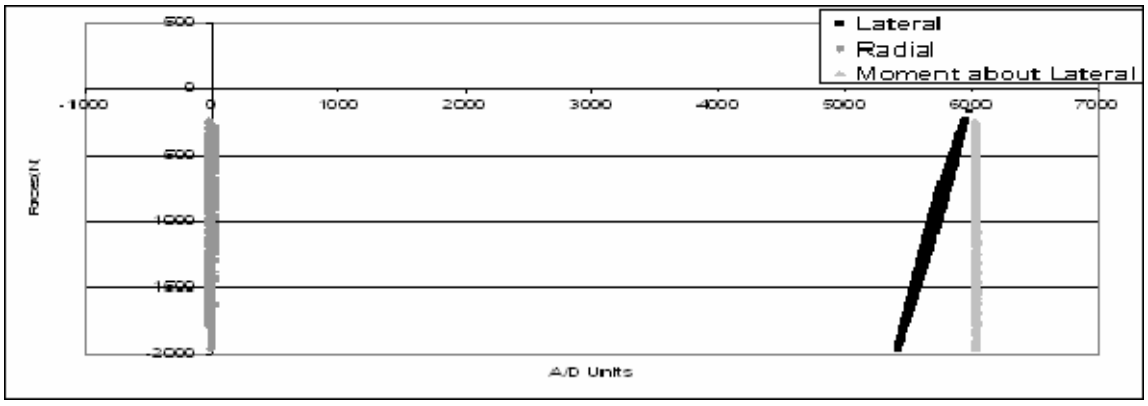

Figure 32 - Cross Axis Sensitivity During Moment about Radial Testing

3.3.8 SMART^{HUBS} – Right Hub Cross Axis Sensitivity

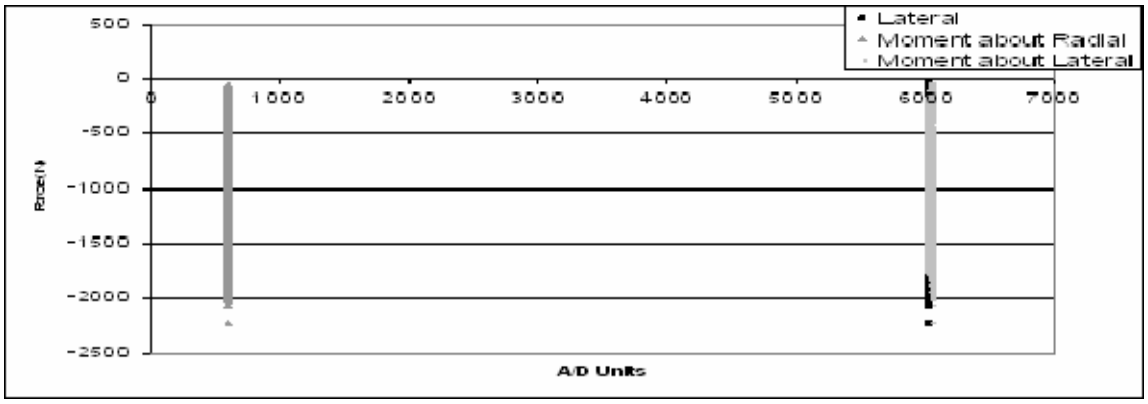

Figure 33 - Cross Axis Sensitivity During Radial Testing

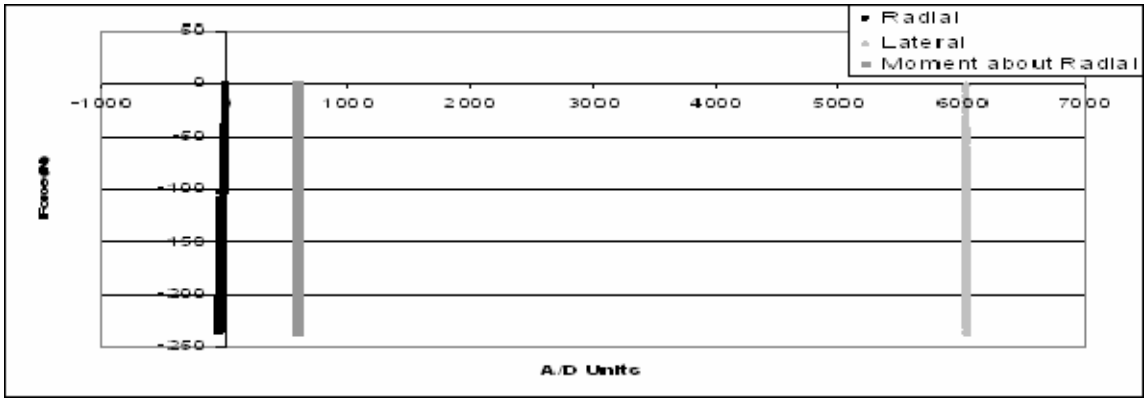

Figure 34 - Cross Axis Sensitivity During Moment about Lateral Testing

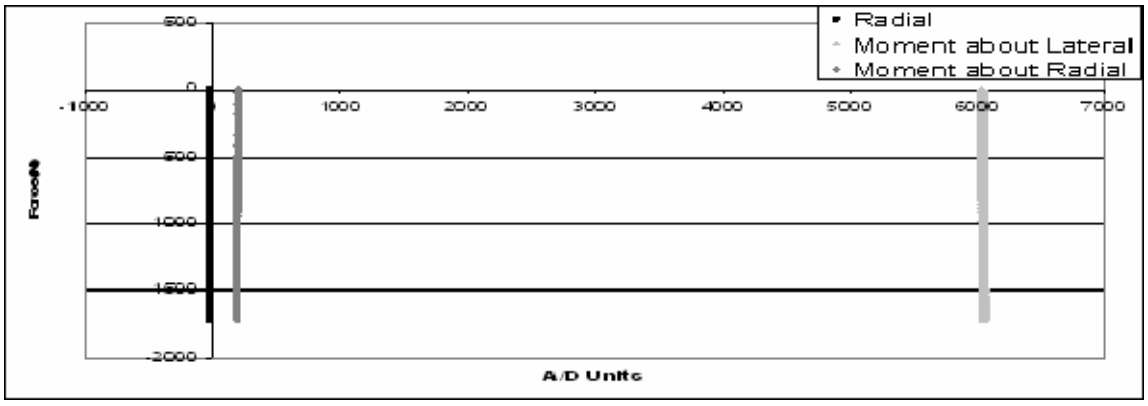

Figure 35 - Cross Axis Sensitivity During Lateral Testing

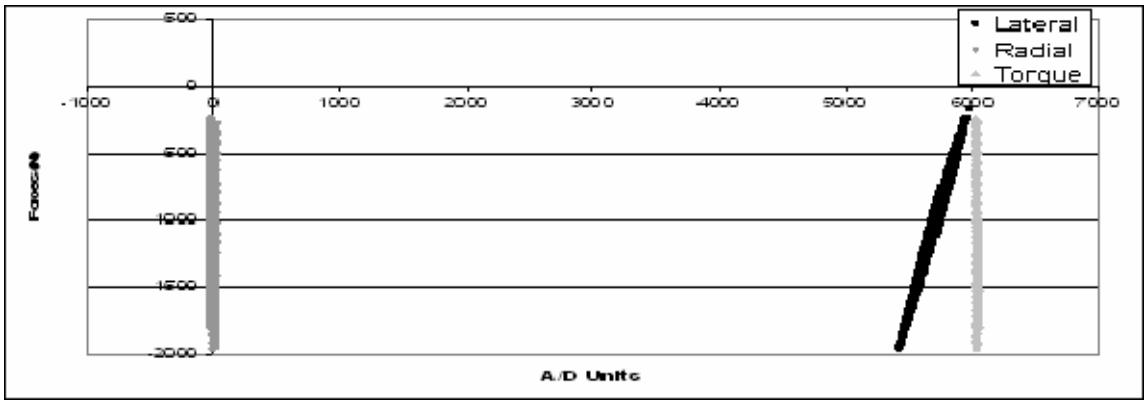

Figure 36 - Cross Axis Sensitivity During Moment about Radial Testing

Table 8 - Cross Axis Sensitivity for the SMART[CASTERS]

Left Caster		Vertical	Fore Aft	Moment
	Vertical	XXX	5.91%	0.24%
	Fore Aft	5.77%	XXX	0.11%
	Moment	0.15%	0.15%	XXX
Right Caster		Vertical	Fore Aft	Moment
	Vertical	XXX	6.53%	0.12%
	Fore Aft	3.30%	XXX	0.15%
	Moment	0.31%	0.29%	XXX

Table 9 - Cross Axis Sensitivity for the SMART^{HUBS}

Left Hub		Radial	Lateral	Moment about Radial	Moment about Lateral
	Radial	XXX	4.00%	0.82%	5.81%
	Lateral	2.67%	XXX	2.21%	1.42%
	Moment about Radial	2.10%	XXX	XXX	0.75%
	Moment about Lateral	4.79%	2.87%	0.28%	XXX
Right Hub		Radial	Lateral	Moment about Radial	Moment about Lateral
	Radial	XXX	1.69%	0.51%	6.24%
	Lateral	1.83%	XXX	2.99%	2.88%
	Moment about Radial	0.59%	XXX	XXX	0.47%
	Moment about Lateral	4.15%	0.68%	0.07%	XXX

The cross axis sensitivities for each direction of testing for both SMART^{HUBS} and SMART^{CASTERS} were calculated. The cross axis sensitivity is the response of directions not being tested during testing of the direction of interest. The range of the cross axis sensitivities was .07% - 6.53% with a mean of 2.14%.

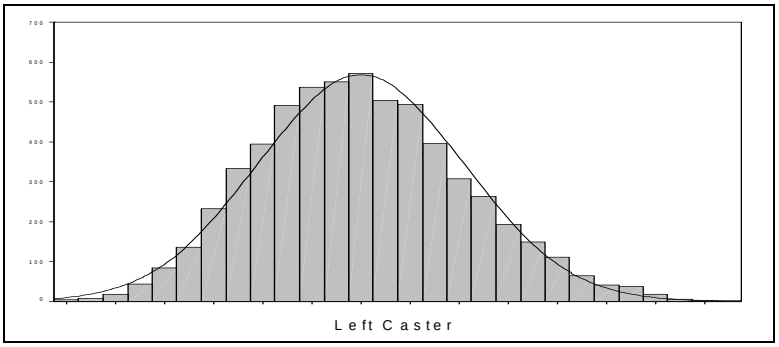

Figure 37 - Left Caster Noise Distribution

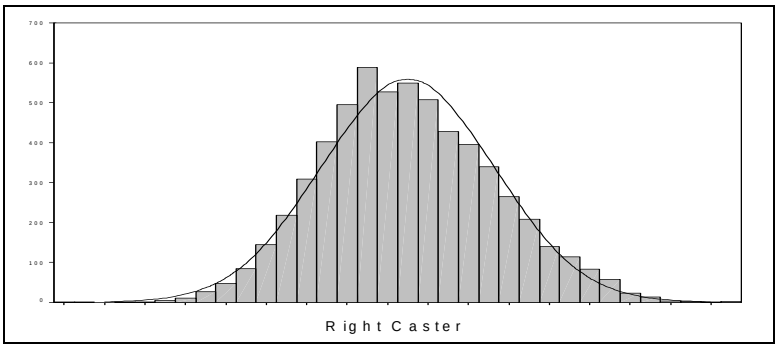

Figure 38 - Right Caster Noise Distribution

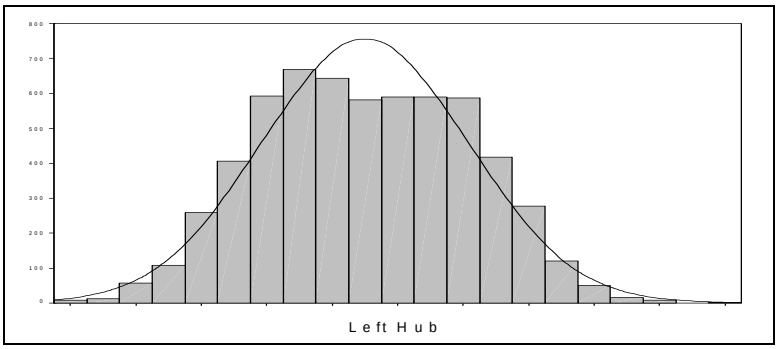

Figure 39 - Left Hub Noise Distribution

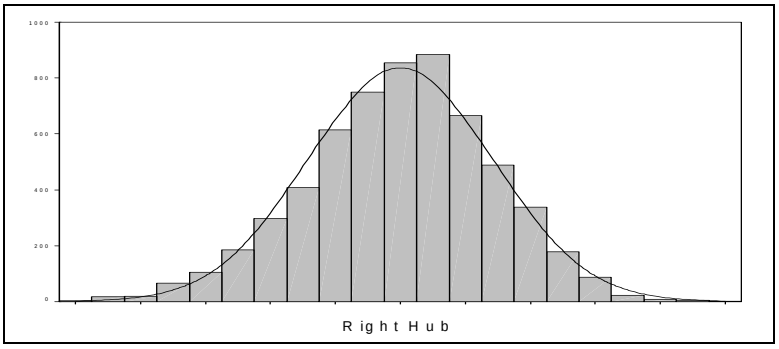

Figure 40 - Right Hub Noise Distribution

The noise of each wheel was tested for normality using a Chi-Square Goodness of Fit test. This statistical test shows how well the normal curve fits the noise distribution. Figures 37-40 show the distribution of both SMART^{HUBS} and SMART^{CASTERS} and Table 10 shows the mean, standard deviation, variance and significance for each wheel.

Table 10 - Results of the noise test for each SMART^{HUBS} and SMART^{CASTERS}

	Mean (N)	Variance	Standard Deviation	P-value for Normality
Left Caster	0.0004	4.428	2.104	**.9880**
Right Caster	-0.0069	18.274	4.274	**.9002**
Left Hub	-0.0005	9.978	3.159	**.9883**
Right Hub	-0.0018	8.155	2.856	**.9598**

3.3.9 Activities of Daily Living Course Force Data

Force data in the vertical direction were collected from the SMART^{HUB} and SMART^{CASTER} for 8 subjects traveling over an activities of daily living course. Force in the vertical direction was calculated for use with future research to examine the relationship between the vertical forces at the SMART^{HUB} and SMART^{CASTER}, and the vertical vibrations transmitted to the seat.

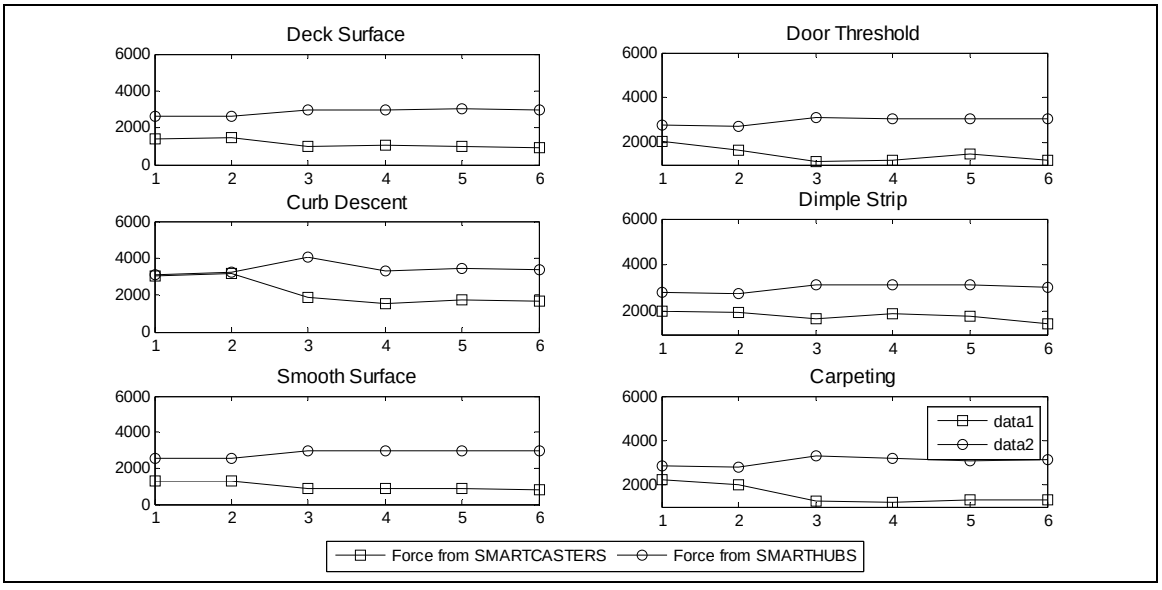

Figure 41 - Average maximum forces for all subjects over each obstacle (1= Invacare Insert, 2= Invacare Suspension, 3=Quickie Insert, 4=Quickie Low, 5=Quickie Middle, 6=Quickie Most)

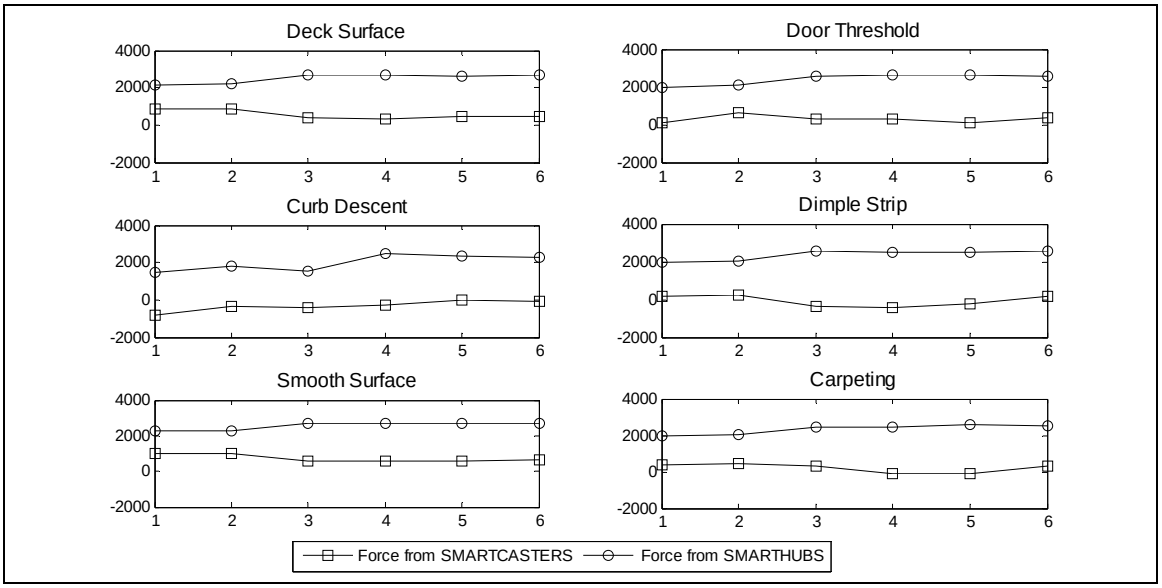

Figure 42 - Average minimum forces for all subjects over each obstacle (1= Invacare Insert, 2= Invacare Suspension, 3=Quickie Insert, 4=Quickie Low, 5=Quickie Middle, 6=Quickie Most)

Force data were compared statistically by converting the total measured force over each obstacle to the frequency spectrum and then evaluating the total spectral power from 1-25 Hz. This frequency range was chosen because the predominant amount of force occurs in this range. Figure 43 shows the force data collected over each obstacle for one trial. The data is normalized to exclude the weight of the wheelchair and the user and show the pure reaction forces. Figure 44 shows the frequency spectrum over each obstacle.

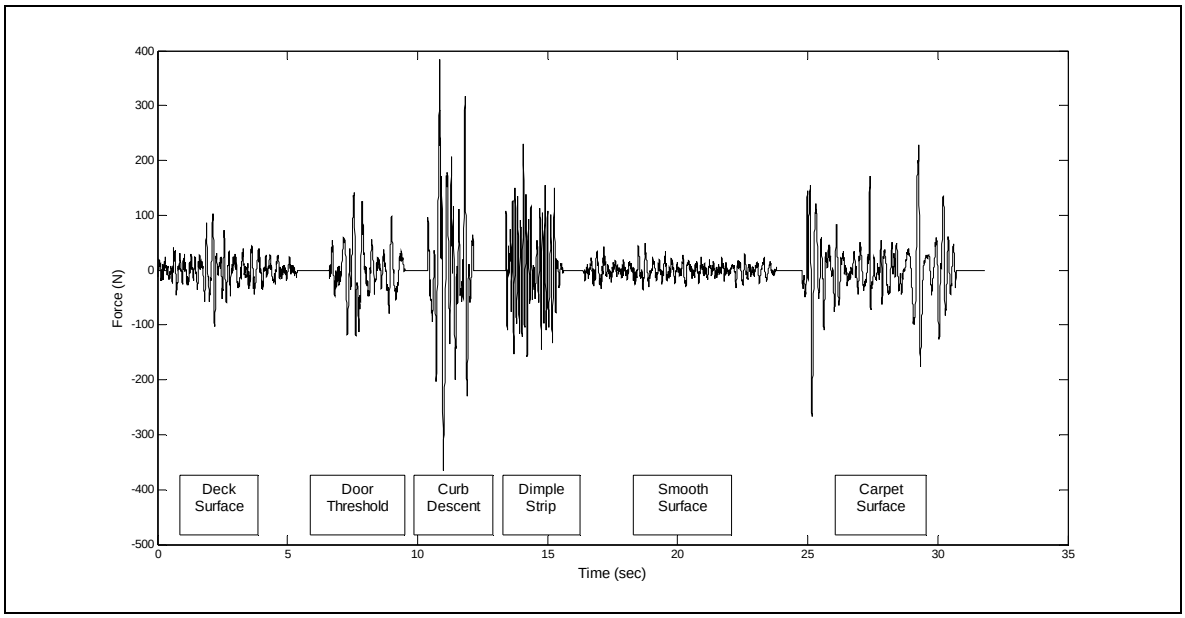

Figure 43 - Example of total Force data during driving over the obstacle course

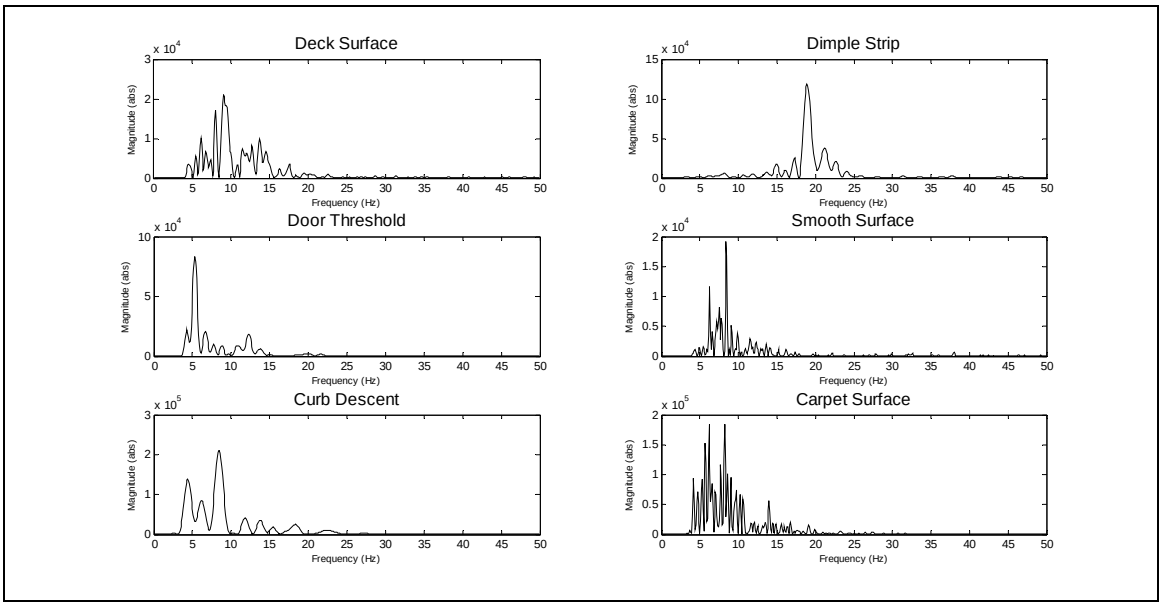

Figure 44 Total Force Frequency Spectra for each obstacle

Mixed model ANOVA of the total force in the vertical direction showed significance differences at three surfaces, the door threshold (p=.0297), the curb descent (p=.0001), and the carpet surface (p=.0001). There were no significant differences among the deck surface (p=.6302), the dimple strip (p=.1389), and the smooth surface (p=.0608). Figure 45 shows the average total force power over 25 Hz for each obstacle.

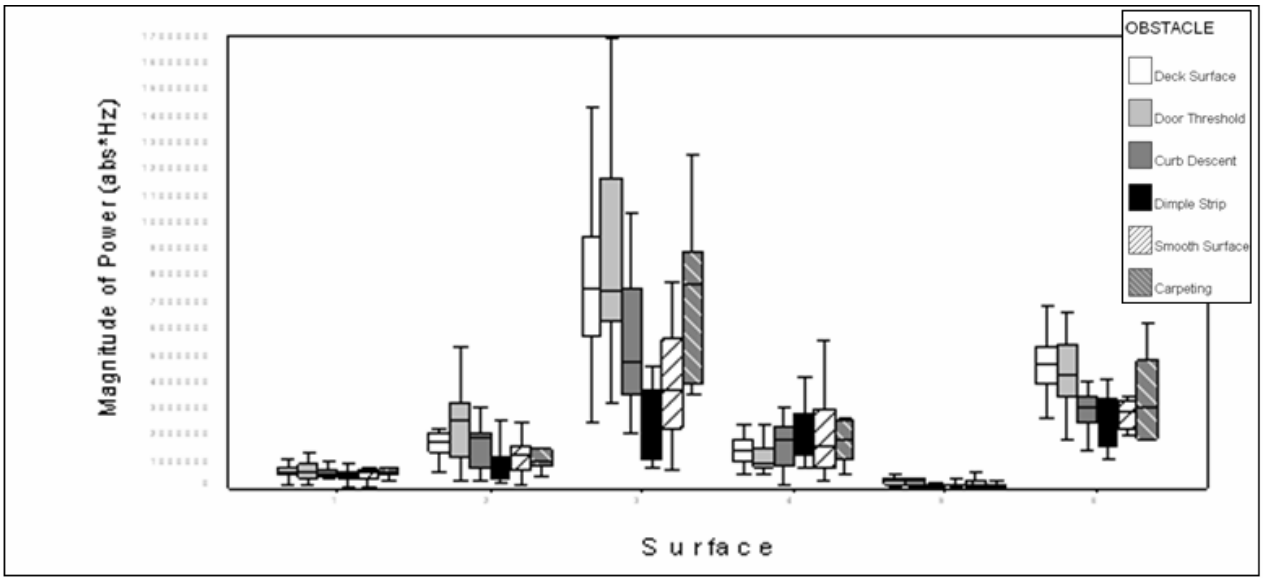

Figure 45 - Average Force for each Suspension Type Over each Surface (1=deck surface, 2=door threshold, 3=curb descent, 4=dimple strip, 5=smooth surface, 6=carpeting)

3.4 DISCUSSION

There are multiple benefits that arise from ground reaction force and moment data collected from the power wheelchair SMART^{HUB} and SMART^{CASTER} during driving. Data collected during real world power wheelchair use can be used to produce more durable and cost effective wheelchairs through finite element analysis. By developing finite element models of power wheelchair frames and using accurate force input collected from the SMART^{HUBS} and SMART^{CASTERS},

power wheelchairs can be made more robust and have a longer lifetime. Additionally, alternate designs and materials can be computer modeled more accurately, and lead to more efficient research and development, better power wheelchairs, and eventually a more cost effective product. Force data can also be used to develop better suspension systems for power wheelchair users, which will make power wheelchairs perform better as well as reduce the amounts of whole-body vibrations that are transmitted to their users.

Linearity of the calibration for each tested direction was greater than 97.5% indicating an excellent relationship between the input forces and the resultant measured voltages. The cross axis sensitivities were also good with the highest value being 6.53% of the direction of interest. The cross axis sensitivities ranged from .07% - 6.53% with an average of 2.14%.

Analysis of the force data revealed significant differences between the six suspension settings at three obstacles; the door threshold, the curb descent, and the carpeting. Each of these three obstacles produces more transient peak forces, rather than oscillatory forces. Obstacles that produce oscillatory forces; the deck surface, the dimple strip and the smooth tile surface did not show any significant differences between suspension settings. This result most likely occurs because the suspensions, specifically the spring elements, have the greatest effect on reducing and absorbing shock forces as opposed to the solid aluminum insert settings which do not absorb any of the force energy.

Limitations of this study include the use of only two wheelchairs. Although when this study began the two wheelchairs tested were two of the most popular, there has been a dramatic increase in the development of suspension power wheelchairs as well as different designs of suspension wheelchairs. Another limitation was the inclusion of only six obstacles. Wheelchair users encounter many different environments over the course of the day, especially with power

wheelchair users traveling longer and further distances. The obstacles tested were chosen based on previous studies and because they are commonly encountered during everyday propulsion [15, 30, 36].

SMART^{HUBS} and SMART^{CASTERS} capable of measuring ground reaction forces and moments were successfully developed, calibrated, and tested. Data collected from these instruments will be used in subsequent sections to evaluate if a mathematical model of the tested suspension power wheelchairs can be developed.

4.0 EVALUATION OF ELECTRIC POWERED WHEELCHAIRS WITH SUSPENSION AND EXPOSURE TO WHOLE-BODY VIBRATION

4.1 INTRODUCTION

Although all major wheelchair companies have in the recent years produced suspension electric powered wheelchairs [Invacare-3G Storm Series Torque SP; Sunrise Medical-Quickie S626; Pride Mobility-Quantum Vibe; Permobil-Chairman2K] minimal research has been conducted to determine if these suspension systems are effective.

Electric powered wheelchair users are at high risk for injury related to whole-body vibration because of the long durations they spend in their wheelchairs on any given day. Cooper et al [17] performed a study characterizing the driving characteristics of PWC users. Results of this study showed that powered wheelchair users travel, on average, 2.55 kilometers per day, and actively use their wheelchairs for 20+ hours per day. Over the course of an eight-hour period, the minimum average vertical vibration that is deemed of potential harm to seated humans by the ISO 2631-1 standard is .5 m/s^2 [31]. This value is almost certainly reached by a power wheelchair user during normal daily activities. Research is necessary to determine the efficacy of suspension systems and determine if they meet requirements for reducing the possibility of secondary injuries to power wheelchair users.

4.1.1 Powered Wheelchair Users

By recent counts (the 2000 United States Census), there are 2.3 million wheelchair users in the United States. This number is expected to grow to 4.3 million by the year 2010 due to the increased life span and advanced surgical and trauma techniques. Of this 2.3 million, about 210,000 use electric powered wheelchairs [40]. As with the total number of wheelchair users in the United States this number is expected to grow dramatically in the coming years.

Minimal research has been conducted evaluating the relationship between electric powered wheelchairs and vibrations that may be experienced during driving. Cooper et al [41] examined the effects of different sidewalk surfaces. Results showed that even during five seconds of riding, electric powered wheelchairs traveling across all surfaces at 1m/s experienced average peak forces exceeding the reduced comfort boundary and at 2 m/s exceeded the fatigue-decreased proficiency boundary. Peak vibrations for some surfaces were approaching the exposure limit boundary. Research is necessary to evaluate electric powered wheelchair propulsion over obstacles that users commonly encounter over a normal day, and assess the effects of whole-body vibrations transmitted to the users.

The Human Engineering Research Labs have been conducting research on the effects of whole-body vibrations acting on wheelchair users for the past ten years. The interest in this research stems from the correlations found between vibrations experienced by humans in the seated position, who, based on the published research, are exposed for less amounts of time than wheelchair users who are often seated for the majority of every day. Other elements may contribute to pain in power wheelchair users. Power wheelchair users who have limited ability to shift their weight over the course of the day and that do not have power seat functions to

facilitate weight shifts may experience similar symptoms (i.e. low back pain, and muscle fatigue) to those caused by exposure to whole-body vibration.

The ISO 2631-1 Standard of Effects of Exposure to Vibrations on Humans began development in 1966 and was published in 1974 [31]. Research on the effect of vibrations on humans dates back before this and has shown a correlation between vibrations and long and short term ailments experienced, such as low-back pain, musculoskeletal disorders, peripheral nervous system disorders, and motion sickness.

The most recent version of the ISO 2631-1 standard defines the acceptable levels of vibrations that can be experienced based on the Health Guidance Caution Zone. It is based in the time domain and defined the average level of vibration based on the exposure time of the subject. For up to 10 minutes of exposure the maximum allowable vibration level is 6.0 m/s^2. At 8 hour of exposure the maximum allowable level is around 0.8m/s^2.

4.1.2 Whole-Body Vibrations on Wheelchair Users

Most of the wheelchair and whole-body vibration research done to this point has been conducted on manual wheelchairs. Van Sickle et al showed that manual wheelchair propulsion over a simulated road course produces vibration loads that exceed the ISO 2631-1 standards for the fatigue-decreased proficiency boundary at the seat of the wheelchair as well as the head of the user [13]. These results may indicate that exposure to whole-body vibration may contribute to fatigue and lead to injury in manual wheelchair users.

In a study by Boninger et al [42], 66% of wheelchair users reported neck pain since acquiring their wheelchair. One of the key reasons believed to be the cause of pain, was the exposure to whole-body vibration. The investigators stated that it is necessary to conduct future

research to investigate the cause of pain in wheelchair users to determine if whole-body vibration is a contributing factor. Tai et al [16] conducted research on ten subjects to quantitatively evaluate the vibration exposure on manual wheelchair users over the course of the day. Results showed that the root mean square of the vibrations collected from the seat of the wheelchair exceeded the ISO 2631-1 fatigue-decreased proficiency boundary standard for all vibration axes after at most 25 minutes. In the vertical and fore-aft axes the vibrations, at some frequencies, exceed the boundary for less than one minute. These results show that for manual wheelchair users traveling over a simulated road course harmful whole-body vibration can be experienced prior to one minute of propulsion.

Cooper et al [28] evaluated vibrations at the seat and the footrest of six manual wheelchairs, specifically three suspension wheelchairs and three non-suspension wheelchairs. Results of this study reported that suspension caster forks significantly reduce the amount of shock and vibration exposure to the user. It was also stated that the systems of the three suspension wheelchairs did not outperform the non-suspension manual wheelchairs and that the systems must be improved in order to perform to their capacity. DiGiovine et al [15, 43] evaluated the differences in seating systems, namely cushions and back supports, at reducing the whole-body vibrations transmitted to manual wheelchair users. They determined that wheelchair users may not be using the most appropriate cushions and back supports to reduce their exposure to whole-body vibration.

Kwarciak et al [29] and Wolf et al [30] performed similar studies using two methods of analysis to evaluate vibrations on suspension and non-suspension wheelchairs while descending curbs of varying heights. Both studies revealed no significant difference in the abilities of the wheelchairs to reduce the amounts of vibrations transferred to the wheelchair user. Kwarciak et

al go on to state that the cause may be in the orientation of the suspension elements and that they might not be oriented properly for maximum dampening of vibration.

The purpose of this study was to evaluate differences in two suspension power wheelchairs to determine if suspension systems in power wheelchairs are capable of reducing the amounts of whole-body vibration transmitted to power wheelchair drivers, and if the levels of WBV that users are exposed to while driving over an obstacle course are at potentially harmful levels according to the ISO 2631-1 standard.

4.2 METHODS

This study includes the use of two suspension electric powered wheelchairs: The Quickie S-626 and the Invacare 3G Torque SP Storm Series. The Quickie S-626 uses an adjustable spring-dampening shock absorption system. The shock absorber can be adjusted to accommodate the mass of the user. The Invacare Storm uses a non-adjustable spring-dampening shock absorber. The wheelchairs were ordered with important matching dimensions, including but not limited to seat width and height, backrest width and height, and drive and caster wheel sizes.

Figure 46 - Invacare and Quickie suspension wheelchairs used for testing

Each subject tested all of the configurations of each suspension wheelchair. These included the Invacare with suspension, the Quickie with suspension set to three settings (most stiff, least stiff, and 50% stiffness), and both wheelchairs with solid inserts to act as non-suspension wheelchairs. Solid inserts were constructed out of 6061T6 aluminum and were used to replace the suspension elements within the frame of the powered wheelchair. Through this research design it can be concluded whether the suspension alone, or if tuning the suspension makes a difference in reducing whole-body vibration.

Twenty able bodied subjects and two wheelchair users were recruited for this study. All subjects completed an inclusion/exclusion criteria questionnaire after signing the informed consent document but prior to participating in the study. All subjects weighed no more than 250 lbs, which is the maximum weight prescribed by the wheelchair manufacturer. Able-bodied subjects weighed on average 74.0 ± 14.2 kg. Body Mass Index (BMI) was also calculated. Average BMI of the able-bodied subjects was 25 ± 3.2.

Eleven males and nine females who were able-bodied were recruited for testing. All subjects were between the ages of 18 and 65 years. All able-bodied subjects used the same standard foam cushion. Two wheelchair users, one male with tetralpalegia (61 kg) and one female with tetralpalegia (69 kg) completed testing to evaluate if differences existed between the able-bodied subjects and users representative of power wheelchair users.

In each of the configurations of the wheelchairs, the subjects traversed an Activities of Daily Living (ADL) course. This course was created with the intention of replicating obstacles that wheelchair users encounter in everyday driving conditions. The course has been used in previous studies for testing wheelchair users in an environment similar to one they might encounter in their daily lives [44]. Obstacles that were included in this study were carpet, smooth tile floor, a truncated dome bump (dimple strip) mat, a simulated door threshold, a two-inch curb descent, and deck surface. Vibrations were collected from a tri-axial accelerometer mounted to a ¼ inch aluminum seat plate during driving over the activities course. Speed of both wheelchairs was set to be 1.4 m/s at the maximum speed, a common speed for wheelchair use. Subjects were asked to drive the wheelchair over the activities of daily living course, and were instructed to drive straight over each obstacle, and to drive at the wheelchair's maximum speed (set to 1.4 m/s). A PC compatible program written in the C programming language was used to collect acceleration data. This program and the instrumentation have been used in previous studies [13, 15, 26]. During the trial the investigator tapped the space bar just before the driver came in contact with an obstacle and just after the driver cleared the obstacle so that respective obstacles could be easily identified for data analysis.

For six of the unimpaired subjects (each tested one suspension setting), a device called a SITBAR (Seat Interface for Transducers indicating Body Acceleration Received) was used to collect accelerations above the cushion (Figure 47). The six subjects were randomly chosen and only one suspension setting was tested for each subject so that subjects would experience as little discomfort as possible.

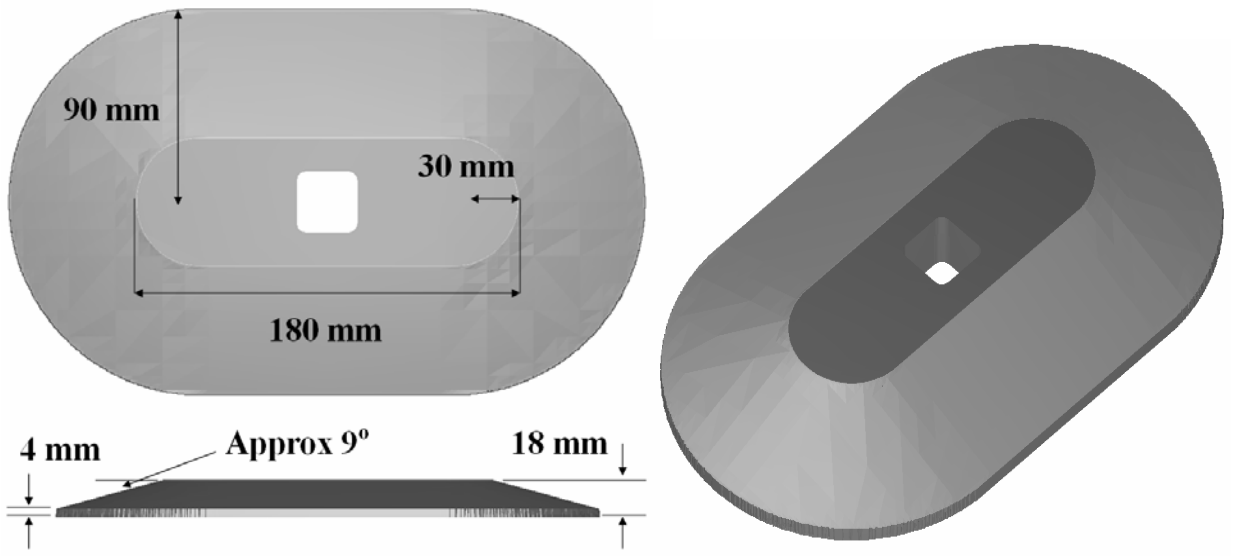

Figure 47 - Top and Isometric View of a CAD drawing of the SITBAR

Each suspension configuration was tested once with the SITBAR. The SITBAR was developed by Whitham and Griffin [10]. It is designed to compress a non-rigid seat (i.e. seat cushions) in a similar way as do human buttocks. The SITBAR was used to determine if the vibrations experience directly above the cushion, i.e. the vibrations that were being directly transmitted to the user were attenuated or intensified.

Figure 48 - Obstacles included in the activities of daily living course

Once accelerations were collected, ISO 2631-1 frequency weightings [31] were applied (Figure 49). The frequency weightings were developed because humans have different responses to vibrations at certain frequencies, specifically in the range of 4-12 Hz. For humans in a seated position there are two specified frequency weightings, one for the vertical direction and one for the fore-aft and lateral directions.

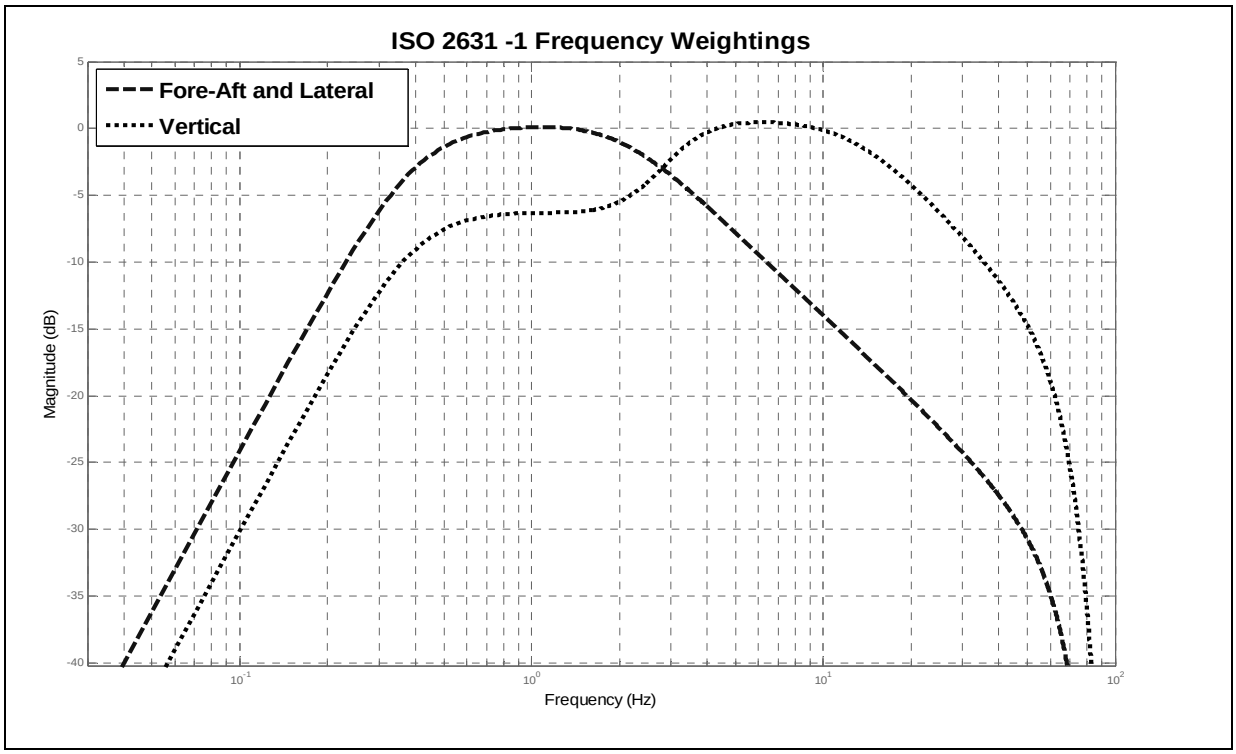

Figure 49 - Frequency Weightings for the Vertical, Fore-Aft and Lateral Directions

Time based vibration calculations were calculated as described by the ISO 2631-1 Standard. The weighted Root-Mean-Square (RMS) calculation is used to assess the effect of vibration on health. The calculation of the RMS is given by Equation 1.

$$RMS = \left[\frac{1}{T} \int_0^T a_w^2(t)\,dt \right]^{\frac{1}{2}} \quad [1]$$

The Vibration Dose Value (VDV) is an additional method of evaluation for time based vibrations. It is more sensitive to peaks than the RMS method and is useful for transient accelerations and for evaluating intermittent vibrations that occur at different time periods. The calculation for the VDV is given by Equation 2.

$$VDV = \left[\int_0^T \left[a_W(t) \right]^4 dt \right]^{\frac{1}{4}} \qquad [2]$$

An additional characteristic of the VDV when comparing it to the RMS is that it is not time dependant. Matlab code for ISO 2631-1 RMS and VDV calculation and frequency weightings can be seen in Appendix C. This is important because it allows short durations of whole-body vibrations to be extrapolated and compared against the ISO 2631-1 Health Guidance Caution Zone. Even if there are periods of rest between periods of vibration, the VDV value remains consistent. When the exposure to vibration consists of more than one period the Total VDV exposure should be calculated. Total VDV (VDV_T) was calculated using Equation 3.

$$VDV_T = \left[\sum_i VDV_i^4 \right]^{\frac{1}{4}} \qquad [3]$$

Figure 50 shows the Health Guidance Caution Zones for the Vibration Dose Value. The lower boundary (8.5 $m*s^{-1.75}$) represents the cutoff for WBV levels that are considered potentially harmful. The upper boundary (17 $m*s^{-1.75}$) represents a level above which health risks are likely.

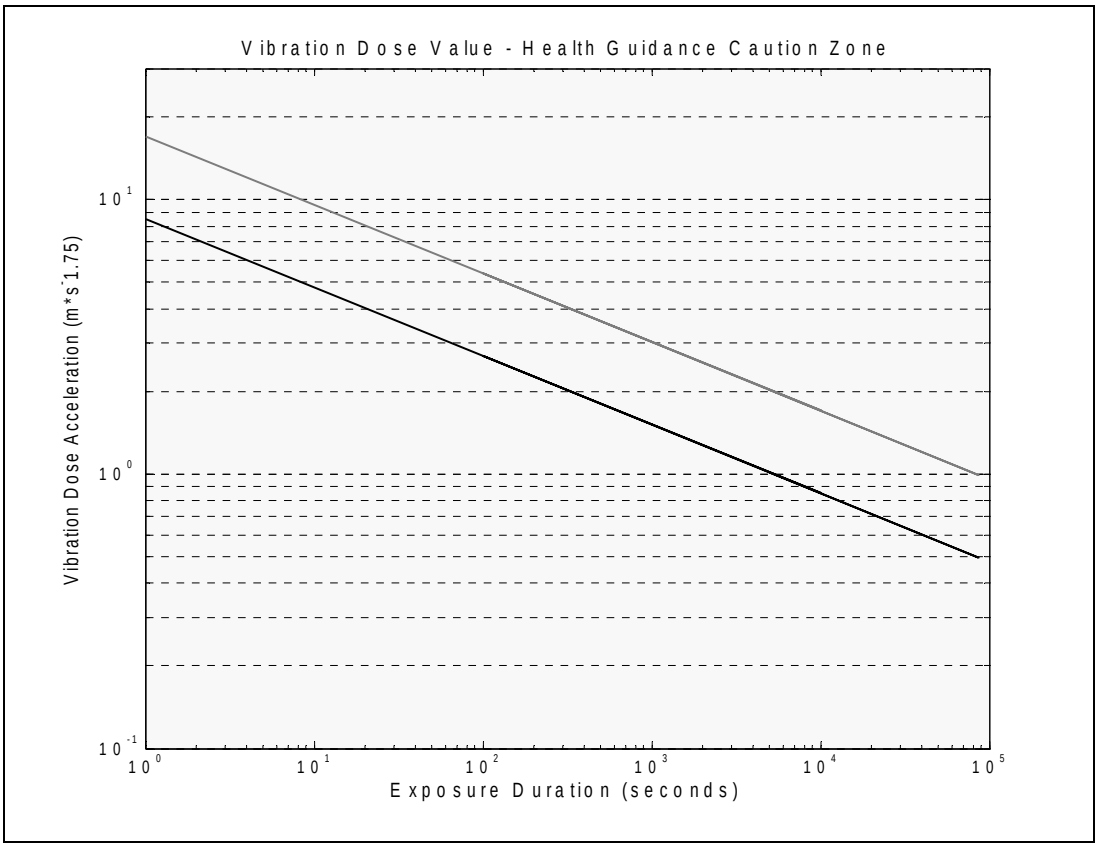

Figure 50 - Health Guidance Caution Zone for the VDV

Transmissibility (*Tm*) at the seat cushion was calculated using the data from the six subjects who tested with the SITBAR from Equation 4. VDV_{output} and VDV_{input} represent the vibration dose value from beneath the cushion (input) and the SITBAR (output) for each suspension setting over each obstacle. The resultant value is the transmissibility in the time domain and is unitless.

$$Tm = \frac{VDV_{output}}{VDV_{input}} \qquad [4]$$

Distributions of all data were examined for normality, and outliers were removed. Data were found to be normally distributed. A Mixed Model ANOVA was used to determine if significant differences existed between the six suspension systems while driving over each of the obstacles within the activities of daily living course. Significance level was set at $p < 0.05$. A mixed model was selected because each of the subjects, the random effect, tested all of the suspension settings, the fixed effect. A Bonferroni Post-hoc analysis was performed on suspension types to determine where significant differences existed.

A Pearson correlation with a significance level of $p < 0.05$ was used to evaluate a correlation existed between body mass index, weight and vibration dose value.

4.3 RESULTS

Statistical analyses of the RMS and VDV data revealed significant differences between the six different suspensions over each of the obstacles in the activities of daily living course.

Post-hoc analyses revealed that for each of the obstacles, significant differences existed between the Invacare suspension and the Invacare solid insert. For the Quickie power wheelchair the solid insert setting was not significantly different from the most-stiff setting for each of the obstacles except the smooth surface. The solid insert setting was significantly different than the lowest and mid stiffness settings for all of the obstacles except the smooth surface and the deck surface.

Pearson correlation over the activities of daily living course revealed no significant correlation between BMI ($p = 0.4288$) and VDV or between weight ($p = 0.2895$) and VDV.

Table 11 shows the average RMS values and the average VDV values and the total VDV values over each of the obstacles. Figure 51 shows the Total VDV ± two standard deviations for each suspension setting of the able bodied subjects while traveling over the activities of daily living course. The Total VDV of the two wheelchair users are shown on the same graph and mostly fall within the two standard deviations of the able bodied subjects.

Table 11 - Average RMS (m/s^2) and VDV ($m/s^{1.75}$) and Total VDV ($m/s^{1.75}$) values over obstacles for each suspension setting

RMS (m/s^2)	Invacare Insert	Invacare Suspension	Quickie Insert	Quickie Least Stiff	Quickie Mid-Stiff	Quickie Most Stiff
Deck	0.15±.05	0.16±.05	0.15±.03	0.15±.03	0.14±.03	0.15±.03
Door	0.56±.27	0.39±.12	0.38±.15	0.28±.10	0.29±.10	0.39±.15
Curb	1.28±.29	0.92±.14	1.42±.24	0.87±.15	1.08±.16	1.36±.27
Dimple	0.42±.06	0.38±.04	0.41±.07	0.36±.05	0.36±.05	0.40±.07
Smooth	0.08±.02	0.07±.02	0.08±.02	0.08±.03	0.08±.02	0.09±.03
Carpet	0.40±.11	0.35±.10	0.47±.12	0.36±.06	0.34±.05	0.43±.12
VDV ($m/s^{1.75}$)	Invacare Insert	Invacare Suspension	Quickie Insert	Quickie Least Stiff	Quickie Mid-Stiff	Quickie Most Stiff
Deck	0.24±.08	0.27±.10	0.26±.05	0.24±.07	0.23±.05	0.25±.06
Door	1.06±.54	0.71±.23	0.77±.33	0.56±.23	0.51±.22	0.77±.35
Curb	2.54±.79	1.60±.32	2.82±.38	1.42±.49	2.05±.40	2.74±.67
Dimple	0.70±.16	0.63±.08	0.68±.14	0.58±.11	0.58±.10	0.67±.15
Smooth	0.14±.04	0.12±.04	0.14±.03	0.13±.07	0.13±.03	0.15±.05
Carpet	0.98±.30	0.83±.21	1.14±.28	0.72±.26	0.70±.23	1.01±.30
Total VDV	**2.58±.84**	**1.65±.35**	**2.85±.44**	**1.46±.51**	**2.06±.42**	**2.76±.69**

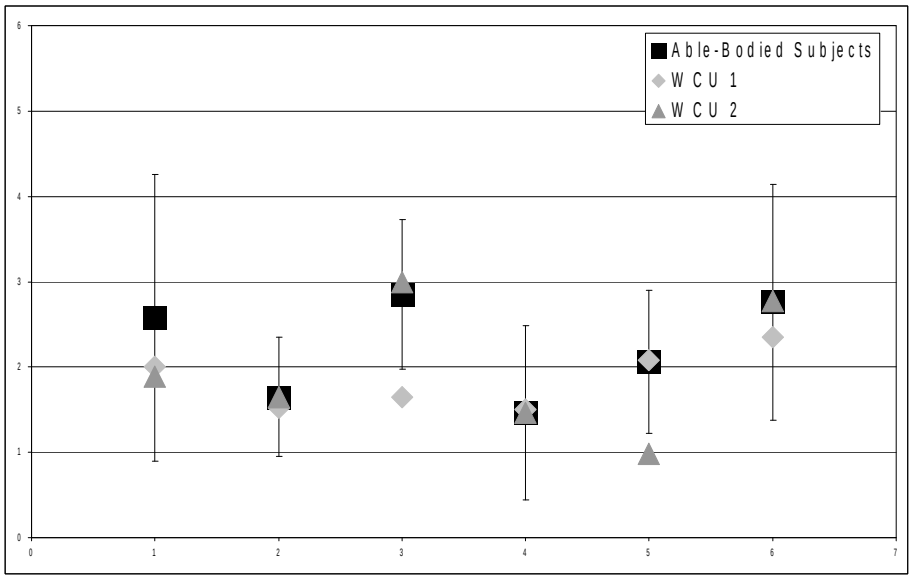

Figure 51 - Total VDV of the able bodied subjects and the Total VDV of the wheelchair users while driving over the activities of daily living course

Figure 52 shows the frequency spectrum of the accelerations at the seat and at the SITBAR collected for the six trials tested with the SITBAR. This figure shows an increase in magnitude above the seat cushion, especially in the 2-8 Hz range. Figure 53 shows an example of the frequency weighted accelerations collected at the seat and the SITBAR during driving over the activities of daily living course. This figure shows that the vibrations above the seat cushion have a higher magnitude than below the cushion.

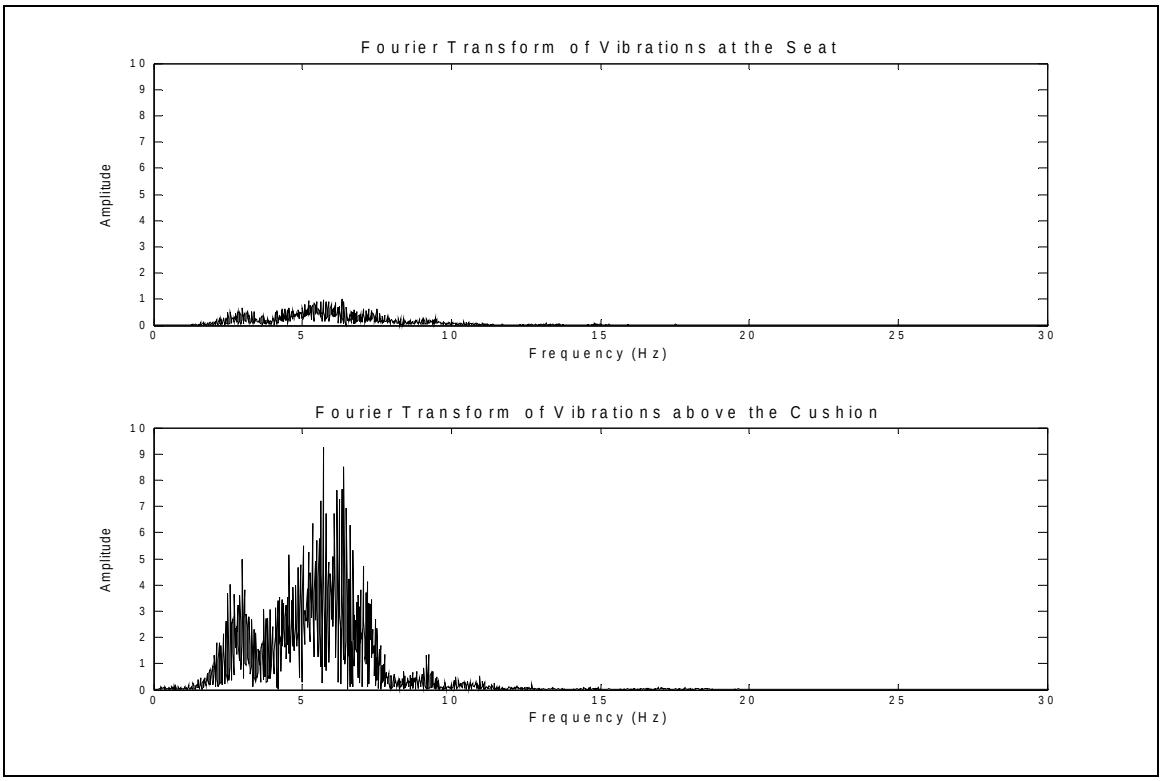

Figure 52 - Frequency Spectra above and below the cushion

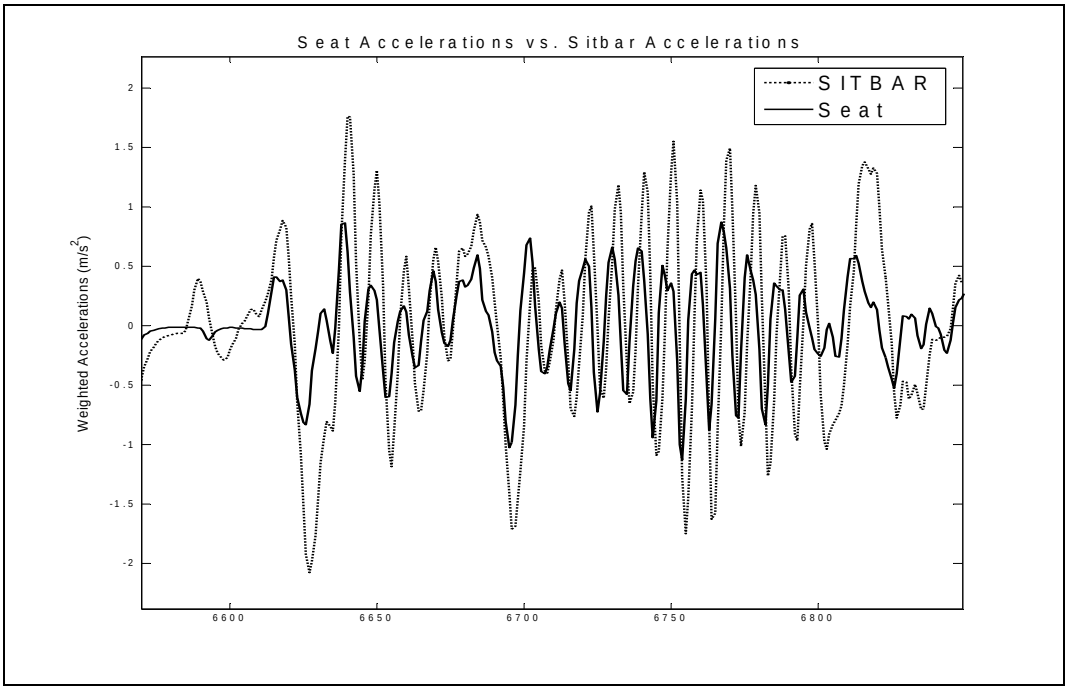

Figure 53 - Seat and SITBAR accelerations over the dimple strip

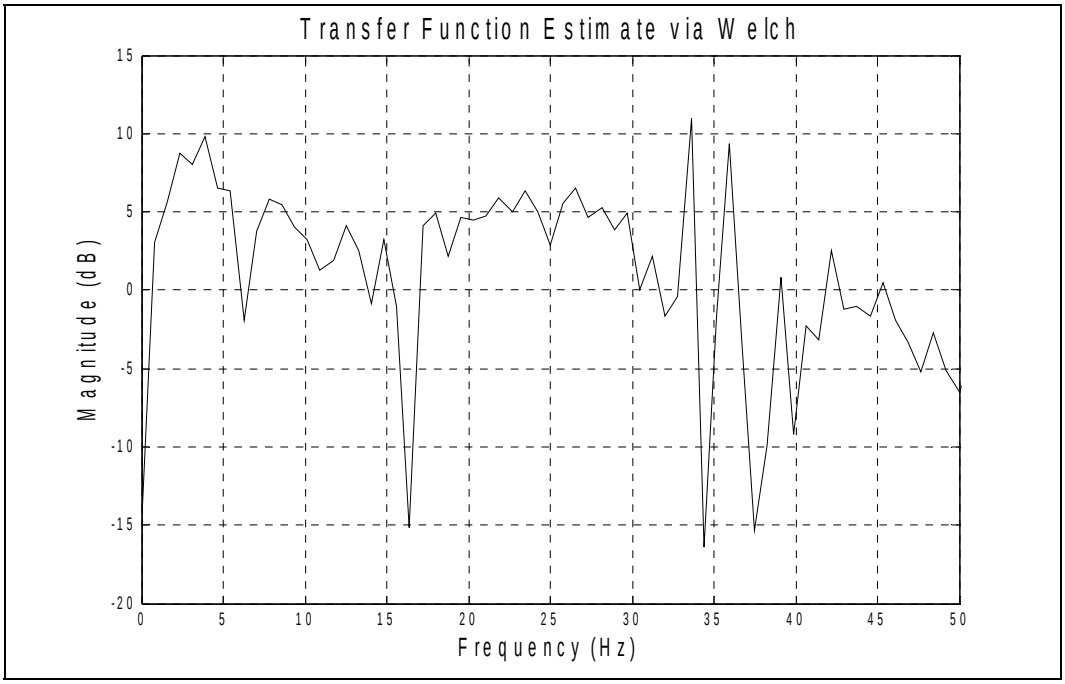

Figure 54 - Transfer function of the seat cushion estimated using measured data

Table 12 shows the transmissibility between the seat accelerometer, below the cushion, and the accelerometer at the human / cushion interface, the SITBAR. The transmissibility ranges from 1.6 to 3.14.

Table 12 - Transmissibility of the cushion for each wheelchair during driving over each of the obstacles

	Invacare Insert	Invacare Suspension	Quickie Insert	Quickie Least-Stiff	Quickie Mid-Stiff	Quickie Most-Stiff
Deck	2.49±.23	2.30±.08	2.64±.31	2.49±.07	2.44±.12	2.52±.06
Door	2.06±.21	1.86±.24	2.37±.49	2.68±.11	2.45±.32	2.84±.88
Curb	1.65±.08	1.60±.14	1.79±.27	2.70±.17	2.17±.17	2.00±.14
Dimple	1.81±.21	1.99±.07	1.83±.12	2.10±.07	2.01±.17	2.13±.12
Smooth	2.85±.39	2.70±.19	2.32±.28	2.16±.16	3.14±.30	2.22±.26
Carpet	2.06±.25	2.54±.13	2.14±.13	2.78±.22	2.35±.05	2.36±.05

Based on these results, further testing was conducted. Transmissibility was evaluated using a 50th percentile male Hybrid Test Dummy (HTD), to collect more data and ensure the validity of the previous results. Results confirmed that the vibrations above the seat cushion were higher than those below the cushion.

Table 13 - Transmissibility of the cushion for the Hybrid Test Dummy traveling over the activities of daily living course

	Transmissibility
Deck	3.14±.18
Door	2.53±.21
Curb	1.76±.21
Dimple	2.15±.37
Smooth	3.42±.93
Carpet	3.34±.24

The total VDV was used to determine the amount of time required before crossing each boundary of the HGCZ. The ISO 2631-1 standard presents an equation to extrapolate vibration levels over long periods of time, based on short durations of vibration exposure.

$$a_{w1}T_1^{1/4} = a_{w2}T_2^{1/4} \quad [5]$$

This equation was applied to the Total VDV and the Total VDV excluding the curb descent, over the activities of daily living course to determine the time of vibration exposure for each suspension setting to cause potentially harmful effects.

Table 14 - Time (in minutes) to cross the Lower and Upper boundaries of the Health Guidance Caution Zone for each of the suspension setting based on the total VDV and Time (in hours) based on total VDV excluding the curb descent

	Lower Boundary Crossing (min)	Upper Boundary Crossing (min)
Invacare Insert	2.06	32.92
Invacare Suspension	11.74	187.81
Quickie Insert	1.21	19.41
Quickie Least Stiff	15.07	241.17
Quickie Mid-Stiff	4.47	71.58
Quickie Most Stiff	1.28	20.52
	Lower Boundary Crossing (hrs)	Upper Boundary Crossing (hrs)
Invacare Insert	0.39	6.21
Invacare Suspension	1.29	20.61
Quickie Insert	0.49	7.88
Quickie Least Stiff	2.11	33.83
Quickie Mid-Stiff	2.42	38.69
Quickie Most Stiff	0.68	10.82

4.4 DISCUSSION

Similar to occupations where whole-body vibrations can be harmful to seated operators, i.e. bus drivers and construction, the reason why wheelchair users are at risk for injury due to exposure from WBV, is because of time of exposure not necessarily experiencing extreme shocks and vibrations. Without significant periods of rest, eight hours as prescribed by the ISO 2631-1 standard, the effects of WBV are cumulative throughout the course of the day, and the longer the exposure time the lower the threshold of non-harmful vibrations.

Results showed that for the Invacare 3G Torque-SP, VDV and RMS experienced by the wheelchair user for the solid insert was significantly different than the suspension for all of the obstacles. For the Quickie S-626, the vibrations experienced from the solid insert trials were significantly higher than the lowest and mid stiffness suspension settings for all obstacles except for the deck surface and the smooth surface. This result most likely occurred because the smooth surface and the deck surface produce low levels of vibrations and do not rely solely on the suspensions to reduce the amounts of transmitted vibration.

Although most of the suspension systems are capable of reducing the amounts of vibration transmitted to the users, the exception being the Quickie S-626 with the most-stiff suspension setting (this setting was not significantly different from the solid insert setting for all obstacles except the smooth surface), the results of the vibration dose values seem to indicate that suspension in power wheelchairs may not reduce vibration enough to reduce probability of injury in powered wheelchair users.

The results from the data collected on two wheelchair users show that the VDV values and total VDV values mostly fall within two standard deviations of the data collected from the able-bodied subjects, with the exception of wheelchair user 1 at the curb descent and wheelchair user 2 at the smooth surface.

Some may argue that powered wheelchair users may avoid obstacles such as a curb descent for any number of reasons. Table 14 shows the time to cross the lower and upper boundaries of the Health Guidance Caution Zone for the Total VDV and for the Total VDV excluding the curb descent. As seen from the results of this analysis, the VDV of the curb descent greatly affects the total VDV over the entire course. However the VDV without the curb descent still crosses the lower boundary of the HGCZ in a modest amount of time (less than 2.5

hours) even with the best suspension. None of the power wheelchairs with suspension cross the upper boundary until almost 11 hours, which is promising. This result is significant based on the amount of time that users spend in their wheelchairs each day. Cooper et al [17] showed that on average wheelchair users at the National Veterans Wheelchair Games spent 20+ hours per day in their wheelchair.

The transmissibility data collected from the SITBAR shows that there are higher levels of vibration being experienced at the human / cushion interface than at the seat below the cushion. DiGiovine et al [15] evaluated the transmissibility between the seat beneath the cushion and at the head during manual wheelchair propulsion. They determined that vibrations measured at the head were generally higher than those at the seat. As shown in Figure 52, the amplitudes are higher at the human / cushion interface than underneath the cushion. This result may occur because of additional input of vibrations at the seat. These vibrations most likely bypass the cushion and travel though the user's legs to cause higher vibrations at the cushion \ user interface. Future work should examine the transmissibility of additional cushions using the SITBAR and compare results from DiGiovine et al [15, 43], and should incorporate additional acceleration inputs at the footrest and the back support to more accurately model the vibrations at the user \ cushion interface.

Limitations of this study include the use of only six obstacles. However these obstacles are a good representation of some of the vibration causing activities that wheelchair users are exposed to during their activities of daily living. Only two suspension wheelchairs were used for this study. At the time the study began the Quickie S-626 and the Invacare 3G Torque SP were two of the most popularly prescribe wheelchairs. Able-bodied subjects were used for data collection. The power wheelchair population is extremely diverse and is not necessarily

characterized by a single type of user. Many power wheelchair users (multiple sclerosis, amputees, muscular dystrophy, elderly, etc.) may show similar responses to able-bodied users. The two wheelchair users tested fell within two standard deviations of the able-bodied users and the testing of more subjects might show an even closer relationship to able bodied users. Additionally, although it is important to apply the results to the wheelchair population, the differences in suspensions in power wheelchairs were being examined.

Researchers will benefit from this data in various ways. The information on the transmissions of vibrations from different suspension systems will lead to improvement in their design and function allowing powered wheelchairs to adequately reduce the amount of whole-body vibrations experienced by their users. The data collected can aid clinicians by providing information that will allow them to prescribe wheelchairs more appropriately based on the users needs. For example if a user with the need for a powered wheelchair has a very active life style it may be more suitable to prescribe them a wheelchair with adequate suspension so as to reduce the amounts of whole-body vibrations they experience, and possibly prevent them from receiving an injury or experiencing pain that may limit their daily activities.

5.0 DEVELOPMENT AND EVALUATION OF A LINEAR SUSPENSION MODEL OF ELECTRIC POWERED WHEELCHAIRS

5.1 INTRODUCTION

The use of suspension or vibration isolation in mechanical systems came into modern form in the late nineteenth century, coincidentally along with the industrial and automotive revolutions [45]. The main use of vibration isolation in any system is to reduce the amount of force or acceleration transmitted to a mass [46-49]. For example for performance purposes as in the case of an automobile engine mount or a large scale machine, or for safety purposes (i.e. operators of heavy machinery, drivers of trucks and buses, or wheelchair users).

Den Hertog's *Mechanical Vibrations* [50] text claims three possible ways of isolation; first is to eliminate the force transmitted to the exposed mass, which is not a practical or probable solution. Second is to alter the mass or the spring constant to move away from the resonance frequency; however this can be difficult because one might not want to alter the system. The last and most applicable method is the addition of a dynamic vibration absorber or a damper.

The use of the spring in the mechanical system is to reduce the force transmitted to the mass of interest. The addition of the damper allows for the reduction of continuing oscillations of a system, which are present with only a spring. Theoretically, if only a spring is used in a system then the oscillatory vibrations will never be fully attenuated because of the exponential characteristics of the system. The use of the damper also contributes to road holding in automobiles, which adds to safety.

Although dampers do contribute to the vibration reduction of a system in most cases they can present some drawbacks as well. Matschinky's text [51] states "Harmonization of springs and dampers always requires a compromise between the demands of handling and comfort". Dampers can reduce the amount of oscillatory vibrations transmitted through a system but can also introduce alternative amplified forces to the system such as impact forces.

In the past decade producers of electric powered wheelchairs have begun adding suspension to their wheelchairs, for many different reasons. Wheelchair users are more independent now than any other time in history due to advances in technology, medicine, and governmental policy as well as other factors. This increased independence brings about encounters with surfaces and obstacles that must be safely negotiated by powered wheelchairs. The use of optimal suspension in powered wheelchairs can allow for better road handling (accompanying the increased speed, and maneuverability of powered wheelchairs), obstacle climbing and negotiation, and the reduction of whole-body vibration transmitted during these increased activities.

The apparent mass method is a means of measuring the dynamic response of the human body when it is exposed to vibrations [52]. The apparent mass, M, is calculated as the quotient of the force, F, and the acceleration, a, in the frequency domain, ωi:

$$M(\omega i) = \frac{F(\omega i)}{a(\omega i)} \qquad [1]$$

Many studies have examined the apparent mass of humans using multiple methodologies; including examining differences between men, women, and children [52], comparing standard sinusoidal vibrations and randomly applied vibrations [53], examining apparent mass of humans exposed to horizontal vibrations [54], and examining differences in apparent mass of automotive

drivers for both passengers and drivers [55]. Results of vibration in the vertical direction showed an apparent mass resonance frequency of 4-5 Hz. For exposure to horizontal vibration there were two resonance peaks at 2.5-3.5 Hz and at 4.5-5.5 Hz. For automotive passengers the resonance frequency occurred at 6.5-8.6 Hz, and for automotive drivers with hands on the steering wheel there were two resonance frequencies at 5.1-8.25 Hz and at 8-12 Hz.

The purposes of this study were to characterize the spring and damper constants of the suspension elements of the Quickie S-626 and the Invacare 3G Torque SP suspension powered wheelchairs, and to develop a mathematical model and examine the apparent mass characteristics of the suspension power wheelchairs.

5.2 METHODS

5.2.1 System Identification of the Suspension Elements

Dynamic system testing [56-57] of the spring-damper suspension elements of both the Invacare 3G Torque SP and the Quickie S-626 was conducted. An Instron Material Testing System (MTS) was used to evaluate the spring and damper constants. A laptop computer was attached to the force and position outputs of the Instron MTS and a LabView (National Instruments Corp. Austin, TX) program was used to collect the resultant outputs. Testing was conducted by inputting sinusoidal displacements of varying amplitudes (0.1 inches - 0.5 inches) and various frequencies (1 Hz – 8 Hz), related to the travel and frequency of the suspension during wheelchair driving, and measuring the output of force. Figure 55 shows the test setup for the suspension from the Invacare 3G Torque SP.

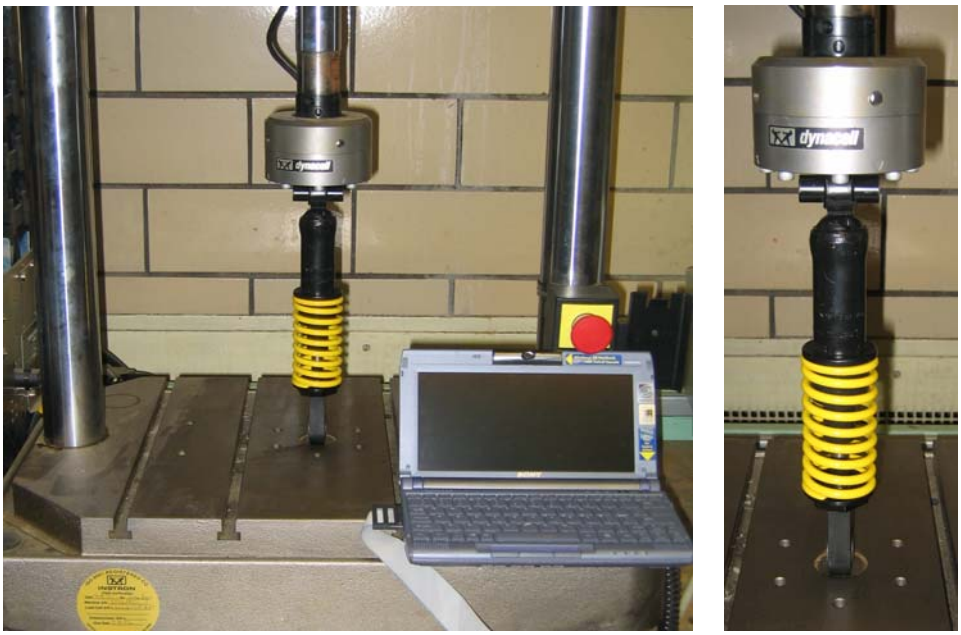

Figure 55 - Instron testing of suspension element for system identification

A system identification using a mathematical multiple regression was done in MATLAB (The Mathworks Inc., Natick, MA). The equation to determine the spring and damper constants, β, is shown below, where F is the measured force and X is a matrix of the measured force and velocity. This equation is a best fit measurement which incorporates the range of displacements and frequencies used in the dynamic testing.

$$\beta = F^T (X^T X)^{-1} X^T \qquad [2]$$

5.2.2 Modeling the Suspension Power Wheelchairs

In order to identify the system parameters, that is the resultant motions of the sprung mass due to an input, the Laplace transform becomes extremely useful [58-60]. The Laplace transform is a method that can be used to solve and analyze differential equations, exactly like the equations of motion for the system of interest. It can be used to investigate systems that change with time and develop a transfer function to evaluate an output from a given input [61].

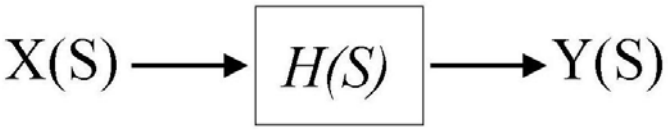

Figure 56 - Laplace Transform giving the transfer function H(S)

Once the transfer function between the input and the output is evaluated, analysis of the system can take place. Another useful tool in the evaluation of differential equations is the Bode plot [62-64]. The Bode plot can be used to show the frequency response of the transfer function of a modeled system. This becomes extremely important in design of any system, because the Bode plot can be applied to a mathematical model and produce realistic results. For example in the sprung mass model the Bode plot can characterize the use of different spring and damper constants and show the effects on the dampening ratio and the natural frequency of the system.

Figures 57 and 58 show the free body diagrams of the Quickie S-626 and the Invacare 3G Torque SP suspension power wheelchairs. These diagrams were used to develop the mathematical model and transfer functions between the input ground reaction vertical forces and the resultant vertical accelerations at the seat.

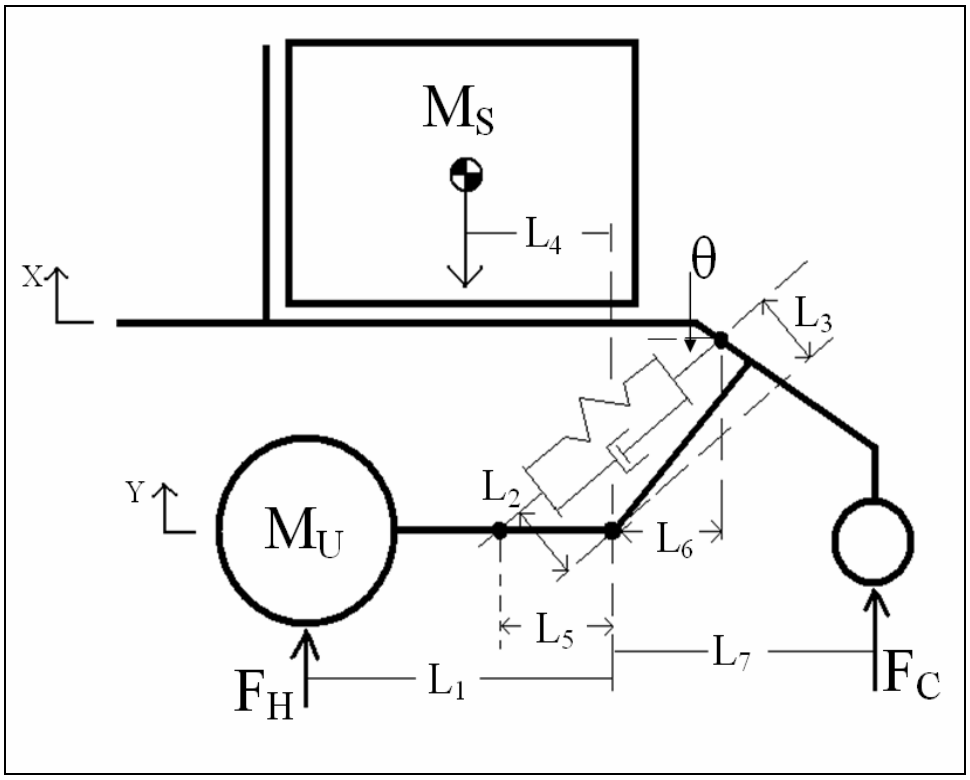

Figure 57 - Free Body Diagram of the Quickie S-626 Power Wheelchair

Figure 57 shows the diagram of the Quickie S-626 Power Wheelchair. M_S is the mass of the user and the frame of the wheelchair and M_U is the mass of the drive motor and wheel, F_H is the force on the hubs, and F_C is the force on the casters. L_1-L_7 represent various important dimensions in the model. X and Y are displacements of the user and frame mass and the drive train mass respectively. K and C are the spring and damper constants of the suspension element. The model parameters were selected to most appropriately represent the dimensions of the wheelchair and the suspension elements. The model is assumed to be linear because the input and output of the equations of motion share the same order.

Equations of Motion for the Quickie S-626 based on the Free Body Diagram Figure 57:

$$0 = M_s \ddot{x}(t) L_4 + 2C(U1) + 2K(U2) \quad [1]$$

$$F_{TOT} = -2M_u \ddot{y}(t) L_1 - 4C(U1) - 4K(U2) \quad [2]$$

$$U1 = \dot{x}(t)\sin(\theta)\frac{L_6 L_3}{L_1} - \dot{y}(t)\sin(\theta)\frac{L_5 L_2}{L_1}t) \quad [3]$$

$$U2 = x(t)\sin(\theta)\frac{L_6 L_3}{L_1} - y(t)\sin(\theta)\frac{L_5 L_2}{L_1}t) \quad [4]$$

$$F_{TOT} = F_{CR} L_7 + F_{CL} L_7 - F_{HR} L_1 - F_{HL} L_1 \quad [5]$$

The Laplace transform of equation 1 is calculated, and $\ddot{Y}(s)$ is solved for in order to substitute into the Laplace transform of equation 2. The values A and B are created in order to simplify the algebra:

$$0 = M_s \ddot{X}(s) L_4 + 2C\left(\frac{\ddot{X}(s)\sin(\theta)L_6 L_3}{L_1 s} - \frac{\ddot{Y}(s)\sin(\theta)L_5 L_2}{L_1 s}\right) + 2K\left(\frac{\ddot{X}(s)\sin(\theta)L_6 L_3}{L_1 s^2} - \frac{\ddot{Y}(s)\sin(\theta)L_5 L_2}{L_1 s^2}\right) \quad [6]$$

$$\ddot{Y}(s)[2A] = \ddot{X}(s)[M_s L_4 + 2B] \quad [7]$$

$$A = \left[\frac{C\sin(\theta)L_5 L_2}{L_1 s} + \frac{K\sin(\theta)L_5 L_2}{L_1 s^2}\right] \quad [8]$$

$$B = \left[\frac{C\sin(\theta)L_6 L_3}{L_1 s} + \frac{K\sin(\theta)L_6 L_3}{L_1 s^2}\right] \quad [9]$$

The Laplace transform of equation 2 is calculated and the value of $\ddot{Y}(s)$ is substituted from equation 7. The transfer function is the output accelerations, $\ddot{X}(s)$, divided by the input forces, $F_{TOT}(s)$:

$$F_{TOT}(s) = -2M_u\ddot{Y}(s)L_1 + \ddot{X}(s)[4B] - \ddot{Y}(s)[4A] \quad [10]$$

$$F_{TOT}(s) = \ddot{X}(s)\frac{M_sL_4 + 2B}{2A}(-2M_uL_1 - 4A) + \ddot{X}(s)[4B] \quad [11]$$

$$F_{TOT}(s) = \ddot{X}(s)\left[\frac{-2M_sL_4M_uL_1 - 4M_sL_4A - 4M_uL_1B - 8AB + 8AB}{2A}\right] \quad [12]$$

Substituting back in for A and B:

$$\frac{\ddot{X}(s)}{F_{TOT}(s)} = \frac{\frac{2C\sin(\theta)L_2L_5}{L_1}s + \frac{2K\sin(\theta)L_2L_5}{L_1}}{-2M_sM_uL_1s^2 - \frac{C\sin(\theta)}{L_1}(4M_sL_2L_4L_5 + 4M_uL_1L_3L_6)s - \frac{K\sin(\theta)}{L_1}(4M_sL_2L_4L_5 + 4M_uL_1L_3L_6)}$$

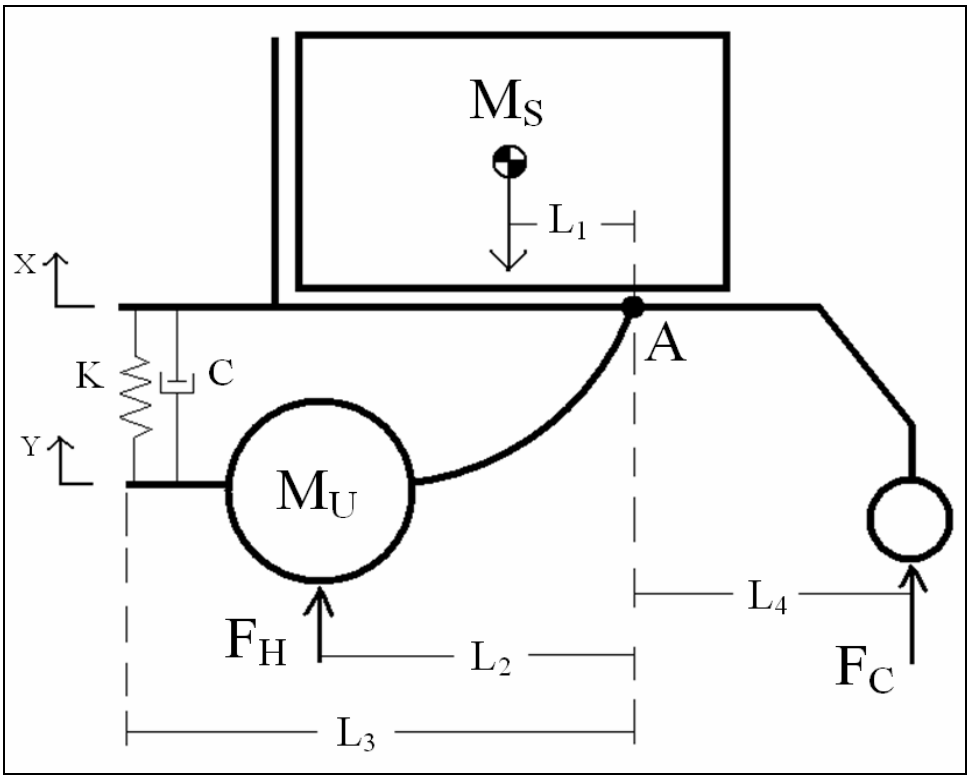

Figure 58 - Free Body Diagram of the Invacare 3G Torque SP Power Wheelchair

Figure 58 shows the diagram of the Invacare 3G Torque SP Power Wheelchair. M_S is the mass of the user and the frame of the wheelchair and M_U is the mass of the drive motor and wheel, F_H is the force on the hubs, and F_C is the force on the casters. L_1-L_4 represent various important dimensions in the model. X and Y are displacements of the user and frame mass and the drive train mass respectively. K and C are the spring and damper constants of the suspension element. The model parameters were selected to most appropriately represent the dimensions of the wheelchair and the suspension elements. The model is assumed to be linear because the input and output of the equations of motion share the same order.

Equations of Motion for the Invacare 3G Torque SP based on the Free Body Diagram Figure 58:

$$0 = M_s\ddot{x}(t)L_1 + 2CL_3\left(\dot{x}(t) - \dot{y}(t)\right) + 2KL_3\left(x(t) - y(t)\right) \quad [14]$$

$$F_{TOT} = -2M_u\ddot{y}(t)L_2 + 4CL_3\left(\dot{x}(t) - \dot{y}(t)\right) + 4KL_3\left(x(t) - y(t)\right) \quad [15]$$

$$F_{TOT} = F_{CR}L_4 + F_{CL}L_4 - F_{HR}L_2 - F_{HL}L_2 \quad [16]$$

The Laplace transform of equation 14 is calculated, and $\ddot{Y}(s)$ is solved for in order to substitute into the Laplace transform of equation 15. The value A is created in order to simplify the algebra:

$$0 = M_s\ddot{X}(s)L_1 + 2CL_3\left(\frac{\ddot{X}(s)}{s} - \frac{\ddot{Y}(s)}{s}\right) + 2KL_3\left(\frac{\ddot{X}(s)}{s^2} - \frac{\ddot{Y}(s)}{s^2}\right) \quad [17]$$

$$\ddot{Y}(s)\left[2A\right] = \ddot{X}(s)\left[M_sL_1 + 2A\right] \quad [18]$$

$$A = \left[\frac{CL_3}{s} + \frac{KL_3}{s^2}\right] \quad [19]$$

The Laplace transform of equation 15 is calculated and the value of $\ddot{Y}(s)$ is substituted from equation 18:

$$F_{TOT}(s) = \ddot{X}(s)\left[4A\right] - \ddot{Y}(s)[2M_uL_2 + 4A] \quad [20]$$

$$F_{TOT}(s) = \ddot{X}(s)\left[4A\right] - \ddot{X}(s)\left[\frac{M_sL_1 + 2A}{2A}\right][2M_uL_2 + 4A] \quad [21]$$

$$F_{TOT}(s) = \ddot{X}(s)\left[\frac{8A^2 - 2M_s L_1 M_u L_2 - 4M_s L_1 A - 4M_u L_2 A - 8A^2}{2A}\right] \quad [22]$$

The transfer function is the output accelerations, $\ddot{X}(s)$ divided by the input forces, $F_{TOT}(s)$:

$$\frac{\ddot{X}(s)}{F_{TOT}(s)} = \frac{2CL_3 s + 2KL_3}{-2M_s M_u L_1 L_2 s^2 - CL_3(4M_s L_1 + 4M_u L_2)s - KL_3(4M_s L_1 + 4M_u L_2)}$$

5.2.3 Apparent Mass

The two suspension power wheelchairs, the Quickie S-626 and the Invacare 3G Torque SP were driven over an obstacle course consisting of six obstacles, a deck surface, a simulated door threshold, a 50 mm curb descent, a truncated dome dimple strip, a smooth tile surface, and a thick pile carpet. Two sets of tests were conducted. In the first test, three Hybrid Test Dummies (HTDs) were driven over the obstacle course. The HTDs were a 5th percentile female (50 kg), a 50th percentile male (75 kg), and a 95th percentile male (100 kg). The second set of testing included 8 subjects, 4 males and 4 females, with an average ± standard deviation mass of 72.88 ± 18.5 kg, and a median and range of 76 kg, and 45.5-94 kg.

Each wheelchair was instrumented with two SMART^{HUBS} and two SMART^{CASTERS} as well as a tri-axial accelerometer placed on the seat of the wheelchair underneath a standard polyurethane foam cushion. The cushion was 43.18 cm x 40.64 cm with a thickness of 5.08 cm and a 6.35 cm pommel. The density of the cushion is 55 kg/m^3. The SMART^{HUBS} and SMART^{CASTERS}, as described earlier, were used to measure the ground reaction forces input to the wheelchair and the accelerometer was used to measure accelerations at the seat during driving over the obstacle course.

The apparent mass frequency spectrum of each HTD and driver were calculated using the cross-spectral density method [52, 53],

$$H(f) = \frac{G_{io}(f)}{G_{ii}(f)} \qquad [24]$$

where G_{io} is the cross spectral density between the force and the acceleration in the frequency domain, and G_{ii} is the power spectral density of the acceleration in the frequency domain. The normalized apparent mass power from 4-12 Hz and the apparent mass power per frequency (i.e. power from 1-2 Hz, 2-3 Hz, etc.) were calculated. The 4-12 Hz range is significant because it is the region of the acceleration frequency spectrum that is considered most dangerous by the ISO 2631-1 Standard on Human Vibration. The apparent mass power per frequency was calculated to observe the resonance frequencies of the apparent mass spectra to compare to results from reviewed literature.

The suspension power wheelchair models that were developed in the previous section were applied to the forces collected from the SMART^{HUBS} and SMART^{CASTERS} during subject testing. The output of this calculation was the theoretical acceleration at the seat of the wheelchair. This result was then compared to the measured accelerations to determine the accuracy of the model.

5.3 RESULTS

5.3.1 System Identification of the Suspension Elements

Figure 59 shows an example of the input of the displacement to the suspension element and the measured force from the Instron MTS versus the force calculated from the system identification. Table 15 shows the resultant calculated spring and damper constants.

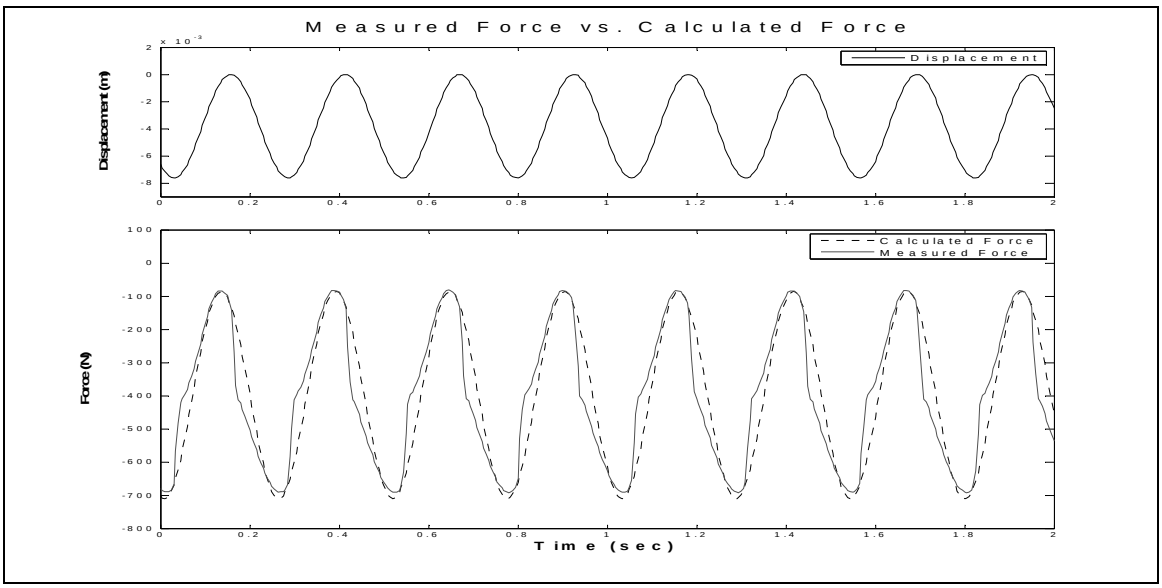

Figure 59 - Measured Displacement and Force from MTS and Calculated Force

Table 15 - Calculated Spring and Damper Constants

	Spring Constant N/m		Damper Constant N*sec/m
Quickie S-626			
Least Stiff Setting	**135,534**		**8,592**
Mid Stiff Setting	**144,490**		**7,224**
Most Stiff Setting	**199,004**		**5,289**
Invacare 3G Torque SP	**82,195**		**3,967**

5.3.2 Modeling the Suspension Power Wheelchairs

Figure 60 shows the Bode diagram of the transfer function of the mathematical model with the spring constant and damper constant values that were measured on the Instron. The transfer function, calculated from the free body diagram and the equations of motion, acts as a low pass filter for both the Invacare and Quickie suspension power wheelchair.

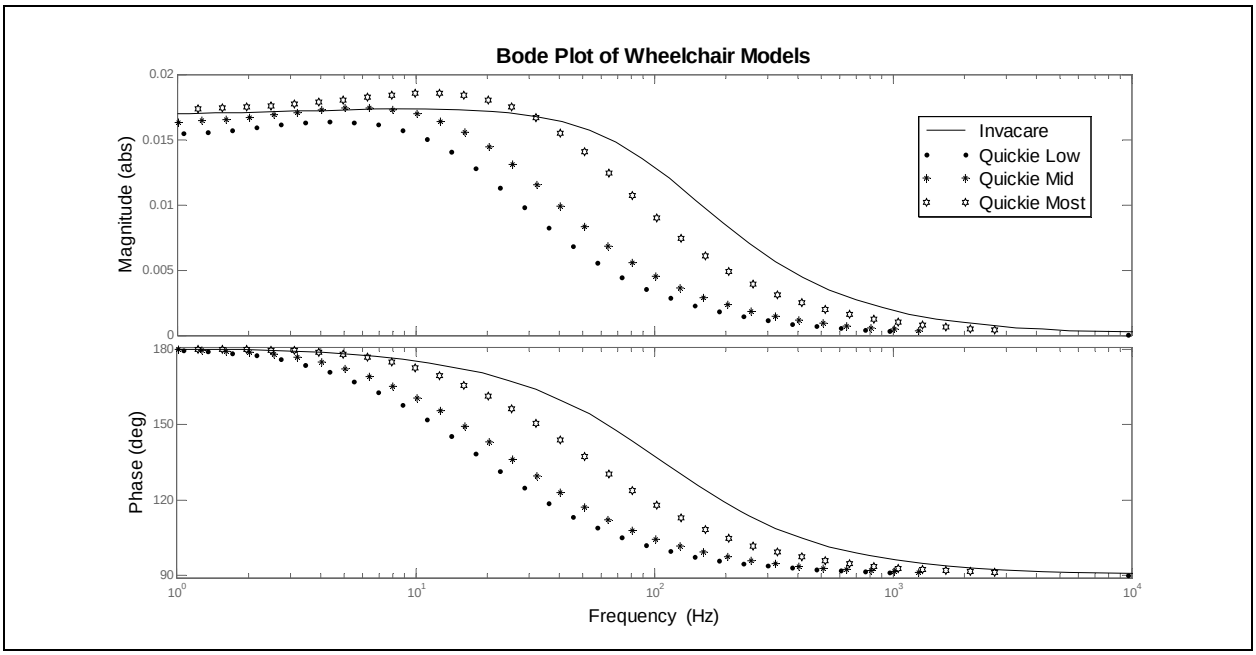

Figure 60 - Bode Diagram of the Transfer Function with spring and damper constants measured from Instron MTS testing.

With the suspension power wheelchairs equipped with the aluminum solid inserts it can be assumed that the spring and damper constants go to infinity. Figure 61 shows the Bode diagram of the suspension wheelchair models with the solid inserts. The transfer function shows that the solid inserts do not increase the amplitude of the transferred forces but simply pass more of the force signal to the seat of the wheelchair.

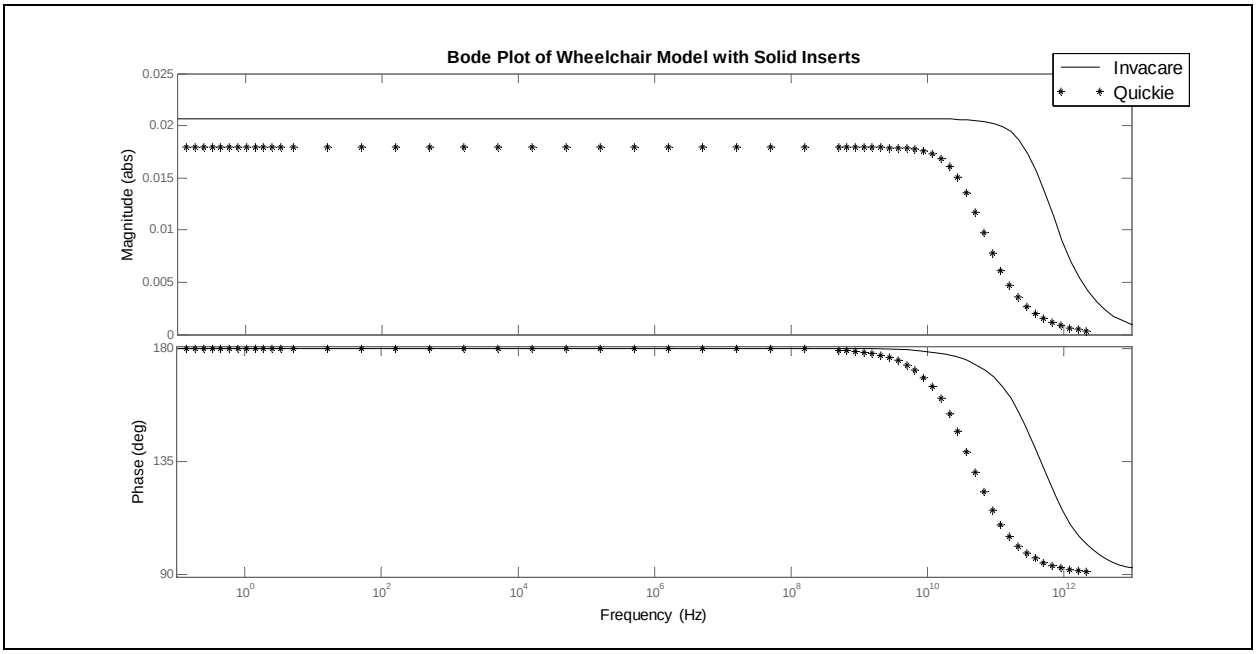

Figure 61 - Bode Diagram of the Transfer Function with the aluminum solid insert

The theoretical model was used to evaluate the accelerations at the seat based on the data collected from the 8 subjects that drove the wheelchairs over the activities of daily living course. These accelerations were then compared to the measured accelerations that were collected during the testing.

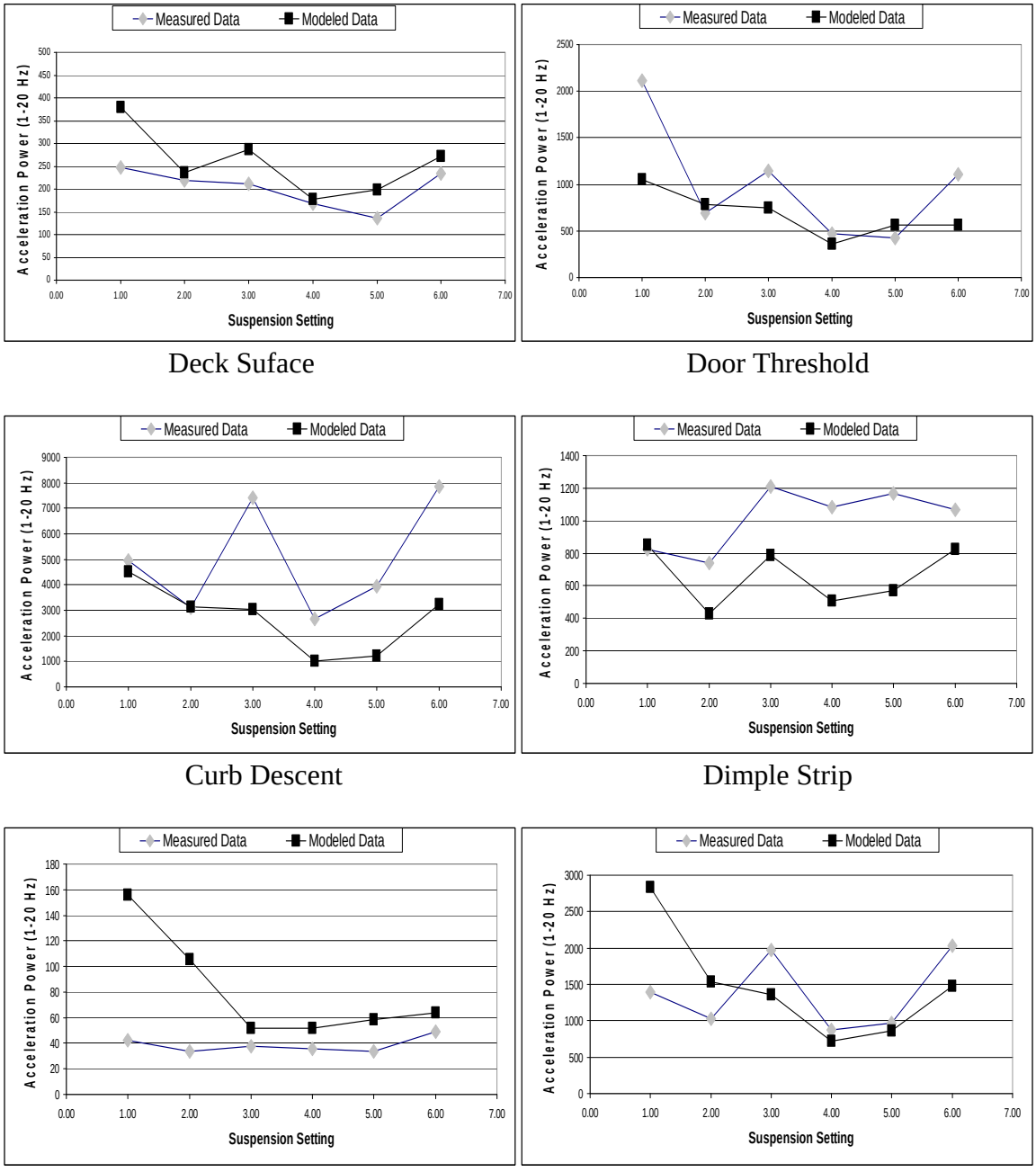

Figure 62 - Average Modeled and Measured Accelerations 1-20 Hz for each Obstacle

Figure 62 shows the average modeled acceleration power from 1-20 Hz and the average measured acceleration power from 1-20 Hz. Figure 63 shows the average modeled acceleration power and the average measured acceleration power from 4-12 Hz.

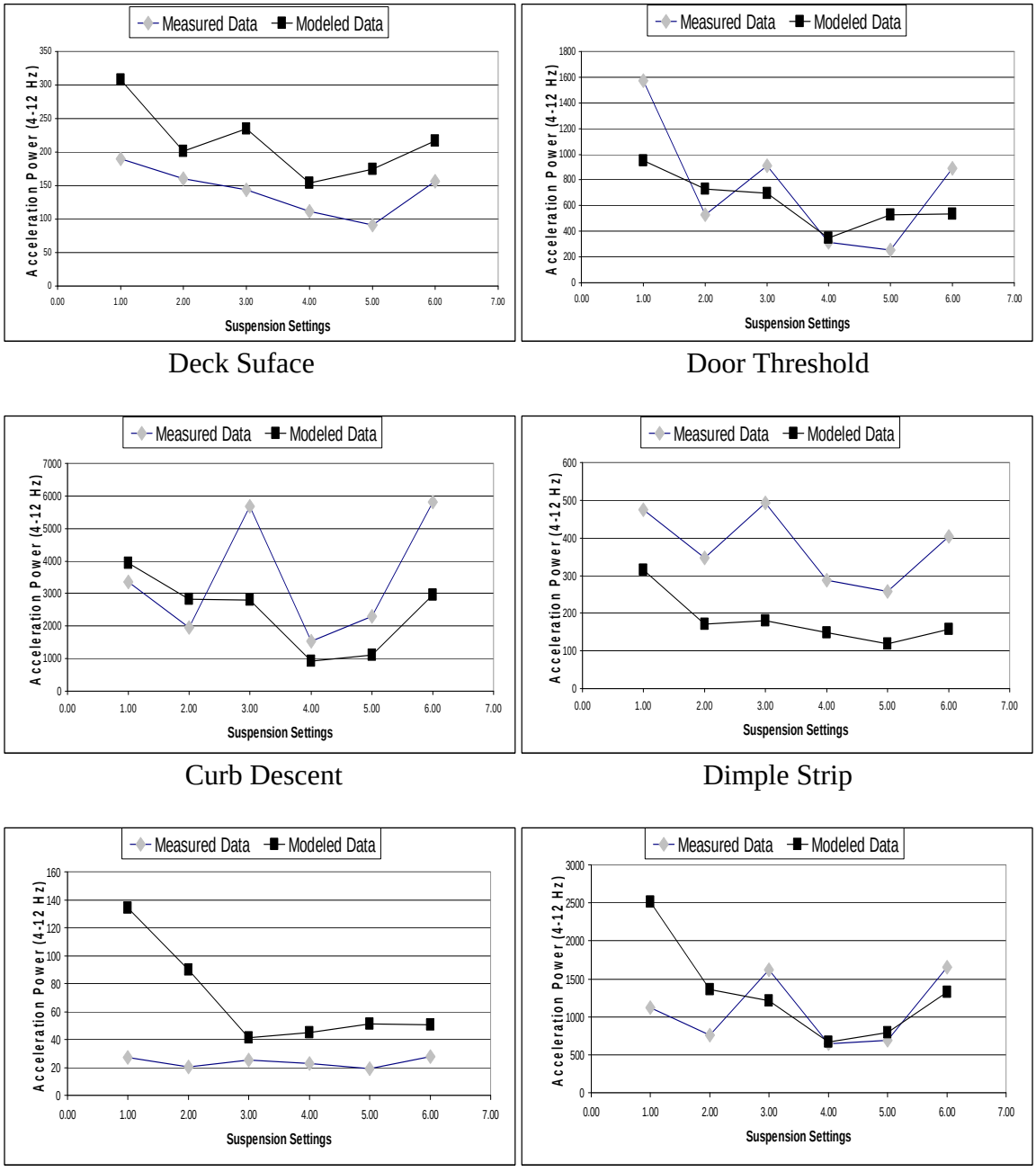

Figure 63 - Average Modeled and Measured Accelerations 4-12 Hz for each Obstacle

A paired t-test ($p<0.05$) and was conducted to determine if the model was effective at determining the accelerations at the seat. Results showed that for the acceleration power of 1-20

Hz the values were significantly different (p=0.024. For the acceleration power of 4-12 Hz the values were not significantly different (p=0.233).

5.3.3 Apparent Mass

The apparent masses of the Hybrid dummies and the 8 test subjects were calculated for each obstacle. Figures 64 and 65 show the apparent mass power per frequency from 1-50 Hz for the Hybrid test dummies and the subjects respectively.

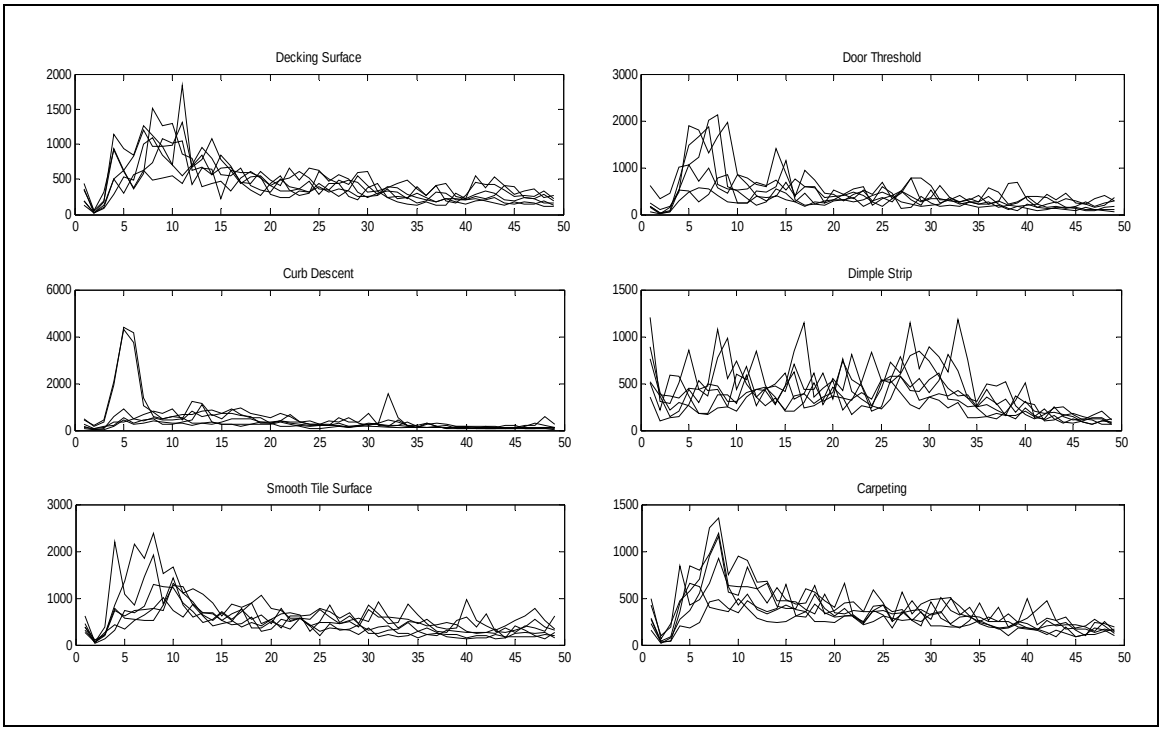

Figure 64 - Apparent Mass power per frequency for the Hybrid Test Dummies over each obstacle

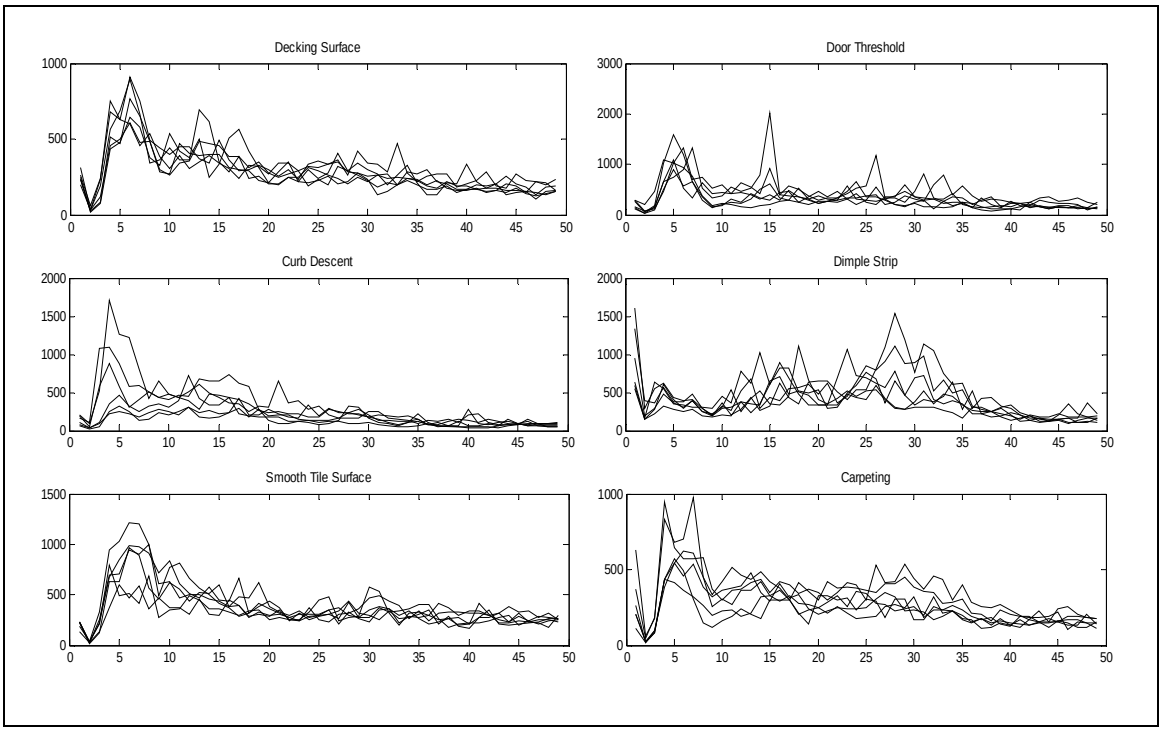

Figure 65 - Apparent Mass power per frequency for the Subjects over each obstacle

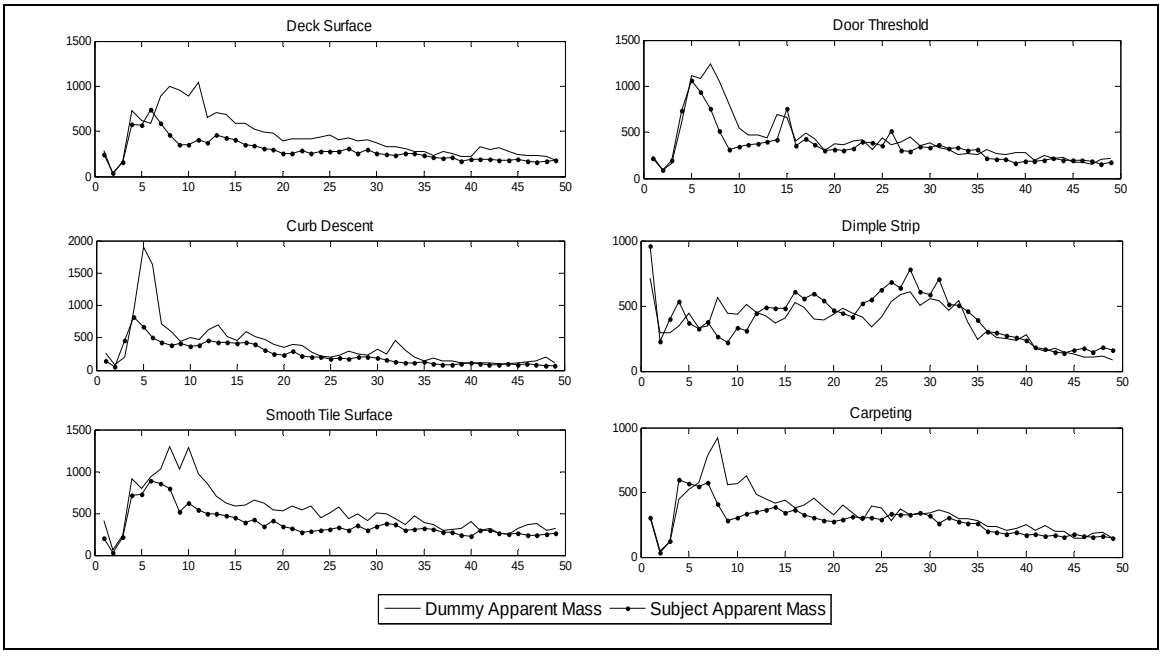

Figure 66 - Average Apparent Mass power per frequency for the Subjects and the Hybrid Test Dummies over each obstacle

Most obstacles show a resonance frequency range of around 5-10 Hz with the exception of the dimple strip, which for both the test dummies and the subjects show a more broadband signal. Also the door threshold shows an additional resonance peak at around 15 Hz.

The normalized apparent mass power was also calculated in the 4-12 Hz range to evaluate if there are significant differences between the suspension elements. An ANOVA (p<0.05) was performed on the data and revealed that significant differences existed between suspension types for the curb descent (obstacle 3) and the carpeting (obstacle 6). There was no significant difference between the suspension settings at the deck surface (obstacle 1), door threshold (obstacle 2), dimple strip (obstacle 4), and the smooth tile surface (obstacle 5).

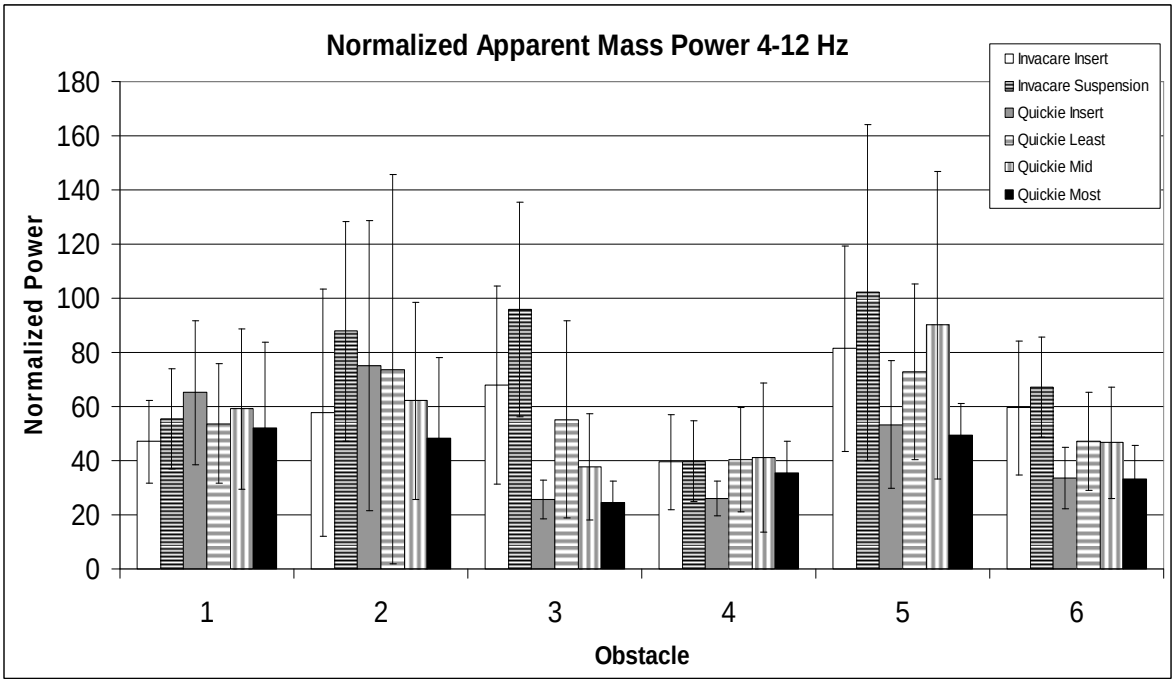

Figure 67 - Normalized Apparent Mass Power at 4-12 Hz for each obstacle (1=deck surface, 2=door threshold, 3=curb descent, 4=dimple strip, 5=smooth surface, 6=carpeting)

5.3.4 Theoretical Model of Suspension Wheelchair

Based on the previous results, a model of a suspension wheelchair with a sprung seat was created. This model was derived from occupations at risk for whole-body vibration (i.e. truck, bus, and tractor drivers, etc.) and suspensions that have been used for these users to attenuate vibration exposure. This model places an additional spring-damper suspension between the frame of the wheelchair and the seat, effectively suspending the wheelchair user within the frame.

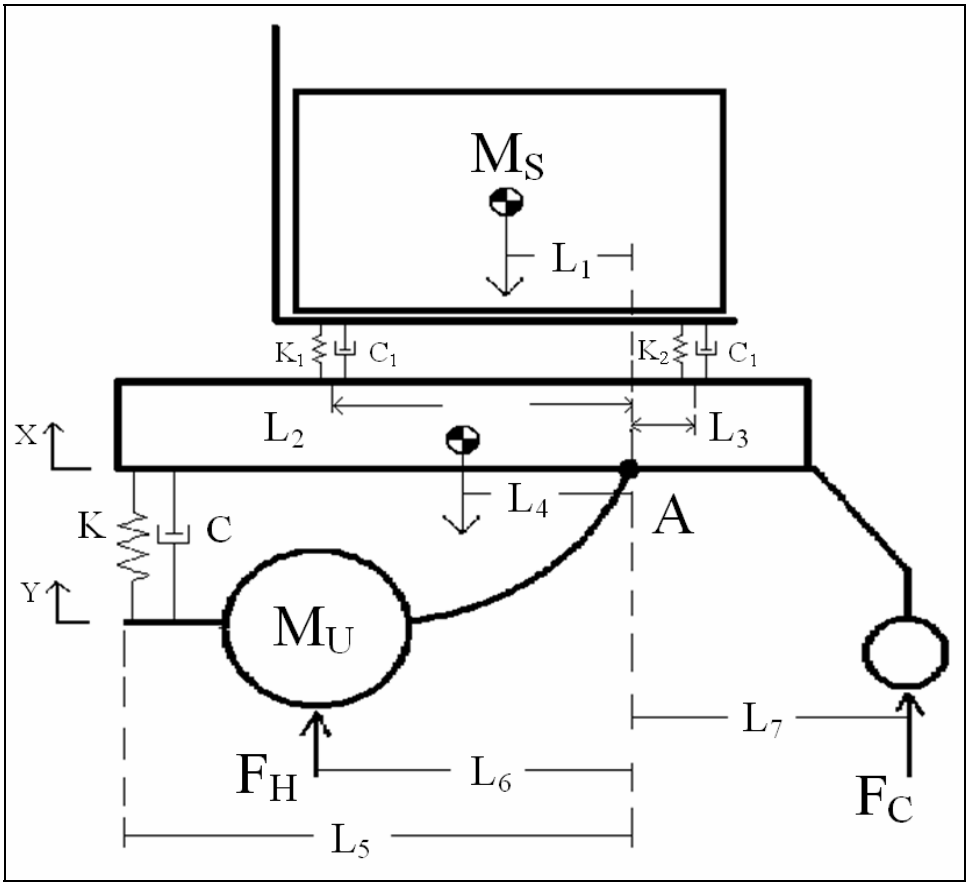

Figure 68 - Free Body Diagram of the Theoretical Suspended Seat on the Invacare 3G Torque SP Power Wheelchair

Figure 68 shows the diagram of the Invacare 3G Torque SP Power Wheelchair with the theoretical suspension seat. M_S is the mass of the user, M_F is the mass of the wheelchair frame, and M_U is the mass of the drive motor and wheel. F_H is the force on the hubs, and F_C is the force on the casters. L_1-L_7 represent various important dimensions in the model. X and Y are displacements of the user and frame mass and the drive train mass respectively. K and C are the spring and damper constants of the suspension element. K1, K2, C1, and C2 are the spring and damper constants of the seat suspension. The model parameters were selected to most appropriately represent the dimensions of the wheelchair and the suspension elements.

Equations 25, 26, and 27 represent the equations of motion for the Invacare 3G Torque SP with suspended seat based on the free body diagram in Figure 68:

$$0 = M_s \ddot{x}(t) L_1 + 2C_1 L_2 \left(\dot{x}(t) - \dot{y}(t)\right) + 2K_1 L_2 \left(x(t) - y(t)\right) - 2C_2 L_3 \left(\dot{x}(t) - \dot{y}(t)\right) - 2K_2 L_3 \left(x(t) - y(t)\right) \quad [25]$$

$$0 = M_s \ddot{y}(t) L_4 + 2C_1 L_2 \left(\dot{y}(t) - \dot{x}(t)\right) + 2K_1 L_2 \left(y(t) - x(t)\right) - 2C_2 L_3 \left(\dot{y}(t) - \dot{x}(t)\right) - 2K_2 L_3 \left(y(t) - x(t)\right) + 2CL_5 \left(\dot{y}(t) - \dot{z}(t)\right) - 2KL_{53} \left(y(t) - z(t)\right) \quad [26]$$

$$F_{TOT} = -2M_u \ddot{z}(t) L_4 + 4CL_5 \left(\dot{z}(t) - \dot{y}(t)\right) + 4KL_5 \left(z(t) - y(t)\right) \quad [27]$$

$$F_{TOT} = F_{CR} L_7 + F_{CL} L_7 - F_{HR} L_6 - F_{HL} L_6 \quad [28]$$

The Laplace Transform of equation 27 is calculated and $\ddot{Z}(s)$ is solved for. Equation 30 will be substituted into the Laplace Transform of equation 26. The value B is created to simplify the algebra:

$$F_{TOT}(s) = \ddot{Z}(s)\left[M_u L_6 + \frac{2CL_5}{s} + \frac{2KL_5}{s^2} \right] + \ddot{Y}(s)\left[-\frac{2CL_5}{s} - \frac{2KL_5}{s^2} \right] \quad [29]$$

$$\ddot{Z}(s) = \frac{F_{TOT}(s) + \ddot{Y}(s)[2B]}{M_u L_6 + 2B} \quad [30]$$

$$B = \left[\frac{2CL_5}{s} + \frac{2KL_5}{s^2} \right] \quad [31]$$

The Laplace Transform of equation 26 is calculated. The value A is created to simplify the equation:

$$0 = \ddot{X}(s)\left[-2A\right] + \ddot{Y}(s)\left[M_F L_4 + 2A + 2B\right] - \ddot{Z}(s)\left[2B\right] \quad [32]$$

$$A = \left[\frac{2C_1 L_2}{s} + \frac{2K_1 L_2}{s^2} - \frac{2C_2 L_3}{s} - \frac{2K_2 L_3}{s^2} \right] \quad [33]$$

After solving equation 32 for $\ddot{Z}(s)$ the value is substituted in equation 29 and $\ddot{Y}(s)$ is solved for; this result is shown in equation 34:

$$\ddot{Y}(s) = \frac{F_{TOT}(s)\left[2B\right] + \ddot{X}(s)\left[2A\right]\left[M_u L_6 + 2B\right]}{(M_u L_6 + 2B)\left[M_F L_4 + 2A + 2B\right] - 4B^2} \quad [34]$$

Finally, the Laplace Transform of equation 25 is calculated and $\ddot{Y}(s)$ from equation 34 is substituted. The value Q is created to simplify the equation:

$$0 = \ddot{X}(s)\left[M_s L_1 + 2A\right] - \ddot{Y}(s)\left[2A\right] \quad [35]$$

$$0 = \ddot{X}(s)\left[M_s L_1 + 2A\right] - \frac{\ddot{X}(s)\left[4A^2\right]\left[M_u L_6 + 2B\right]}{Q} - \frac{F_{TOT}(s)\left[2A\right]\left[2B\right]}{Q} \quad [36]$$

$$Q = (M_u L_6 + 2B)\left[M_F L_4 + 2A + 2B\right] - 4B^2 \quad [37]$$

$$\frac{F_{TOT}(s)}{\ddot{X}(s)} = \frac{(M_s L_1 + 2A)(Q) - 4A^2(M_u L_6 + 2B)}{4AB} \quad [38]$$

Substituting for A, B, and Q, the Transfer Function becomes:

$$\frac{\ddot{X}(s)}{F_{TOT}(s)} = \frac{N1 + N2 + N3}{D1 + D2 + D3 + D4 + D5} \quad [39]$$

$$N1 = 4s^2(C_1 L_2 CL_5 - C_2 L_3 CL_5) \quad [40]$$

$$N2 = 4s(K_1 L_2 CL_5 - K_2 L_3 CL_5 + C_1 L_2 KL_5 - C_2 L_3 KL_5) \quad [41]$$

$$N3 = 4(K_1 L_2 KL_5 - K_2 L_3 KL_5) \quad [42]$$

$$D1 = s^4(M_S L_1 M_u L_6 M_F L_4) \quad [43]$$

$$D2 = s^3(2(M_S L_1 M_u L_6 + M_F L_4 M_u L_6)(2C_1 L_2 - 2C_2 L_3) + 2(M_S L_1 M_u L_6 + M_F L_4 M_S L_1)(2CL_5)) \quad [44]$$

$$D3 = 4s^2(2(M_S L_1 M_u L_6 + M_F L_4 M_u L_6)(2C_1 L_2 - 2C_2 L_3) + 2(M_S L_1 M_u L_6 + M_F L_4 M_S L_1)(2KL_5) + (M_S L_1 + M_u L_6 + M_F L_4)(C_1 L_2 CL_5 - C_2 L_3 CL_5)) \quad [45]$$

$$D4 = s(M_S L_1 + M_u L_6 + M_F L_4)(K_1 L_2 CL_5 - K_2 L_3 CL_5 + C_1 L_2 KL_5 - C_2 L_3 KL_5) \quad [46]$$

$$D5 = 4(M_S L_1 + M_u L_6 + M_F L_4)(K_1 L_2 KL_5 - K_2 L_3 KL_5) \quad [47]$$

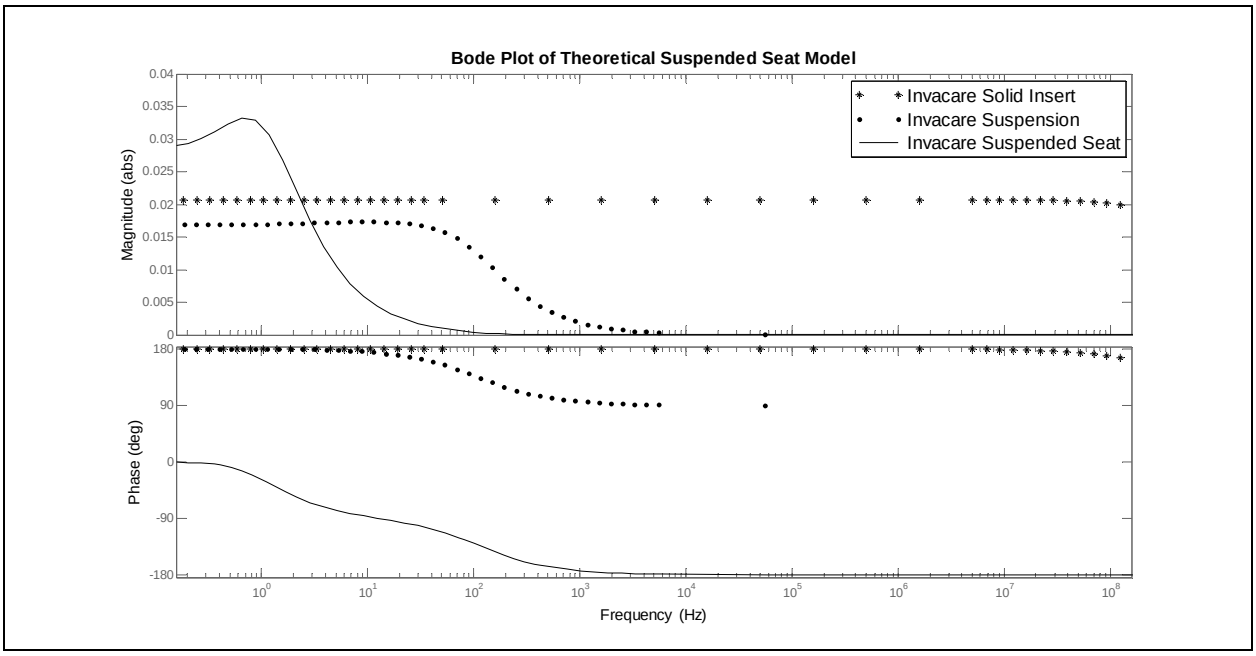

Figure 69 - Bode Diagram of the Invacare 3G Torque SP with aluminum solid inserts, suspension and a theoretical suspended seat

Figure 69 shows the Bode diagram of the Invacare 3G Torque SP with solid inserts, suspension and the theoretical suspension under the seat. The values that were used for the spring and damper constants were K1=K2=1000 N/m and C1=C2=300 N*sec/m. These values were selected to show that suspension at the seat can theoretically reduce the transmission of vibration to users. Further work should be done to design and test power wheelchair seat suspension.

5.4 DISCUSSION

An isolator that can reduce the amount of vibration in a system [65-67], in this case, transmission of whole-body vibrations to wheelchair users, and at the same time increase the performance of electric powered wheelchairs would be invaluable.

As seen in the above Bode plots (Figures 60 and 61) that show the frequency response of the system, the transfer function between the input and the output of the system is represented as a low pass filter. This makes physical sense because the resultant acceleration at the seat is at least an order of magnitude lower than the input force and because of the damper, the high frequency oscillatory vibrations are dissipated. The low pass filter can account for both of these transitions between the input and output.

The suspension can reduce the amount of harmful vibrations in two ways. First the system parameters, namely the spring constant, can be adjusted to decrease the passed amplitude as much as possible. This will reduce the magnitude of the vibrations experienced by the user. The second option is to shift the frequency away from the harmful 4-12 Hz region designated by the ISO 2631-1 standard.

Based on the results shown in the Bode plots two things are immediately apparent. The system does a good job of reducing the amplitude of the input force of the system. The second is that as both the spring constant and the damper constant increase the cutoff frequency of the low pass filter increases as well, which means that more of the force data gets passed through the system. This can be seen in the Bode plots of the suspension wheelchairs fitted with the solid aluminum inserts. This becomes important because, based on the Fourier spectrum analysis of the force data, most of the higher magnitude energy is located at lower frequencies. Therefore in order to adequately reduce the harmful whole-body vibrations transmitted to wheelchair users,

the spring and damper constants would have to be very low. Theoretically this seems acceptable but when thinking about the physical reality this becomes an impossibility.

With a very low spring constant and damper constant some of the lower frequencies of forces would be cut out. However, at the same time, there would be much more residual oscillatory vibration transmitted due to the low damper constant. Additionally the very low spring constant would cause a lot of bouncing in the system, especially during starting and stopping. This result can be shown through a simulation of the transfer function by applying a step input and an impulse input. The step input represents an oscillatory input and the impulse input represents a transient shock input. The results of this simulation can be seen in Appendix E. As the spring and damper constants are decreased, the amplitude and the resonance oscillations of the resultant signal increase for both inputs. This is important to powered wheelchair users because a large proportion have limited upper trunk control. Any additional inertia during starting and stopping may cause large forces and motions of the upper body and may result in larger fore-aft vibrations and possibly tips and falls.

The comparison between the measured accelerations and the accelerations calculated from the model showed that in the 1-20 Hz range, the measured accelerations were significantly higher than the modeled acceleration (p=0.024). However for the 4-12 Hz range the measured accelerations and the modeled accelerations were not significantly different (p=0.233). Looking at the spectra of the force data in Chapter 3, most of the force transmission occurs in the 4-12 Hz range. A predominant amount of the measured accelerations also occurs in the 4-12 Hz range, arising from the natural frequency of the human body. However there may be additional measured vibrations in the 1-4 Hz and 12-20 Hz range, causing the measured values to be significantly higher than the modeled values. This can be accounted for in future research in

multiple ways. It may be more appropriate to develop a computer model of the power wheelchairs including more specific frame characteristics and a more detailed human user model including anthropometric measurements and segment masses. Also it would be useful to collect additional vibration data from the footrest of the wheelchair and from the wheelchair frame and include that data in the model.

The apparent mass calculated from the measured forces and accelerations were consistent with literature cited in that the resonance frequencies occur in the 5-10 Hz range, with the exception of the dimple strip which presents as more of a broadband signal. Results showed that significant differences in the average normalized apparent mass only existed at the curb descent and at the carpeting. For these two obstacles the Invacare with suspension and the Quickie in the Low and Middle suspension settings had significantly higher apparent masses than their respective solid insert trials. This result shows that for these two obstacles, which happen to produce shock vibrations, the output accelerations are significantly lower for the suspension settings than the solid insert settings, which is confirmed by the results in the previous section. This difference in apparent masses at the curb descent and the carpeting shows that when wheelchairs are exposed to shocks, the suspension elements are good at lowering the transmission of that shock to the user. The apparent mass calculation may be a good metric for use in future research to determine the effectiveness of suspension in wheelchairs. The apparent mass may be more effective at showing different levels of transmission in various wheelchairs with suspension and at what specific frequencies those differences occur at.

The model that explores suspending the wheelchair seat by placing additional suspension elements between the frame and the seat showed interesting results. The Bode plot of the model with a spring-damper suspended seat shows a reduction in the cutoff frequency of the low pass

filter rather than an attenuation of the amplitude. There is actually an increase in the passed amplitude followed by a far steeper cutoff transition when compared to the original model. However, because the peak occurs at around 2.5 Hz which is not within the 4-12 Hz range considered most harmful by the ISO 2631-1 Standard, this model may still attenuate the vibrations at the seat. Additionally, the parameters of the seat suspension can be further explored to identify an optimized setting that may reduce more vibrations.

Limitations of this study include the use of only two suspension power wheelchairs. As mentioned in a previous section at the inception of this study, the two wheelchairs tested were among the most popular and commonly prescribed on the market. The wheelchair model, although very complete in including all measured inputs and outputs as well as the physical measurements of the wheelchairs, did not include certain elements such as the material characteristics of the frame and the drive wheel and caster tires that may contribute to different results. Also a more detailed user mass should be included in the model as well incorporating segment lengths and masses.

Future work should examine a complete model of a power wheelchair. Only two models of power wheelchair were examined, and since the inception of this study new suspension power wheelchairs have become available. However the basic science of modeling a power wheelchair was examined and could be applied to any power wheelchair to examine the effectiveness of the suspension system. Based on the development of the power wheelchair models in this paper, additional mathematical models should be developed of current power wheelchairs that are available on the market. These models can be compared to determine the effectiveness of these power wheelchairs at reducing vibration transmitted to users. Future work should also include the further exploration of seat suspension, specifically what type to use (spring, air, elastomer,

etc.) and what spring and damper constant values should be used. Following this, a prototype power wheelchair with suspended seat should be developed and tested.

When wheelchair companies began adding suspension to electric powered wheelchairs, the reduction of transmissions of whole-body vibrations to wheelchair users may not have been a top priority. Instead they may have concentrated on increasing the maneuverability, handling, and durability which are all extremely important factors. However with the increases in these other features, wheelchair users became more independent and were therefore exposed to higher and more frequent vibration requiring vibration reduction as well as enhanced performance.

6.0 CONCLUSION

The overall focus of this work was to evaluate the effect of whole-body vibrations on power wheelchair users. Before this work began very little data existed on the amounts of whole-body vibration experienced by power wheelchair users during driving. Data on other populations that are exposed to vibration while in a seated position have been thoroughly examined [2-12] and have shown that chronic injuries such as low-back pain and disc degeneration, and acute effects such as motion sickness, and muscle fatigue and spasm. The wheelchair user population is exposed to whole-body vibration under similar circumstances in that they are exposed while in a seated position and the time of exposure is high. Vibrations experienced by manual wheelchair users have been reported and have shown that manual wheelchair users are exposed to levels of whole-body vibration that could be considered harmful [13-16]. Other studies have been conducted to examine other factors involved in the amount of whole-body vibration transmitted to manual wheelchair users, including cushion selection and type of wheelchair, i.e. rigid frame, folding frame, or suspension manual wheelchairs [28-30, 38, 43, 44].

Previous studies have examined manual and power wheelchair driving over different sidewalk surfaces [26, 41]. Results have shown that differences exist between sidewalk surfaces, and that there are certain interlocking paver surfaces that transmit lower amounts of vibration to wheelchair users than a standard poured concrete surface. This work examined the differences in nine sidewalk surfaces as well as examining changes in surfaces longitudinally. Results showed that there were significant changes in the amount of transmitted vibration over

time, however there was no recognizable pattern of that change. Collection of data at additional times could reveal a more distinct pattern of significant or non-significant changes due to wear over time. Other factors come into play when recommending interlocking concrete pavers for use in access routes used by wheelchair users. Cost may be an important factor to consider. However while the standard poured concrete surface may be less costly to install initially, the interlocking paver surfaces may cost less long term because maintenance only involves removing damaged pavers and replacing them as opposed to replacing the entire surface. Another factor is that wear and heaving of the pavers may result in higher vibration exposures over time. However, because maintenance of surfaces can be addressed by fixing individual pavers this problem can be absolved easily.

Unique ground force and moment sensors ($SMART^{HUB}$ and $SMART^{CASTER}$) for use on power wheelchairs were developed, and tested. The application of this data can provide potential improvements in both power wheelchair frame durability and primarily for the benefit of this research, suspension in power wheelchairs. Data can be used in conjunction with a finite element analysis of power wheelchair frames to enhance durability and cost effectiveness. Data can also be used to improve power wheelchair controllers. By incorporating the drive wheel forces and torques into controller models, algorithms can be developed to enhance performance and safety during driving.

Following the first development and calibration of the $SMART^{HUBS}$ and $SMART^{CASTERS}$ there were problems that arose with calibration and the data collection. The calibration was incomplete because the wheels were not dynamically tested. In the second attempt, the forces applied to the $SMART^{HUBS}$ and $SMART^{CASTERS}$ during calibration were sinusoidal with varying frequency and magnitude, which allowed for a more appropriate calibration through realistic

application of forces and moments. Secondly, after the first development of the SMART^{HUBS} and SMART^{CASTERS}, the data gathered from the strain gages during testing became noisy and began experiencing dropout. This degradation most likely occurred from poor bonding and a loss of contact with the titanium sensor. This problem was remedied with the second attempt by applying a polymer coating over each strain gage following the bonding and wiring.

After learning from the mistakes in the first development attempt, the SMART^{HUBS} and SMART^{CASTERS} were successfully developed and calibrated and were then used to evaluate the forces experienced during driving over an activities of daily living course. The results of these testing showed differences in measured forces between suspension settings over three of the six tested obstacles (the door threshold, the curb descent, and the carpeting). This result most likely occurs because these three obstacles produce transient shock forces as opposed to the oscillatory forces produced by the other obstacles. The suspension elements in the wheelchairs most likely have the greatest impact at reducing shocks and therefore attenuate some of the force while driving over these obstacles.

Two different suspension power wheelchairs were tested to determine if differences existed between suspensions and if suspension in power wheelchairs is effective at reducing the amounts of whole-body vibrations transmitted to drivers. Results showed that for drivers traveling over an activities of daily living course, suspension was effective at reducing the amount of vibration transmitted, however the levels of vibration may not be attenuated enough to adequately reduce secondary injury in power wheelchair users. Another interesting finding is that, through the use of the SITBAR, transmissibility of the foam cushion used by subjects was found to amplify the amounts of vibration transmitted directly at cushion / user interface. . This result may occur from vibration input at the feet of the user. A model, incorporating user

anthropometrics and acceleration inputs from beneath the cushion, the feet, and the SITBAR, could provide valuable information on the relationship between the vibrations measured beneath the cushion and at the feet and the vibrations that are transmitted directly to the user.

A model of a suspension power wheelchair was developed consisting of the input forces at the drive wheels and casters, and the mass of the frame and the subject separated by the suspension elements. Through a mathematical assessment of this model a transfer function was established. Results showed that the model was good at predicting the accelerations at the seat in the 4-12 Hz range however the model underestimated the accelerations in the 1-20 Hz range. A more complete computer model including more specific frame characteristics and more detailed user parameters such as segment lengths and masses, and the inclusion of additional vibration outputs, at the footrest and at on the frame could remedy this discrepancy.

An alternative model was also examined. This model was a prospective theoretical model that included added suspension elements between the frame and the seat. Results showed the possibility of additional attenuation of vibrations at the seat through a reduction in passed frequencies of vibration. The model shows a shift in the cutoff frequency rather than a reduction in the amplitude of the signal. A great benefit of this type of model is that alternative suspension characteristics (i.e. the spring and damper constants), suspensions (i.e. elastomer, or air springs), and suspension placements can be examined and compared. These results are promising and could result in a new suspension model of power wheelchairs specifically designed to reduce whole-body vibrations transmitted to wheelchair users.

Overall the results from this work show that, suspension power wheelchairs are capable of reducing vibrations transmitted to power wheelchair users. However based on the results from the whole-body vibration testing and modeling of the suspension wheelchairs, it seems that

suspension in power wheelchairs is more appropriately designed for handling and performance. By no means are these unimportant factors, especially since power wheelchair users are more active than any other time in history, probably due to advancements in power wheelchair designs, including suspension. These suspension systems provide added safety and performance to power wheelchairs by maintaining ground contact with wheels and increasing traction to drive wheels. However, because power wheelchair users are more active and frequently encounter obstacles that can cause transmission of harmful shocks and vibrations, suspension becomes more important, and even though suspension was found to attenuate vibration it may not be sufficient to reduce injury.

Future work should first more closely examine the levels of whole-body vibration that power wheelchair users experience during their normal activities. The use of data loggers has become extremely useful in recent years at examining the activity levels of wheelchair users [17] and similar technology should be developed to examine accelerations during power and manual wheelchair use over extended periods of time (i.e. days and eventually weeks). This data can be used to more appropriately study the possible long term effects of whole-body vibration on power wheelchair users by more clearly understanding levels of vibration that power wheelchair users experience and what activities are causing the vibrations. Evaluating the vibration doses that users are exposed to during their day will provide more information as to the health effects that wheelchair users may experience over time due to WBV. Additionally, exposure to whole-body vibration may cause some wheelchair users to drive less due to the effects. Users with diagnoses such as MS, ALS, or with high Spinal Cord Injury, who's energy levels change dramatically from day to day and throughout the day may experience higher levels of fatigue and pain due to WBV exposure. Future studies may be able to measure this increase in fatigue and

pain by incorporating questionnaires and subject journals, along with the collection of vibrations throughout the day.

This data should also be used to examine more detailed power wheelchair models with the intent of developing a power wheelchair that can further attenuate the amounts of whole-body vibrations transmitted to users. Mathematical models of more current power wheelchairs should be developed and compared to determine their effectiveness at reducing the transmission of whole-body vibration. The transfer function responses of current power wheelchairs can be compared to evaluate the amplitudes and the cutoff frequency of the vibrations that are transmitted. Manual wheelchairs can also be evaluated and compared using mathematical models, and like the work done in section 5.3.4, theoretical designs of suspension manual wheelchairs can be tested.

With the use of more advanced computer modeling, a power wheelchair with suspension specifically intended to reduce vibrations should be developed, examining alternative suspension placement, inclusion of additional suspension elements specifically at the seat, different suspension materials (i.e. air, elastomers, metal springs). Additionally, active suspension has become an area of interest in occupations concerned with whole-body vibration exposure and the automotive injury. The theory behind active suspension is to evaluate the vibrations being experienced by the system in real time (i.e. vibrations while driving a bus), and adjust the suspension of the system to maximum the attenuation of vibration output (i.e. exposure of whole-body vibration to the driver). The benefit of active suspension is that it may further reduce the transmission of whole-body vibration to users. Some negatives of active suspension are that it adds weight to the system, and also requires addition energy to drive suspension changes.

With additional research and development more effective suspension power wheelchairs, with specific designs to reduce exposure to whole-body vibration, can be produced that can reduce or eliminate acute and chronic ailments in users and can improve quality of life.

APPENDIX A

COMPUTER AIDED DESIGN DRAWINGS FOR SMART^{HUB} AND SMART^{CASTER}

Core Sensor for the SMART^{CASTER}

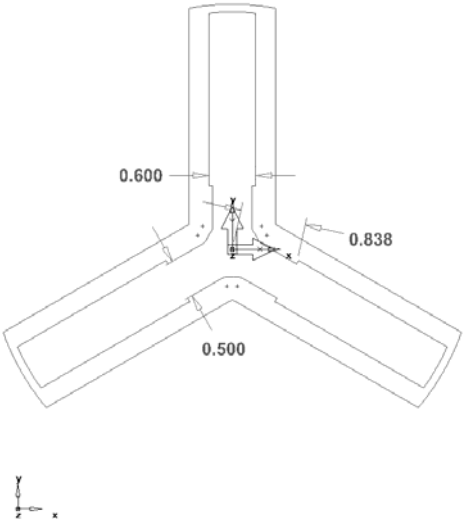

Outer Hub for the SMART^{CASTER}

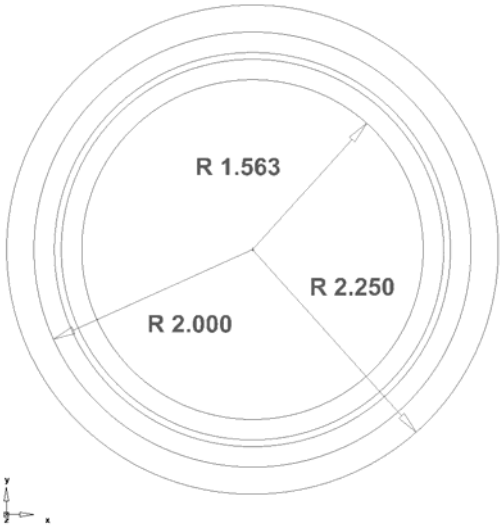

Inner Hub for the SMART^{CASTER}

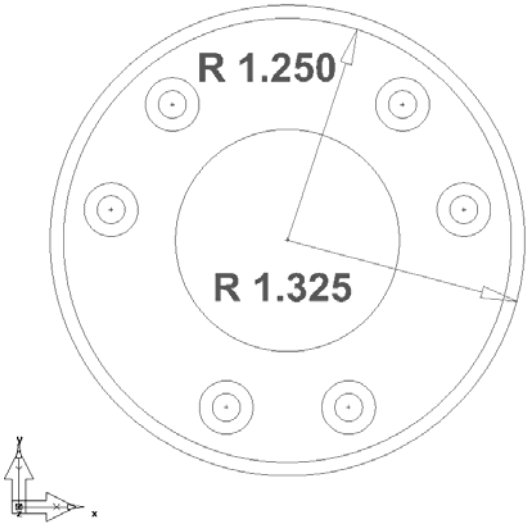

Solid Model of finished SMART^{CASTER}

Core Sensor for the SMART^{HUB}

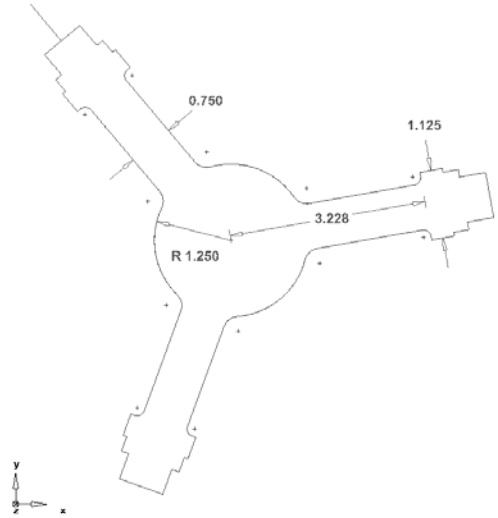

Outer Hub for the SMART^{HUB}

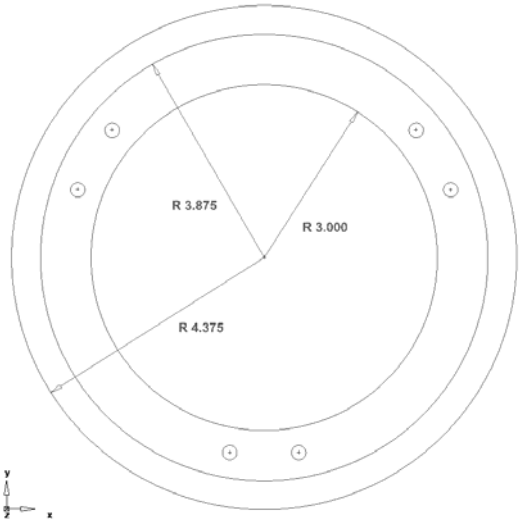

Solid Model of finished SMART^{CASTER}

PARTS LIST

SMART^{CASTER}

Core Sensor

1. Titanium Alloy Plate Stock (Grade 5 – 6AL-4V)
2. 0.75" OD x 0.625" ID x 0.25" Carbide Bushings
3. 350 Ohm, Dual Pattern, General Purpose Strain Gages
4. 0.0625” x 0.0625” Key Stock

Inner Hub

1. 6061-T6 Aircraft Aluminum Plate Stock
2. Kaydon Reali-Slim Bearings 2” ID x 2.5” OD

Outer Hub

1. 6061-T6 Aircraft Aluminum Plate Stock

SMART^{HUB}

Core Sensor

1. Titanium Alloy Plate Stock (Grade 5 – 6AL-4V)
2. 1.125" OD x 1" ID x 0.5" Carbide Bushings
3. 350 Ohm, Dual Pattern, General Purpose Strain Gages

Outer Hub

1. 6061-T6 Aircraft Aluminum Plate Stock

Data Logger

1. Tattletale Model 8v2 Pin and Socket with 1 MB SRAM
2. 5x3 in Bus Exp Board for Tattletale 8v2
3. PC Serial Interface Cable

Amplifier Board

1. Prototype Amplifier Board (Diagram provided in Appendix B)
2. Li-Ion 7.2V, 1800mAh Digital Camcorder Batteries
3. SN74LS74AN IC Dual D-Type Flip-Flop 14-DIP
4. IC LP Instrumentation Amplifier 8 DIP
5. Resistor 510 OHM 1/8W 5% CARBON FILM
6. Resistor 10K OHM 1/8W 5% CARBON FILM
7. Resistor 200 OHM 1/8W 5% CARBON FILM
8. Potentiometer 5.0K OHM 3/8" SQ CERM SL MT

APPENDIX B

SCHEMATIC OF AMPLIFIER BOARD FOR SMART^{HUB} AND SMART^{CASTER}

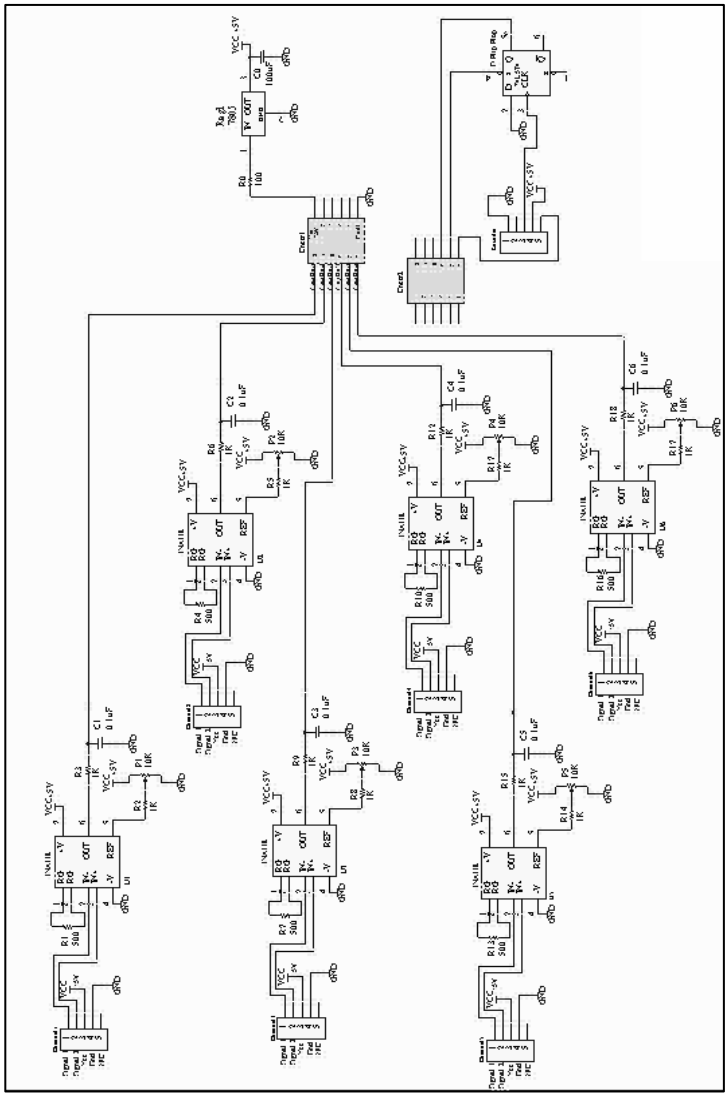

APPENDIX C

MATLAB CODE FOR ACCELERATION DATA ANALYSIS

```
files=['mt12_iin.thr';'mt12_isu.thr';'mt12_qin.thr';...
    'mt12_qls.thr';'mt12_qmi.thr';'mt12_qmo.thr'];

RMS1=[];
VDV1=[];

%Data in the vertical direction is analyzed
%for each suspension setting (1-6)

for i=1:6
    string=['x=importdata(''',files(i,:),''');'];
    eval(string);

    %calibration constant for the seat accelerometer(4g)
    k_acc=.3633;

    %sampling frequency
    fs=200;

    acc_x=k_acc*(x(:,1)-mean(x(1:50,1)));
    acc_y=k_acc*(x(:,2)-mean(x(1:50,2)));
    acc_z=k_acc*(x(:,3)-mean(x(1:50,3)));

    figure
    plot(acc_z)
    hold on
    plot(x(:,12)*20,'r')

    weighting_filter_design_v5;

    m=find(x(:,12)==1);

%Each obstacle in the trial is defined by a start and stop marker.
%Obstacles are devided and weighting filter
%is applied to acceleration data.
    vert_1_1=filter(numd_wk,dend_wk,acc_z(m(1):m(2)));
```

```
    vert_1_2=filter(numd_wk,dend_wk,acc_z(m(3):m(4)));
    vert_1_3=filter(numd_wk,dend_wk,acc_z(m(5):m(6)));
    vert_1_4=filter(numd_wk,dend_wk,acc_z(m(7):m(8)));
    vert_1_5=filter(numd_wk,dend_wk,acc_z(m(9):m(10)));
    vert_1_6=filter(numd_wk,dend_wk,acc_z(m(11):m(12)));
    vert_2_1=filter(numd_wk,dend_wk,acc_z(m(13):m(14)));
    vert_2_2=filter(numd_wk,dend_wk,acc_z(m(15):m(16)));
    vert_2_3=filter(numd_wk,dend_wk,acc_z(m(17):m(18)));
    vert_2_4=filter(numd_wk,dend_wk,acc_z(m(19):m(20)));
    vert_2_5=filter(numd_wk,dend_wk,acc_z(m(21):m(22)));
    vert_2_6=filter(numd_wk,dend_wk,acc_z(m(23):m(24)));
    vert_3_1=filter(numd_wk,dend_wk,acc_z(m(25):m(26)));
    vert_3_2=filter(numd_wk,dend_wk,acc_z(m(27):m(28)));
    vert_3_3=filter(numd_wk,dend_wk,acc_z(m(29):m(30)));
    vert_3_4=filter(numd_wk,dend_wk,acc_z(m(31):m(32)));
    vert_3_5=filter(numd_wk,dend_wk,acc_z(m(33):m(34)));
    vert_3_6=filter(numd_wk,dend_wk,acc_z(m(35):m(36)));

%The Root Mean Square (RMS) and Vibration Dose Value (VDV) calculations.
%Values are calculated for each obstacle
    RMS=[sqrt(trapz((vert_1_1).^2)/(length(vert_1_1))),...
        sqrt(trapz((vert_1_2).^2)/(length(vert_1_2))),...
        sqrt(trapz((vert_1_3).^2)/(length(vert_1_3))),...
        sqrt(trapz((vert_1_4).^2)/(length(vert_1_4))),...
        sqrt(trapz((vert_1_5).^2)/(length(vert_1_5))),...
        sqrt(trapz((vert_1_6).^2)/(length(vert_1_6))),...
        sqrt(trapz((vert_2_1).^2)/(length(vert_2_1))),...
        sqrt(trapz((vert_2_2).^2)/(length(vert_2_2))),...
        sqrt(trapz((vert_2_3).^2)/(length(vert_2_3))),...
        sqrt(trapz((vert_2_4).^2)/(length(vert_2_4))),...
        sqrt(trapz((vert_2_5).^2)/(length(vert_2_5))),...
        sqrt(trapz((vert_2_6).^2)/(length(vert_2_6))),...
        sqrt(trapz((vert_3_1).^2)/(length(vert_3_1))),...
        sqrt(trapz((vert_3_2).^2)/(length(vert_3_2))),...
        sqrt(trapz((vert_3_3).^2)/(length(vert_3_3))),...
        sqrt(trapz((vert_3_4).^2)/(length(vert_3_4))),...
        sqrt(trapz((vert_3_5).^2)/(length(vert_3_5))),...
        sqrt(trapz((vert_3_6).^2)/(length(vert_3_6)))];

    VDV=[(trapz((vert_1_1).^4)/fs)^.25,(trapz((vert_1_2).^4)/fs)^.25,...
        (trapz((vert_1_3).^4)/fs)^.25,(trapz((vert_1_4).^4)/fs)^.25,...
        (trapz((vert_1_5).^4)/fs)^.25,(trapz((vert_1_6).^4)/fs)^.25,...
        (trapz((vert_2_1).^4)/fs)^.25,(trapz((vert_2_2).^4)/fs)^.25,...
        (trapz((vert_2_3).^4)/fs)^.25,(trapz((vert_2_4).^4)/fs)^.25,...
        (trapz((vert_2_5).^4)/fs)^.25,(trapz((vert_2_6).^4)/fs)^.25,...
        (trapz((vert_3_1).^4)/fs)^.25,(trapz((vert_3_2).^4)/fs)^.25,...
        (trapz((vert_3_3).^4)/fs)^.25,(trapz((vert_3_4).^4)/fs)^.25,...
        (trapz((vert_3_5).^4)/fs)^.25,(trapz((vert_3_6).^4)/fs)^.25];

    RMS1=[RMS RMS1];
    VDV1=[VDV VDV1];
end

%Trial 1 = Invacare Solid Insert
%Trial 2 = Invacare Suspension Element
%Trial 3 = Quickie Solid Insert
```

```
%Trial 4 = Quickie Least Stiff
%Trial 5 = Quickie Mid Stiff
%Trial 6 = Quickie Most Stiff

%Obstacle 1 = Deck Surface
%Obstacle 2 = Door Threshold
%Obstacle 3 = Curb Descent
%Obstacle 4 = Dimple Strip
%Obstacle 5 = Smooth Concrete
%Obstacle 6 = Carpet

%Data is organized so that each RMS and VDV value is assigned to the
%corresponding suspension system and obstacle
trial=[6*ones(18,1);5*ones(18,1);4*ones(18,1);3*ones(18,1);2*ones(18,1);1*one
s(18,1)];
obs=[1;2;3;4;5;6];
obs2=[obs;obs;obs;obs;obs;obs;obs;obs;obs;obs;obs;obs;obs;obs;obs;obs;obs;obs
];
final_matrix=[obs2 trial RMS1' VDV1'];

save mt12_final.xls final_matrix -ascii -tabs;
```

MATLAB CODE FOR ISO 2631-1 FREQUENCY WEIGHTINGS

```
%function [numd_wk, dend_wk, numd_wd, dend_wd]=weighting_filter_design_v5
%Weighting based on ISO 2631-1:1997, Annex A
%numd_wk==numerator used in the filter.m function for the vertical
accelration weighting
%dend_wk==denomenator used in the filter.m function for the vertical
accelration weighting
%numd_wd==numerator used in the filter.m function for the horizontal
accelration weighting
%dend_wd==denomenator used in the filter.m function for the horizontal
accelration weighting
%
%USE WEIGHTING_FILTER_DESIGN_V4 TO EXAM PLOTS OF THE WEIGHTING FUNCTIONS
%REMOVE THE '%%' TO EXAMINE FILTERS IN LAPLACE DOMAIN AND TO PLOT
%   THE WEIGHTING FILTERS FOR THE VERTICAL ACCELERATION AND THE HORIZONTAL
ACCELERATIONS
%
%NOTE: s==p. p is used in the standards in lieu of s. s and p are just the
laplace operator
%Low pass filter
%
%                   2
%               w2
%Hl(s)=------------------------
%       2                     2
%      s  + sqrt(2)*w2*s + w2
%
%High pass filter
%                   2
%                  s
%Hh(s)=------------------------
%       2                     2
%      s  + sqrt(2)*w1*s + w1
%
%where  w1=2*pi*f1
%           w2=2*pi*f2
%
%Acceleration-Velocity Transition Filter
%            2
%            w4           2
%        ------ * s + w4
%          w3
%Hac(s)=------------------------
%        2     w4        2
%       s  + -----*s + w4
%              Q4
%Upward step
%
%            2    w5           2
%           s  + ---- * s + w5
%                Q5
%
```

```
%Hs(s)= ------------------------------
%            2    w6          2
%           s  + ---- * s + w6
%                Q6
%
Fs=200; %Sampling Frequency
w1_k=2*pi*0.4; %High pass cut-off frequency in hertz
w1_d=w1_k;
w2_k=2*pi*100; %Low pass cut-off frequency in hertz
w2_d=w2_k;
w3_k=2*pi*12.5;
w3_d=2*pi*2.0;
w4_k=2*pi*12.5;
w4_d=2*pi*2.0;
w5_k=2*pi*2.37;
w6_k=2*pi*3.35;

Q4_k=0.63;
Q4_d=0.63;
Q5_k=0.91;
Q6_k=0.91;
%Low Pass Filter
num_l_k=w2_k^2;
den_l_k=[1 , w2_k*sqrt(2), w2_k^2];
num_l_d=w2_k^2;
den_l_d=[1 , w2_d*sqrt(2), w2_d^2];
%Transform from s-domain to z-domain using a bilinear transformation
[numd_l_k, dend_l_k]=bilinear(num_l_k, den_l_k, Fs);
[numd_l_d, dend_l_d]=bilinear(num_l_d, den_l_d, Fs);

%High Pass Filter
num_h_k=[1 0 0];
den_h_k=[1, w1_k*sqrt(2), w1_k^2];
num_h_d=[1 0 0];
den_h_d=[1, w1_d*sqrt(2), w1_d^2];
%Transform from s-domain to z-domain using a bilinear transformation
[numd_h_k, dend_h_k]=bilinear(num_h_k, den_h_k, Fs);
[numd_h_d, dend_h_d]=bilinear(num_h_d, den_h_d, Fs);

%Acceleration-Velocity Transition Filter
num_t_k=[(w4_k^2/w3_k), w4_k^2];
den_t_k=[1, w4_k/Q4_k, w4_k^2];
num_t_d=[(w4_d^2/w3_d), w4_d^2];
den_t_d=[1, w4_d/Q4_d, w4_d^2];
%Transform from s-domain to z-domain using a bilinear transformation
[numd_t_k, dend_t_k]=bilinear(num_t_k, den_t_k, Fs);
[numd_t_d, dend_t_d]=bilinear(num_t_d, den_t_d, Fs);

%Upward step Filter
num_s_k=[1, w5_k/Q5_k, w5_k^2];
den_s_k=[1, w6_k/Q6_k, w6_k^2];
%num_s_d=1;
%den_s_d=1;
%Transform from s-domain to z-domain using a bilinear transformation
[numd_s_k, dend_s_k]=bilinear(num_s_k, den_s_k, Fs);
%NOTE:  The upward step filter for the horizontal direction is unity so
```

```
%           we don't need to worry about it.

%Combine Filters in s-domain (aka laplace)
num_h_l_k=conv(num_l_k, num_h_k);
num_h_l_d=conv(num_l_d, num_h_d);
den_h_l_k=conv(den_l_k, den_h_k);
den_h_l_d=conv(den_l_d, den_h_d);
num_t_s_k=conv(num_t_k, num_s_k);
den_t_s_k=conv(den_t_k, den_s_k);
num_wk=conv(num_h_l_k, num_t_s_k);
num_wd=conv(num_h_l_d, num_t_d);
den_wk=conv(den_h_l_k, den_t_s_k);
den_wd=conv(den_h_l_d, den_t_d);

%[numd_w_k, dend_w_k]=bilinear(num_w_k, den_w_k, Fs);
%[numd_w_d, dend_w_d]=bilinear(num_w_d, den_w_d, Fs);

%Combine Filters in the z-domain
    %Weightings for vertical accelerations
numd_h_l_k=conv(numd_l_k, numd_h_k);
dend_h_l_k=conv(dend_l_k, dend_h_k);
numd_t_s_k=conv(numd_t_k, numd_s_k);
dend_t_s_k=conv(dend_t_k, dend_s_k);
numd_wk=conv(numd_h_l_k, numd_t_s_k);
dend_wk=conv(dend_h_l_k, dend_t_s_k);
    %Weightings for horizontal accelerations (fore-to-aft & lateral)
numd_h_l_d=conv(numd_l_d, numd_h_d);
dend_h_l_d=conv(dend_l_d, dend_h_d);
numd_wd=conv(numd_h_l_d, numd_t_d);
dend_wd=conv(dend_h_l_d, dend_t_d);
```

APPENDIX D

CODE FOR DATA COLLECTION USING THE TATTLETALE 8V2 DATA LOGGER

```
/*********************************************************************/

#include    <TT8.h>           /* Tattletale Model 8 Definitions */
#include    <tat332.h>  /* 68332 Tattletale (7,8) Hardware Definitions */
#include    <sim332.h>  /* 68332 System Integration Module Definitions */
#include    <qsm332.h>  /* 68332 Queued Serial Module Definitions */
#include    <tpu332.h>  /* 68332 Time Processing Unit Definitions */
#include    <dio332.h>  /* 68332 Digital I/O Port Pin Definitions */
#include    <tt8pic.h>  /* Model 8 PIC Parallel Slave Port Definitions */
#include    <tt8lib.h>  /* definitions and prototypes for Model 8 library */

#include    <stdio.h>
#include    <stdlib.h>
#include    <userio.h>

/*Create Variables*/

int         Delay;
void        SetupIRQ2(void);
void        IRQ2Handler(void);

int         count = 0;        /*right*/
int         count1 = 0;       /*left*/
int         speed;
int         direction;
int         fwd_bwd;
int         trigger;
ulong       revolution=0;
ulong       revolution1=0;
int         i;
int         n;
int         direction_left = 0;
int         direction_right = 0;

/*********************************************************************
**    main
*********************************************************************/
void main(void)
```

```
      {
      InitTT8(NO_WATCHDOG,TT8_TPU);
      printf ("start\n");
      SetupIRQ2();
      TPUSetPin(7,1);
      TPUSetPin(8,1);
      Delay=0;

      count = 0;
      count1 = 0;

/*Enable the Trigger to start data collection*/

      while (trigger == 0)
      {     trigger = TPUGetPin(11);
            DelayMilliSecs(20);
            printf("%5d \n",trigger);
      }
      DelayMilliSecs(3000);
for(;;)
      {

/*Create Additional Variables for Data Storage*/

{
 short ch0,ch1,ch2,ch3,ch4,ch5,Ax1,Ax2,Ay1,Ay2,Az1,Az2,AD6,AD7,Pin_input;
 long i;
 long TickRate;              /* The current rate of the system clock */
 long sample;
 char cmd;                   /* The current sample number */
 short *valuePtr;            /* Pointer to stored values */
 XmdmErr  ErrorCode;         /* Error Code for Xmodem send */
 short MaxValue, MinValue;   /* data analysis variables */
 long  RunningSum, AveValue; /* same */
 ushort Tpoints;

 TickRate = GetTickRate();      /* Gets the current clock rate */
 valuePtr = malloc( 900000 ); /* allocate mem */

 /*printf("\nLogging\n");*/
 Sleep(0);                      /* Initialize sleep counter    */
 Tpoints=5;

/*Data Collection - create the six data channels data logger*/

  ch0= AtoDReadMilliVolts(0);
  ch1=AtoDReadMilliVolts(1);
  ch2=AtoDReadMilliVolts(2);
  ch3=AtoDReadMilliVolts(3);
  ch4=AtoDReadMilliVolts(4);
  ch5=AtoDReadMilliVolts(5);
      }

/*Begin Data Collection*/

for (i=0;i<=9999;i++) /*Collect 10000 points*/
```

```
{
Sleep(200);
valuePtr[i*7]=AtoDReadMilliVolts(0);
valuePtr[i*7+1]=AtoDReadMilliVolts(1);
valuePtr[i*7+2]=AtoDReadMilliVolts(2);
valuePtr[i*7+3]=AtoDReadMilliVolts(3);
valuePtr[i*7+4]=AtoDReadMilliVolts(4);
valuePtr[i*7+5]=AtoDReadMilliVolts(5);
valuePtr[i*7+6]=count;
}
printf("\n Set Baud Rate 38400, Download Data \n");
SerSetBaud(38400L,0);
while(ErrorCode = XmodemSendMem(valuePtr, 56000,1120))
printf("Load Failed, Try Again \n");
printf("Load Complete \n");
}

/*************************************************************************
**    SetupIRQ2 interrupt
**
*************************************************************************/

void SetupIRQ2(void)
      {
static ExcCFrame  efp2;
      PConfInp(F,2);          /* disallow IRQ1 interrupts here */
      InstallHandler(IRQ2Handler, Level_2_Interrupt, &efp2);
      PConfBus(F,2);          /* allow IRQ1 interrupts here */
      }
/*************************************************************************
**    IRQ2Handler
**    Get Encoder Data
*************************************************************************/
void IRQ2Handler (void)
{
      PConfInp(F,2);
      direction_right = TPUGetPin(1);
      fwd_bwd = TPUGetPin(5);
      if (fwd_bwd == 1)
      {
            count=count-1;
            if (count == -1)
            {count = 499;
            }
                        }
       else
      {
      count++;   }

      TPUSetPin(8,0);
      TPUSetPin(8,1);
      if (count > 499)
            {count = 0;
            }
      PConfBus(F,2);
}
```

APPENDIX E

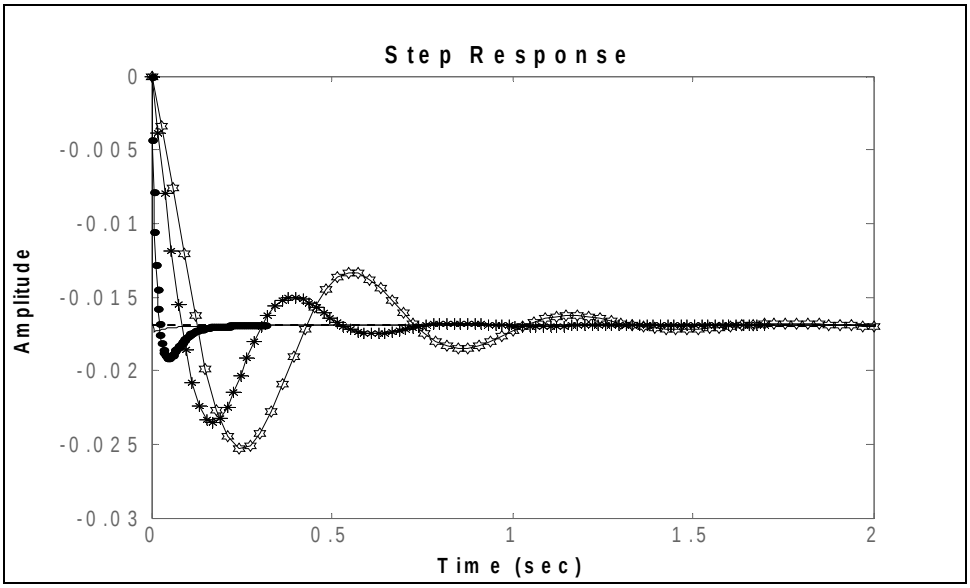
Step Response
Amplitude
Time (sec)
0
-0.005
-0.01
-0.015
-0.02
-0.025
-0.03
0
0.5
1
1.5
2

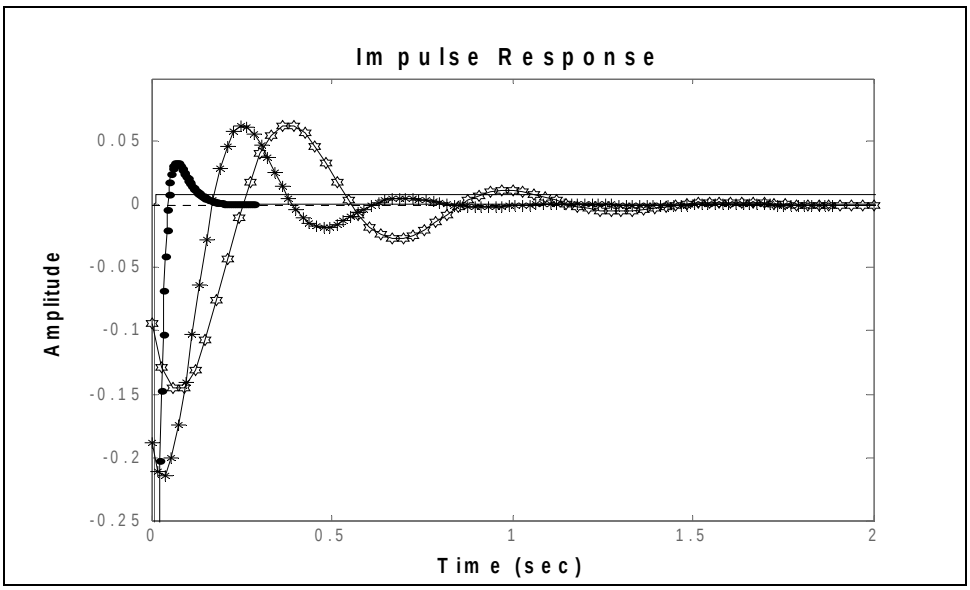
Impulse Response
Amplitude
Time (sec)
0.05
0
-0.05
-0.1
-0.15
-0.2
-0.25
0
0.5
1
1.5
2

BIBLIOGRAPHY

[1] Dieckmann D. A study of the influence of vibration on man. *Ergonomics*. 1957; 1: 347-355.

[2] Seidel H, Heide R. Long term effects of whole-body vibration: a critical review of the literature. *Int Arch Occup Environ Health*. 1986; 58: 1-26.

[3] Kumar A, Varghese M, Mohan D, Mahajan P, Gulati P, Kale S. Effect of whole-body vibration on the low back: a study of tractor-driving farmers in North India. *Spine*. 1999; 24: 2506-2523.

[4] Magnusson M, Pope MH, Wilder DG, Areskoug B. Are occupational drivers at an increased risk for developing musculoskeletal disorders? *Spine*. 1996; 21: 710-717.

[5] Lings S, Leboeuf-Yde C. Whole-body vibration and low back pain: A systematic critical review of the epidemiological literature 1992-1999. *Int Arch Occup Environ Health*. 2000; 73: 290-297.

[6] Pope M, Wilder DG, Magnusson ML. A review of studies on seated whole body vibration and low back pain, *Proc Inst Mech Eng*. 1999; 213: 435-446.

[7] Fairley T. Predicting the discomfort caused by tractor vibration. *Ergonomics*. 1995; 38: 2091-2106.

[8] Dupuis H, Hartung E, Haverkamp M. Acute effects of transient vertical whole-body vibration. *Int Arch Occup Environ Health*. 1991; 63: 261-265.

[9] Mansfield N, Griffin MJ. Difference threshold for automobile seat vibration, *Appl Ergon*. 2000; 31: 255-261.

[10] Griffin MJ. *Handbook of Human Vibrations*. San Diego CA: Academic Press Inc; 1990: 173-186.

[11] Harris CM, Piersol AG, eds. *Harris' Shock and Vibration Handbook*. 5th ed. New York NY: McGraw-Hill Co Inc; 2002: 42.1-42.60.

[12] Nachemson AL, Jonsson E, eds. *Neck and Back Pain; The Scientific Evidence of Causes, Diagnosis, and Treatment*. Philadelphia PA: Lippincott Williams &Wilkins Inc; 2000: 100-106.

[13] VanSickle D, Cooper R, Boninger M, DiGiovine C. Analysis of vibrations induced during wheelchair propulsion. *J Rehabil Res Dev*. 2001; 38: 409-421.

[14] VanSickle DP, Cooper RA, Boninger ML. Road loads acting on manual wheelchairs. *IEEE Trans Rehabil Eng*. 2000; 8(3): 371-384.

[15] DiGiovine C, Cooper R, Wolf E, Fitzgerald S, Boninger M, Guo S. Whole-body vibration during manual wheelchair propulsion with selected seat cushions and back supports. *IEEE Trans Rehabil Eng*. 2003; 11(3): 311-322.

[16] Tai C, Liu D, Cooper RA, DiGiovine MM, Boninger ML. Analysis of vibrations during manual wheelchair propulsion. *Saudi Journal of Disability and Rehabilitation*. 1998; 4(3): 186-191.

[17] Cooper RA, Thorman T, Cooper R. Driving characteristics of electric powered wheelchair users: How far, fast and often do people drive? *Arch Phys Med Rehabil*. 2002; 83: 250-255.

[18] Thompson C, Belanger M. Effects of vibration in inline skating on the Hoffman reflex, force and proprioception. *Med Sci Sports Exerc*. 2002; 34 (12): 2037-2044

[19] Frendo F, Sgueglia M, Vitale E, Hippoliti R. Analysis of motorscooter ride comfort. *Conference of Automotive and Transportation Technology*. SAE: Paris, France; 2002

[20] Mansfield NJ, Griffin MJ. Effect of magnitude of vertical whole-body vibration on absorbed power for the seated human. *Journal of Sound and Vibration*. 1998; 215(4): 813-825.

[21] Bovenzi M, Hulshof, CTJ. An updated review of epidemiologic studies on the relationship between exposure to whole-body vibration and low back pain. *Journal of Sound and Vibration*. 1998; 215(4): 595-611.

[22] Griffin MJ, Vertical vibration of seated subjects: Effects of posture, vibration level, and frequency. *Aviat Space Environ Med*. 1975; 46 (3): 269-276.

[23] Wan Y, Schimmels JM. Optimal seat suspension design based on minimum "simulated subjective response". *J Biomed Eng*. 1997; 119: 409-416.

[24] Nishiyama K, Taoda K, Kitahara T. A decade of improvement in whole-body vibration and low back pain for freight container tractor drivers. *Journal of Sound and Vibration*. 1998; 215(4): 635-642.

[25] Wilder D, Magnusson ML, Fenwick J, Pope M. The effect of posture and seat suspension design on discomfort and back muscle fatigue during simulated truck driving. *Appl Ergon*. 1994; 25(2): 66-76.

[26] Wolf EJ, Pearlman J, Cooper RA. Vibration exposure of individuals using wheelchairs over sidewalk surfaces. *Disabil Rehabil*. 2005; 27(23): 1443-1449.

[27] Maeda S, Futatsuka M, Yonesaki J, Ikeda M, Relationship between questionnaire survey results of vibration complaints of wheelchair users and vibration transmissibility of manual wheelchair. *Environmental Health Prevention Medicine*. 2003; 8: 82-89.

[28] Cooper RA, Wolf EJ, Fitzgerald SG, Boninger ML, Ulerich R, Ammer WA. Seat and footrest shocks and vibrations in manual wheelchairs with and without suspension, *Arch Phys Med Rehabil*. 2003; 84: 96-102.

[29] Kwarciak AM, Cooper RA, Wolf EJ. Effectiveness of rear suspension in reducing shock exposure to manual wheelchair users during curb descents. *Proceedings of the 25th Annual RESNA Conference*. Minneapolis, MN; 2002.

[30] Wolf, E.J., Cooper, R.A., and Kwarciak, A.M. Analysis of whole-body vibrations of suspension manual wheelchairs: utilization of the absorbed power method. *Proceedings of the 25th Annual RESNA Conference*. Minneapolis, MN; 2002.

[31] *ISO 2631-1 - Evaluation of Human Exposure to Whole-Body Vibration - Part 1: General Requirements*. Geneva, Switzerland. International Standards Organization; 1997.

[32] *The problem and measures of interlocking block pavement for eyesight or walking disabled people*. Interlocking Block Association of Japan; 1993: 6-24.

[33] Asato K, Cooper RA, Robertson RN, Ster JF. SMART^{Wheels}: Development and testing of a system for measuring manual wheelchair propulsion dynamics. *IEEE Trans Biomed Eng*. 1993; 40: 1320-1324.

[34] Van Der Woude LHV, Veeger HEI, Rozendal RH. propulsion technique in handrim wheelchair ambulation. *J Med Eng Technol*. 1989; 13: 136-141.

[35] Richter WM, Rodriguez R, Woods KR, Axelson PW. Vinyl coated handrim biomechanics: Balancing ergonomic pros and cons. *Proceedings of the 28th Annual RESNA Conference*. Atlanta, GA; 2005.

[36] VanSickle DP. *Realistic Road Loads and Rider Comfort for Manual Wheelchairs* [dissertation]. Pittsburgh, PA: University of Pittsburgh; 1997.

[37] Baldwin JD, Thacker JG. Characterizations of the dynamic stress response of manual and powered wheelchair frames. *J Rehabil Res Dev*. 1993; 30: 224-232.

[38] Wolf EJ, Cooper RA, DiGiovine CP, Boninger ML, Guo S. Using the absorbed power method to evaluate effectiveness of vibration absorption of selected seat cushions during manual wheelchair propulsion. *Med Eng Phys*. 2004; 26: 799-806.

[39] Webster JG, ed. *The Measurement, Instrumentation, and Sensors Handbook*. Danvers, MA: CRC Press LLC; 1999: 22.9-22.10.

[40] LaPlante MP. Demographics of wheeled mobility device users. *Conference on Space Requirements for Wheeled Mobility*. Buffalo, NY; 2003.

[41] Cooper RA, Wolf EJ, Fitzgerald SG. Evaluation of selected sidewalk pavement surfaces. *J Spinal Cord Med*. 2004; 27(5): 468-475.

[42] Boninger ML, Cooper RA, Fitzgerald SG. Investigating neck pain in wheelchair users. *Am J Phys Med Rehabil*. 2003; 82(3): 197-202.

[43] DiGiovine CP, Cooper RA, Wolf EJ, Fitzgerald SG, Boninger ML. Analysis of whole-body vibration during manual wheelchair propulsion: A comparison of seat cushions and back supports for individuals without disability, *Assist Technol*. 2003; 15: 129-144.

[44] DiGiovine MM, Cooper RA, Boninger ML, Lawrence BM, VanSickle DP, Rentschler AJ. User assessment of manual wheelchair ride comfort and ergonomics. *Arch Phys Med Rehabil*. 2000; 81: 490-494.

[45] Dimarogonas M. *Vibration For Engineers*. Upper Saddle River, NJ: Prentice Hall PTR; 1996: 1-30.

[46] Wong JY. *Theory of Ground Vehicles*. New York, NY: John Wiley & Sons Inc; 1993: 353-360.

[47] Gillespie TD. *Fundamentals of Vehicle Dynamics*, Warrendale, PA: SAE Inc; 1992: 147-151.

[48] Doebelin EO. *System Dynamics*, New York, NY: Marcel Dekker Inc; 1998: 521-562.

[49] Sinha NK, Kuszta B. *Modeling and Identification of Dynamic Systems*. Boston, MA: Kluwer Academic Pub; 1983: 289-300.

[50] Den Hartog JP. *Mechanical Vibrations*. 4th ed. New York, NY: McGraw-Hill Professional; 1956.

[51] Matschinsky W. *Road Vehicle Suspensions*. London, UK: Professional Engineering Publishing Lmtd; 2000: 60-67;

[52] Fairely, TE, Griffin MJ. The Apparent Mass of the Seated Human Body: Vertical Vibration. *Journal of Biomechanics*. 1989; 22: 81-94.

[53] Mansfield NJ, Maeda S. Comparison of the Apparent Mass of the Seated Human Measured Using Random and Sinusoidal Vibration. *Industrial Health*. 2005; 43: 233-240.

[54] Mansfield NJ, Lundstrom R. The Apparent Mass of the Human Body Exposed to Non-Orthogonal Horizontal Vibration. 1999; 32: 1269-1278.

[55] Rakheja S, Stiharu I. Seated Occupant Apparent Mass Characteristics Under Automotive Postures and Vertical Vibration. 2002; 253: 57-75.

[56] Juang JN. *Applied System Identification*. Upper Saddle River, NJ: Prentice Hall PTR; 1994: 15-31.

[57] Walter E. *Identification of Parametric Models*, New York, NY: Springer Verlag Inc; 1997: 83-129.

[58] Day WD. *Introduction to Laplace Transforms for Radio and Electrical Engineers*. New York, NY: Interscience Publishing Inc; 1960.

[59] LePage WR. *Complex Variables and Laplace Transforms for Engineers*. New York, NY: McGraw-Hill Book Company Inc; 1961.

[60] Kuhfittig PKF. *Introduction to the Laplace Transform*. New York, NY: Plenum Press; 1978.

[61] Levine WS, ed. *The Control Handbook*. Boca Raton, FL: CRC Press Inc; 1996: 118-192.

[62] Westphal LC. *Sourcebook of Control Systems Engineering*. London, UK: Chapman & Hall; 1995: 461-491.

[63] Phillips CL, Harbor RD. *Feedback Control Systems*. 4th ed. Upper Saddle River, NJ: Prentice Hall PTR; 2000: 115-131.

[64] Granthom WJ, Vincent TL. *Modern Control Systems, Analysis and Design*. New York, NY: John Wiley & Sons Inc; 1993: 136-142.

[65] Tamboli JA, Joshi SG. Optimum design of a passive suspension system of a vehicle subjected to actual random road excitations. *Journal of Sound and Vibration*. 1999; 219: 193-205.

[66] Liu K, Liu J. The damped dynamic vibration absorbers: revisited and new result. *Journal of Sound and Vibration*. 2005; 284: 1181-1189.

[67] Alkhatib R, Nakhaie Jazar G, Golnaraghi MJ. Optimal design of passive linear suspension using genetic algorithm, *Journal of Sound and Vibration*. 2004; 275: 665-691.